NONLINEAR ISOLATORS FOR SHOCK AND RANDOM EXCITATIONS

ME 1999
N

A Thesis Submitted

in Partial Fulfillment of the Requirements

for the Degree of

Doctor of Philosophy

by

N. CHANDRA SHEKHAR

to the

DEPARTMENT OF MECHANICAL ENGINEERING
INDIAN INSTITUTE OF TECHNOLOGY KANPUR

September, 1999

14 JUN 2000 ME
CENTRAL LIBRARY
I. I. T., KANPUR
No. A 131094

TH
[illegible]
[illegible]

A131094

Dedicated to

Many excellent teachers who motivated me from my school days to Ph. D programme. Some of them are :

Mr. K. Bhadraiah, Government High School, Railway Gate, Warangal (1976-79)
Mr. Rama Chandra Mouli, Government Polytechnic, Warangal (1979-86)
Mr. A. Ranga Rao, Government Polytechnic, Warangal (1983-86)
Professor J.V. Subramaniam, College of Engg., Osmania Univ., Hyderabad (1986-90)
Professor B.L. Dhoopar, Indian Institute of Technology, Kanpur (1990-92)
Professor M.M. Oberai, Indian Institute of Technology, Kanpur (1990-93)
Professor N.G.R. Iyengar, Indian Institute of Technology, Kanpur (1990-99)
Professor A.K. Mallik, Indian Institute of Technology, Kanpur (1990-99)

Certificate

It is certified that the work contained in this thesis entitled **Nonlinear Isolators for Shock and Random Excitations** by N. CHANDRA SHEKHAR, has been carried out under our supervision, and that this work has not been submitted elsewhere for a degree.

H. Hatwal
Professor

A.K. Mallik
Professor

Department of Mechanical Engineering

I.I.T. Kanpur

September, 1999

Acknowledgements

I would like to express my deep sense of gratitude to Professor A.K. Mallik and Professor H. Hatwal, for their invaluable suggestions and constructive criticism which helped me a lot during the course of this work. Working with them in the last seven years has been a good learning experience. I also thank them for going through the manuscript carefully and making it readable. I owe a great debt to them for their personal help at various stages during my stay here.

I would like to thank specially, Professor A.K. Mallik, who introduced me to the area of Nonlinear Vibrations during my M.Tech programme.

I am indebted to Professors N.N. Kishore, N.G.R. Iyengar, M.M. Oberai, A. Ghosh, Prashant Kumar, B.L. Dhoopar, C. Venkobachar, N.S. Vyas, K. Ramesh, G. Biswas, B. Dasgupta, P.M. Dixit, S.G. Dhande, K. Banerjee, M.R.M. Rao, S.P. Mohanty and U.B. Tewari for their help.

Thanks are also due to Dr. B. Ravindra, Dr. Shyamal Chatterjee, Dr. Jakka Venkatesh, Dr. Regalla Srinivasa Prakash, Dr. Rajiv Tewari, Dr. Anirvan Dasgupta, Dr. U.S. Dixit, Dr. S.V. Rao, Dr. K. Srinivasan, Dr. Sajja Chandrasekhar Rao, Dr. Appaji Rao, Dr. I. Sridhar, Dr. P.M.V. Subba Rao, Dr. P.V.M. Rao, Dr. Sanjeev Swamy, Dr. Rahul Konnur, Dr. P.V.S.N. Murthy, Dr. Ligy Philip, Dr. Premananda Bera and Dr. N. Venkata Reddy for their help and encouragement.

I thank N.D. Reddy, V.S.N.K. Prasad, S.B.S. Rao, K. Ramu, A.K. Agarwal, S.K.

Rathore, Sanath Agarwal, S. Ravi, P. Muthu, Goutam Chakraborty, Goutam Pohit, Animesh Chatterjee, Ahmed Ali Khan, K. Harikishan Reddy, Mr. Jayaramkumar Sir, Sudhakar and P.S. Rao for being such good friends. I also acknowledge my association with T.S. Rao, Keshava Reddy, Maroutu Rama Rao, Prasad, M.V. Rao, N.S. Reddy, Vaddi Durga Prasad, Saya Srinivas, Nidamarthi Srinivas, Challa Srinivasa Rao, P.V.S.N. Murthy, Soumen Roy, DBN, Kothapalli, Duvvala, Kandakattla, A. Mallikarjun, Singireddy Sridhar, Ghanta Srikanth, Kagitha Uma Maheswar Rao, Birru Rajkumar, Shiva Prasad, Rahul, Boora Kumara Swamy, Piyush Chandra Srivastava, Male Ravikumar, Kyatham Vasishta, Dantamshetty Satish Kumar, N.J.M. Reddy and Late P. Srinivas Babu.

I am thankful for the help I got from Mr. M.M. Singh and Mr. S. Chakrapani.

I thank my parents who instilled in me the determination and hard work. I am extremely indebted to my father, Sri. Nyalapogula Mallaiah Garu, and my brother Krishna for keeping me away from all the tensions. I thank my sister Smt. V. Sridevi, my brother-in-law Sri. Vangari Rajeshwar Rao, and their kids Sanjana and Kautilya. I thank them for making my stay enjoyable whenever I stayed with them. I also thank Suresh (Kanna), Sridhar and Chitti.

Finally, I wish to express my thanks to my wife, Bhagyalaxmi, who, till date, relieved me from the household responsibilities. I thank her for possibly sacrificing her ambitions to stay with me at IIT Kanpur. She provided an excellent home and family life. The amazing amount of patience she has shown so far is a big surprise for me. I sincerely believe I could not have completed this dissertation without her cooperation. She continues to be my best friend.

Nyalapogula Chandra Shekhar

Synopsis

Insertion of a vibration isolator between the source and receiver of vibration is a very common method of vibration control. The function of an isolator is to reduce the magnitude of motion transmitted from the foundation to the receiver or to reduce the magnitude of force transmitted from the source to the foundation.

Shock refers to the transient response following a sudden change in some motion variable as experienced by, for example, an aircraft while landing, a vehicle while encountering a bump on the road or the foundation of a forging machine when the hammer is dropped on the anvil. The simplest idealization of shock isolation system is a single degree-of-freedom (SDOF) model in which the masses are considered to be concentrated and the flexible members are considered to be massless. Then, the isolator is assumed to be massless with linear stiffness and linear damping. The foundation is taken as ideally rigid. Analysis of such linear shock isolation systems have been widely reported in the literature.

A large class of isolator systems is also subjected to random excitation. For example, the landing gear of an aircraft (while taxiing on the runway) and a vehicle suspension are subjected to track induced random excitations. Isolators of ground base structures are subjected to earthquakes which again can be modelled as random excitations. In the most general case, the excitation can be a combination of transient, periodic or random disturbances. A brief review of previous work on shock isolators and random

vibration isolators especially with reference to vehicle vibration control is provided in the first chapter of the thesis.

Nonlinearity is ubiquitous in nature. Linearity is an approximation to reality. In shock and vibration systems, isolators such as air springs, elastomeric dampers and wire-rope isolators are inherently nonlinear. Assumption of Hooke's law for springs and linear viscous damping for dampers is done just for mathematical simplicity. Sometimes, the amplitudes of steady-state vibration are small enough to justify the assumption of linearity. However, the transient displacements and velocities may often be sufficiently large when the nonlinearity in springs and dampers cannot be ignored.

The primary objective of this thesis is to analyze the role of nonlinearity in both the stiffness and damping on the performance of shock isolation systems.

In chapter 2, base excited nonlinear SDOF isolator model has been considered. A simple technique combining the straightforward perturbation method with Laplace transform is used for obtaining solution in closed form. This method is applicable for any order of nonlinearity, both in the restoring and damping forces, expressed in the form of polynomials. However, the results are obtained with only cubic nonlinearity both in the restoring and damping forces. Three types of base excitations, namely, the rounded step, the rounded pulse and the oscillatory step are considered. Analytical results obtained by the present method are compared with those obtained by direct numerical integration. It has been shown that a critical value of the positive coefficient of the cubic damping term maximizes the peak values of relative and absolute displacements. This is true for any power-law damping force with an index greater than 1. Numerical results are included for a typical elastomeric damper which can be modelled by a combination of linear viscous damping and a dissipative quadratic damping with a negative coefficient. It is observed that the overall performance of a shock isolator improves if the nonlinear damping term is symmetric and quadratic

with a negative coefficient as exhibited by elastomers up to a certain value of the amplitude of deformation. It has been established that the nonlinearity in damping predominantly affects the shock isolator response, whereas the effect of nonlinearity in stiffness is insignificant. So, in the subsequent chapters only the damping (and not the stiffness) is taken to be nonlinear.

The performance of the isolator system considered in chapter 2 is re-examined under force shock excitations. These results are included in chapter 3. Unlike with base excitation, the presence of nonlinearity in the damping force is seen to marginally improve the performance of a linear isolator if the system is excited by a shock force on the mass.

In the presence of inherent nonlinear cubic damping in a nonlinear shock isolator with base excitation, four different modifications of the isolator are considered to improve its performance. These modifications are (i) an isolator with a Coulomb damper, (ii) a three element isolator with the nonlinear damper mounted elastically, (iii) an isolator with vibration absorber and (iv) a two stage isolator. Overall, it is seen that the three element and two stage isolators are preferable in the presence of nonlinear cubic damping. These results are presented in chapter 4.

In chapter 5, a two degree-of-freedom (2-DOF) model for a vehicle undergoing heave and pitch motions is investigated for shock excitations. It is assumed that the vehicle is moving with a constant speed so that the rear wheels are subjected to the same input as the front wheels but with a time delay. Both coupled and decoupled symmetric systems are considered. It is shown that the decoupled symmetric system gives optimum isolation performance. Like in SDOF systems, nonlinear damping is detrimental to 2-DOF systems for shock excitation with a two element isolator. A three element isolator nullifies the adverse effect of the nonlinear damping in the 2-DOF system as well.

The vehicle model considered in chapter 5 is investigated again with random excitation. This study is presented in chapter 6. Here, the front and rear suspensions are subjected to the same filtered white noise but with some time delay governed by the speed of the vehicle. Shinozuka's spectral method is used for generation of the random process. Monte-Carlo simulation has been employed to find the response of the vehicle.

The major conclusions of the present thesis are listed below.

(i) A simple analytical method has been developed using perturbation technique in conjunction with Laplace transform to determine the transient response of an SDOF system in the presence of nonlinear, dissipative shock isolators. It is observed that in most cases, the closed form perturbed solution matched well with the numerically integrated results.

(ii) It has been established that the effect of nonlinear damping is more predominant than the effect of nonlinear stiffness so far as the performance of shock isolators for base excitation is concerned. The presence of nonlinear n^{th} power-law damping, with a positive coefficient and the index n greater than unity, is harmful for base excited shock isolators. However, quadratic damping with a negative coefficient improves the performance of a shock isolator.

(iii) With force excitation, the presence of nonlinearity in damping does not deteriorate the performance of a shock isolator, rather it marginally improves the performance of a linear shock isolator.

(iv) To improve the performance of a shock isolator with base excitation, in the presence of nonlinear cubic damping, four methods, namely, Coulomb damped isolator, three element isolator, vibration absorber and two stage isolator have been considered. Overall, a three element isolator and a two stage isolator are preferable in the presence of nonlinear cubic damping.

(v) 2-DOF coupled nonlinear asymmetric systems behave like a symmetric system

for a particular choice of parameter values. At very high speeds and for forward centre of mass, high damping and high stiffness at the front suspension rather than at the rear suspension give the optimum response for the decoupled system.

(vi) The detrimental effect of nonlinear cubic damping in a two element isolator and its mitigation by using a three element isolator are exhibited by both SDOF and 2-DOF models.

(vii) With a random base excitation, 'Stochastic Resonance' type phenomenon is observed for both heave and pitch displacements when the damping is linear. Unlike for shock excitations, in this case the nonlinear cubic damping reduces heave and pitch displacements. However, the presence of nonlinearity in the damping force increases both heave and pitch accelerations.

Contents

Certificate i

Acknowledgements ii

Synopsis iv

Table of Contents ix

List of Figures xiii

List of Symbols xviii

1 INTRODUCTION 1

1.1 Introduction 1

1.2 Review of Previous Work 4

1.2.1 Shock Isolators 4

1.2.2 Random Vibration Isolators 6

1.3 Objectives and Organization of the Present Work 11

2 RESPONSE OF NONLINEAR DISSIPATIVE SHOCK ISOLATORS TO DISPLACEMENT EXCITATION 14

2.1 Introduction 14

2.2 Equations of Motion 17

2.3 Types of Input Displacements of The Base 17

2.4 Closed Form Solutions 24
2.4.1 Zeroth Order Solution 25
2.4.2 First Order Solution 29
2.4.3 Second Order Solution 31
2.5 Results and Discussions 31
2.5.1 Validation of Closed Form Solutions 31
2.5.2 Effect of Nonlinear Damping 38

3 RESPONSE OF NONLINEAR DISSIPATIVE SHOCK ISOLATORS TO FORCE EXCITATION 45
3.1 Introduction 45
3.2 Equations of Motion 46
3.3 Results and Discussions 48
3.3.1 Effect of Nonlinear Damping 51

4 PERFORMANCE OF NONLINEAR ISOLATORS AND ABSORBERS TO SHOCK EXCITATIONS 58
4.1 Introduction 58
4.2 Equations of Motion 60
4.2.1 Type 1 Isolator : Shock Isolator with a Coulomb Damper 60
4.2.2 Type 2 Isolator : Three Element Shock Isolator 60
4.2.3 Type 3 Isolator : Transient Vibration Absorber 63
4.2.4 Type 4 Isolator : Two Stage Shock Isolator 65
4.3 Results and Discussions 67
4.3.1 Type 1 Isolator 70
4.3.2 Type 2 Isolator 71
4.3.3 Type 3 Isolator 75
4.3.4 Type 4 Isolator 81

5 2-DOF HEAVE-PITCH MODEL OF A VEHICLE FOR SHOCK EXCITATION 86
5.1 Introduction . . . 86
5.2 System Models . . . 87
5.2.1 Model I . . . 87
5.2.2 Model II . . . 91
5.3 Theoretical Analysis for Special Cases . . . 93
5.3.1 Symmetric System . . . 93
5.3.2 Decoupled System . . . 94
5.3.3 Linear System . . . 96
5.4 Input from The Road Irregularities . . . 97
5.5 Results and Discussions . . . 98
5.5.1 Effect of Linear Damping . . . 101
5.5.2 Effect of Nonlinear Damping . . . 104

6 2-DOF HEAVE-PITCH MODEL OF A VEHICLE FOR RANDOM EXCITATION 112
6.1 Introduction . . . 112
6.2 Equations of Motion . . . 113
6.3 Road Profile Model . . . 114
6.4 Monte Carlo Simulation . . . 116
6.5 Results and Discussions . . . 118

7 CONCLUSIONS 126
7.1 Conclusions . . . 126
7.2 Scope of Future Work . . . 128

REFERENCES 130

APPENDIX

A Solution of Ordinary Second Order Differential Equations for Three Special Non-homogeneous Functions 141

B Laplace Transform of Equation (5.41) and Its Inverse 145

List of Figures

2.1 Non-linear base excited system 16

2.2 The rounded step displacement 19

2.3 The rounded pulse displacement 20

2.4 The oscillatory displacement step 22

2.5 Comparison of analytical and numerical results for the cubic nonlinearity in stiffness only. $\zeta = 0.1, \gamma = 20, \epsilon = 0.01, \epsilon_1 = 1, \delta_1 = 0$. $\diamond$ zeroth order, $*$ first order, $\triangleright$ second order, —— numerical. Curve (a): the rounded step displacement; curve (b): the rounded pulse displacement; curve (c): the oscillatory displacement step. . . . 33

2.6 Comparison of analytical and numerical results for the cubic nonlinearity in damping only for the rounded step displacement. $\zeta = 0.1$, $\epsilon = 0.01$, $\epsilon_1 = 0$, $\delta_1 = 1$ $\gamma = 20$ $\diamond$ zeroth order, $*$ first order, $\triangleright$ second order, —— numerical. 34

2.7 Comparison of analytical and numerical results for the cubic nonlinearity in damping only for the rounded pulse displacement. $\zeta = 0.1$, $\epsilon = 0.01$, $\epsilon_1 = 0$, $\delta_1 = 1$ $\gamma = 20$ $\diamond$ zeroth order, $*$ first order, $\triangleright$ second order, —— numerical. 35

2.8 Comparison of analytical and numerical results for the cubic nonlinearity in damping only for the oscillatory displacement step. $\zeta = 0.1$, $\epsilon = 0.01$, $\epsilon_1 = 0$, $\delta_1 = 1$ $\gamma = 20$ $\diamond$ zeroth order, $*$ first order, $\triangleright$ second order, —— numerical. 36

2.9 Comparison of analytical and numerical results for the cubic nonlinearity in damping only for the oscillatory displacement step. $\zeta = 0.1$, $\epsilon = 0.01$, $\epsilon_1 = 0$, $\delta_1 = 1$ $\gamma = 1$ $\diamond$ zeroth order, $*$ first order, $\triangleright$ second order, —— numerical. 37

2.10 The effect of nonlinear cubic damping on the relative displacement for the rounded displacement step. $\gamma = 50$, $\zeta = 0.1$, $\epsilon^* = 0$. —— $\delta^* = 0$, $\diamond$ $\delta^* = 0.01$, $*$ $\delta^* = 0.05$, $\twoheadrightarrow$ $\delta^* = 0.1$ 39

2.11 The effect of nonlinear cubic damping on the relative velocity for the rounded displacement step. $\gamma = 50$, $\zeta = 0.1$, $\epsilon^* = 0$. —— $\delta^* = 0$, $\diamond$ $\delta^* = 0.01$, $*$ $\delta^* = 0.05$, $\twoheadrightarrow$ $\delta^* = 0.1$ 40

2.12 The effect of nonlinear cubic damping on the velocity for the rounded displacement step. $\gamma = 50$, $\zeta = 0.1$, $\epsilon^* = 0$. —— $\delta^* = 0$, $\diamond$ $\delta^* = 0.01$, $*$ $\delta^* = 0.05$, $\twoheadrightarrow$ $\delta^* = 0.1$ 41

2.13 The effect of nonlinear cubic damping on the acceleration for the rounded displacement step. $\gamma = 50$, $\zeta = 0.1$, $\epsilon^* = 0$. —— $\delta^* = 0$, $\diamond$ $\delta^* = 0.01$, $*$ $\delta^* = 0.05$, $\twoheadrightarrow$ $\delta^* = 0.1$ 42

2.14 The effect of nonlinear quadratic damping on the acceleration for the rounded step. $\gamma = 50$, $\zeta = 0.1$, $\epsilon^* = 0$. —— $\delta^* = 0$, $\diamond$ $\delta^* = 0.01$, $\triangleright$ $\delta^* = -0.01$ 44

3.1 Non-linear force excited system 46

3.2 The rounded step force excitation. 49

3.3 The rounded pulse force excitation. 50

3.4 The effect of nonlinear cubic damping on the displacement for the rounded step force excitation. $\gamma = 50$, $\zeta = 0.1$. —— : $\delta^* = 0$, ... : $\delta^* = 0.05$ 52

3.5 The effect of nonlinear cubic damping on the velocity for the rounded step force excitation. $\gamma = 50$, $\zeta = 0.1$. —— : $\delta^* = 0$, ... : $\delta^* = 0.05$ 53

3.6 The effect of nonlinear cubic damping on the acceleration for the rounded step force excitation. $\gamma = 50$, $\zeta = 0.1$. —— : $\delta^* = 0$, ... : $\delta^* = 0.05$ 54
3.7 The effect of nonlinear cubic damping on the displacement for the rounded pulse force excitation. $\gamma = 1$, $\zeta = 0.1$. —— : $\delta^* = 0$, ... : $\delta^* = 0.05$ 55
3.8 The effect of nonlinear cubic damping on the velocity for the rounded pulse force excitation. $\gamma = 1$, $\zeta = 0.1$. ——: $\delta^* = 0$, ... : $\delta^* = 0.05$ 56
3.9 The effect of nonlinear cubic damping on the acceleration for the rounded pulse force excitation. $\gamma = 1$, $\zeta = 0.1$. ——: $\delta^* = 0$, ... : $\delta^* = 0.05$ 57

4.1 Type 1 Isolator 61
4.2 Type 2 Isolator 62
4.3 Type 3 Isolator 64
4.4 Type 4 Isolator 66
4.5 SDR and RDR curves for type 1 isolator as a function of γ for the rounded step displacement. I. linear damping $\zeta = 0.1$, II. linear + cubic damping $\zeta = 0.1, \delta^* = 0.01$, III. linear + Coulomb damping $\zeta = 0.1, \delta_f = 0.5$ and IV. linear + cubic + Coulomb damping $\zeta = 0.1, \delta^* = 0.01, \delta_f = 0.5$ (suffix S for SDR and R for RDR). 68
4.6 SAR curves in dB for type 1 isolator as a function of γ for the rounded step displacement. I. linear damping $\zeta = 0.1$, II. linear + cubic damping $\zeta = 0.1, \delta^* = 0.01$, III. linear + Coulomb damping $\zeta = 0.1, \delta_f = 0.5$ and IV. linear + cubic + Coulomb damping $\zeta = 0.1, \delta^* = 0.01, \delta_f = 0.5$ . . . 69
4.7 SDR and RDR curves for type 2 isolator as a function of γ for the rounded step displacement. I. linear damping $\zeta = 0.1$, II. linear + cubic damping $\zeta = 0.1, \delta^* = 0.01$, V. type 2 isolator $\zeta = 0.1, \delta^* = 0.01, n = 1$ (suffix S for SDR and R for RDR). 72
4.8 SAR curves in dB for type 2 isolator as a function of γ for the rounded step displacement. I. linear damping $\zeta = 0.1$, II. linear + cubic damping $\zeta = 0.1, \delta^* = 0.01$, V. type 2 isolator $\zeta = 0.1, \delta^* = 0.01, n = 1$. 73

4.9 The effect of stiffness ratio (n) on the SDR in type 2 isolator for the rounded step displacement at $\gamma = 50$ ($\zeta = 0.1, \delta^* = 0.01$) 74
4.10 SDR curves for type 3 isolator as a function of γ for the rounded step displacement. I. linear damping $\zeta = 0.1$, II. linear + cubic damping $\zeta = 0.1, \delta^* = 0.01$, VI. type 3 isolator $\zeta = 0.1, \delta^* = 0.01, n = 1, \delta_2 = 0.01, \mu = 0.5$ 76
4.11 SDR curves for type 3 isolator as a function of γ for the oscillatory displacement step. I. linear damping $\zeta = 0.1$, II. linear + cubic damping $\zeta = 0.1, \delta^* = 0.01$, VI. type 3 isolator $\zeta = 0.1, \delta^* = 0.01, n = 1, \delta_2 = 0.01, \mu = 0.5$ 77
4.12 SAR curves in dB for type 3 isolator as a function of γ for the rounded step displacement. I. linear damping $\zeta = 0.1$, II. linear + cubic damping $\zeta = 0.1, \delta^* = 0.01$, VI. type 3 isolator $\zeta = 0.1, \delta^* = 0.01, n = 1, \delta_2 = 0.01, \mu = 0.5$ 78
4.13 SAR curves in dB for type 3 isolator as a function of γ for the rounded pulse displacement. I. linear damping $\zeta = 0.1$, II. linear + cubic damping $\zeta = 0.1, \delta^* = 0.01$, VI. type 3 isolator $\zeta = 0.1, \delta^* = 0.01, n = 1, \delta_2 = 0.01, \mu = 0.5$ 79
4.14 Curve (a): The effect of stiffness ratio (n) on the SDR in type 3 isolator, for the rounded step displacement at $\gamma = 50$ ($\zeta = 0.1, \delta^* = 0.01, \delta_2 = 0.01, \mu = 0.5$). Curve (b): The effect of mass ratio (μ) on the SDR in type 3 isolator, for the rounded step displacement at $\gamma = 50$ ($\zeta = 0.1, \delta^* = 0.01, \delta_2 = 0.01, n = 1.0$) 80
4.15 SDR curves for type 4 isolator as a function of γ for the rounded step displacement. I. linear damping $\zeta = 0.1$, II. linear + cubic damping $\zeta = 0.1, \delta^* = 0.01$, VII. type 4 isolator $\zeta = 0.1, \delta^* = 0.01, n = 1, \delta_2 = 0.01, \mu = 0.1$ 82

4.16 SAR curves in dB for type 4 isolator as a function of γ for the rounded step displacement. I. linear damping $\zeta = 0.1$, II. linear + cubic damping $\zeta = 0.1, \delta^* = 0.01$, VII. type 4 isolator $\zeta = 0.1, \delta^* = 0.01, n = 1, \delta_2 = 0.01, \mu = 0.1$ 83
4.17 The effect of mass ratio (μ) on the SDR in type 4 isolator, for the rounded step displacement at $\gamma = 50$ ($\zeta = 0.1, \delta^* = 0.01, \delta_2 = 0.01, n = 1.0$) . . . 84

5.1 Heave-Pitch Model I 88
5.2 Heave-Pitch Model II 89
5.3 Effect of Linear Damping on HDR and PDR for Model I 99
5.4 Effect of Linear Damping on HAR for Model I 100
5.5 Effect of Linear Damping on PAR for Model I 102
5.6 Comparison of Model I and II for HDR and PDR, linear damping case 105
5.7 Comparison of Model I and II on HAR and PAR, linear damping case 107
5.8 Effect of Nonlinear Damping on HDR and PDR 108
5.9 Effect of Nonlinear Damping on HAR and PAR 109
5.10 Comparison of Model I and II for HDR and PDR, nonlinear damping case110
5.11 Comparison of Model I and II for HDR and PDR, nonlinear damping case111

6.1 Comparison of generated autocorrelation function with target autocorrelation function. Y_1: target; g: generated. 119
6.2 Effect of nonlinear damping on RMS Heave displacement. 122
6.3 Effect of nonlinear damping on RMS Heave acceleration in dB. 123
6.4 Effect of nonlinear damping on RMS Pitch displacement. 124
6.5 Effect of nonlinear damping on RMS Pitch acceleration in dB. 125

List of Symbols

a	distance from the center of mass to the front axle
b	distance from the center of mass to the rear axle
c_0	linear damping coefficient
c_1	nonlinear damping coefficient
c_2	linear damping coefficient of the secondary system
c_3	nonlinear damping coefficient of the secondary system
c_{10}	linear damping coefficient of the front tyre
c_{11}	nonlinear damping coefficient of the front tyre
c_{20}	linear damping coefficient of the rear tyre
c_{21}	nonlinear damping coefficient of the rear tyre
c_f	Coulomb damping coefficient
E	expectation operator
h	horizontal lag
i	$\sqrt{-1}$
I	moment of inertia
k_0	linear stiffness constant
L	vehicle wheel base
m	mass
m_2	secondary mass
q	road roughness parameter
R	non-dimensional radius of gyration (see equation 5.8 and page 91)
R_y	autocorrelation function of random process y
s	horizontal distance variable
$sgf(x)$	= -1 if $x < 0$
	= 0 if $x = 0$
	= +1 if $x > 0$

S_y	power spectral density of random process y
t	time
t_0	time delay
T	non-dimensional time (see page 17, equation (2.2))
T_p	non-dimensional time period (see page 18, equation (2.5))
T_0	non-dimensional time delay (see page 95, case II)
V	vehicle forward speed
$W(t)$	white noise process
x	vertical displacement of the center of mass
y_1	base excitation due to road irregularities at the front tyre
y_2	base excitation due to road irregularities at the rear tyre
α	offset parameter (see pages 90 and 91, equation (5-6))
δ	Dirac-delta function
δ^*	non-dimensional nonlinear damping coefficient (see page 17, equation (
δ_f	non-dimensional Coulomb damping coefficient (see page 60, equation (
Δ	non-dimensional relative displacement (see page 17, equation (2.2,
ϵ^*	non-dimensional nonlinear stiffness coefficient (see page 17, equation (
ϕ_n	random phase angle
γ	shock severity parameter
λ	wavelength
μ	mass ratio
ν	wave number
θ	angle of rotation about center of mass
σ	standard deviation of road irregularity
τ	time lag
ω	circular frequency
ω_0	linear natural frequency
Ω	non-dimensional frequency (see page 116, equation (6.17))
ζ	non-dimensional linear damping ratio (see page 17, equation (2.2),
$\lfloor x \rfloor$	largest integer $\leq x$
$\lceil x \rceil$	smallest integer $\geq x$
$\mid x \mid$	absolute value of x

Chapter 1

INTRODUCTION

1.1 Introduction

Vibration and shock phenomena are omnipresent. Many occur in nature and many in man-made devices and structures. Quite often vibration and shock are not desirable and the interest lies in reducing it. Insertion of a vibration isolator between the source and receiver of vibration is a very common method of vibration control. The function of an isolator is to reduce the magnitude of motion transmitted from the foundation to the equipment or to reduce the magnitude of force transmitted from the equipment to the foundation.

Shock is a transient condition. The equilibrium of a system is disrupted either by suddenly applied forces or by increment of force or by sudden change in the motion. This disruption and its ensuing reaction of the system to restore equilibrium constitutes condition of shock.

Examples of shock are aircraft landing, braking and gust loading, missile launching and braking, transportation of fragile equipment, accidental collision of vehicles, drop forging machine, vehicle running on a bump, high speed fluid entry, explosions, gunfire,

etc.

The subject of shock is exceedingly complex because the suddenly applied forces and sudden motions cause mechanical structures to vibrate in a transient manner, and in many natural modes simultaneously. In the application of shock isolators to an actual equipment, the location of isolators are determined largely by practical mechanical considerations. In general, this results in types of non-symmetry and coupled modes not well adopted to analysis by simple means. It is convenient in the design of shock isolators to idealize the system as one having symmetry and uncoupled modes of vibration. In the simplified analysis the masses are considered to be concentrated and the flexible members are massless. The effect of this simplification is to discard the higher modes of vibration. The much less complex analysis of a single degree-of-freedom (SDOF) system then becomes applicable. Mounted equipment and isolators assembly is represented by a mass-spring-dashpot system.

There is a considerable justification for this simplification because the cushioning afforded by the isolator reduces the suddenness of forces and motions, and thereby tends to reduce the response of structures in their higher modes of vibration.

A different form of idealization is required when the equipment is flexible; e.g., a large relatively flexible aircraft subjected to landing shock. Then it is important to represent the aircraft as a system with several degrees-of-freedom.

Isolation of vibration or shock signifies the temporary storage of energy and its subsequent release substantially in its entirety but in a different time relation. Isolation is thus distinct from the absorption or dissipation of energy. The effectiveness of an isolator is sometimes enhanced by limited dissipation of energy but this is a secondary consideration in its function.

A large class of physical systems operate in random vibration environment. These include: aerospace systems excited by atmospheric and boundary layer turbulence and

jet noise; aircraft and vehicles subjected to track induced vibrations; ground based structures excited by earthquakes and wind; and offshore structures excited by wind and hydrodynamic wave-induced loads. A probabilistic approach, based on random vibration analysis, provides a rational and consistent basis for the analysis and design of such systems.

In the most general case, the excitation can be a combination of transient, periodic or random disturbances. It is therefore clear that the optimum design of an isolator for a general type of excitation is probably not feasible and in practice an isolator will be designed for only one set of environmental conditions.

The linear shock isolation problems have been widely reported in the literature. Nonlinearity is ubiquitous in nature. Linearity is an approximation to reality. In shock and vibration systems, isolators such as air springs, elastomeric dampers and wire-rope isolators are inherently nonlinear. Assumption of Hooke's law for springs and linear viscous damping for dampers is done just for mathematical simplicity. Sometimes, the amplitudes of steady-state vibration are small enough to justify the assumption of linearity. However, the transient displacements may often be sufficiently large when the nonlinearity in springs and dampers cannot be ignored.

The primary objective of this thesis is to analyze the role of nonlinearity in both the stiffness and damping on the performance of shock isolation systems. In the present work, the isolation system is modelled as SDOF and 2-DOF systems with shock excitation. At the end, 2-DOF vehicle model has been considered for both shock and random base excitations.

1.2 Review of Previous Work

The amount of literature available on the general problem of shock and random vibration isolation is too vast to be considered in detail. In this section, the literature pertinent to the present work is discussed. An overview of the research work in different areas, connected with the present problem, is categorized under the following headings:

(i) Shock Isolators,

(ii) Random Vibration Isolators

1.2.1 Shock Isolators

Linear shock isolation problems are discussed in several books [1-4]. Snowdon [4] presented the response of a nonlinear shock isolator modelled as a nonlinear elastic (tangent and inverse tangent elasticity) spring parallel to a viscous damper. He concluded that a soft spring (inverse tangent elasticity) performs better than a hard spring. In reference [5], Snowdon compared the performance of a dual-phase damper mounting system with that of a linear, simple mounting system. Guntur and Sankar [6] reported the performances of different kinds of dual-phase damper mounting system and compared these with that of a linear, simple mounting system. Hundal [7] reviewed the literature on pneumatic shock absorbers and isolators. Hundal [8] has also compared the performances of shock isolators with linear and quadratic damping with a base input in the form of an acceleration pulse of rectangular shape.

By using the concept of a variable friction force, Mercer and Rees [9] proposed a new form of shock isolator which is adaptive in its action but is still composed of entirely passive elements. Eshleman and Rao [10] have investigated shock isolation characteristics of six types of elements: (a) helical coil spring, (b) ring spring, (c) friction snubber,

(d) liquid spring, (e) pneumatic spring, and (f) solid rubber elastomer. They concluded that the friction snubber-helical spring combination yielded the best isolation of all the elements. Hundal [11] describes the analysis of response of a pneumatic shock isolator to base acceleration of rectangular and half-sine shape pulses. The isolator consists of a pneumatic damper in parallel with a linear spring. Hundal [12] has also presented the analysis and response of a symmetric pneumatic absorber with orifice damping. The modelling and response of a pneumatic shock isolator are presented in reference [13]. The isolator consisted of a symmetric pneumatic spring with self-damping and was subjected to a velocity pulse. In reference [14], an unsymmetric pneumatic shock isolator is considered. An investigation on a linear shock isolator subjected to a velocity pulse is included in reference [15].

The concept of an 'on-off' damper employing the feedback signals from directly measurable variables is proposed in reference [16]. A control scheme utilizing the directly measurable relative position and relative velocity signals to produce the command signal is configured. For larger values of shock severity, the 'on-off' dampers perform extremely superior to any passive damper.

The shock isolation characteristics of semi-active isolators based on two different control schemes are presented in reference [17]. In the first type, the control depends on the absolute and relative velocities of the sprung mass while in the second type it depends on the relative displacement and the relative velocity. Both employ continuous control of damper forces as opposed to 'on-off' control. The damper forces are generated by modulating its orifice areas for fluid flow. The constraint on damper force is that the energy associated with it is always dissipated. It is seen that both the semi-active control schemes can simultaneously reduce the acceleration and the relative displacement, something passive linear isolators cannot do.

Various analytical methods are available in the literature [18-32] for transient analy-

sis of nonlinear systems, namely, the linearization method [19], the ultraspherical polynomial method [20-22] and Lighthill's extension of Poincare's perturbation method [23]. A simple-straight forward perturbation method is developed in [32] by using Laplace transforms.

1.2.2 Random Vibration Isolators

Numerous papers have so far been published on random vibration isolators especially with reference to vehicle vibration control. In reference [33] various vehicle models have been presented. Hrovat [34] studied the preview control applied to a linear, two-dimensional (2-D), four-degree- of-freedom, half-car model. The model includes vehicle sprung mass pitch and heave dynamics and front and rear unsprung masses. Linear Quadratic (LQ) control formulation has established that the preview based on front wheel input can contribute up to 70% reduction of vehicle r.m.s acceleration, for a given suspension travel, and up to 50% reduction in tire deflection for a given acceleration level. In reference [35], a fully active fail safe suspension is reported for the 4-DOF model using the optimal regulator theory. Root mean square (r.m.s) bounce and pitch absolute acceleration transmissibility of the sprung mass and of maximum suspension and tire deflections are presented for semi-active suspensions. Both passive and active schemes have been considered. In reference [36], the response of a vehicle moving over a non-homogeneously rough flexible track supported over a complaint foundation has been obtained for variable and constant velocity runs. The characteristics of the vehicle and track mode responses are expressed in closed form for both heave-pitch and heave-roll models. A quarter car suspension system model, containing a controllable damper with a limited range of coefficient values, a limited adjustment system bandwidth and a realistic elastic mounting to the car body has been optimized for operation on a random road [37]. The optimization has been carried out through a novel numerical method. In

reference [38], an approximate state-space method for obtaining the time varying mean and covariance of the response of nonlinear systems excited by non-stationary random process is presented. Redfield and Karnopp [39] analyzed a two-degree-of-freedom model for its performance sensitivity as a function of the system's feedback gains. A two-degree-of-freedom (1/4 car model) has also been used to evaluate alternative linear control laws [40]. Hac [41] considered decentralized control of active vehicle suspensions with preview of road irregularities using a two-degree-of-freedom vehicle model. He has also studied the problem of active suspension control of a two-degree-of- freedom vehicle traveling on a randomly profiled road [42].

Kirk [43] has investigated the influence of nonlinear spring stiffness characteristics on the effectiveness of vibration isolators with linear damping, subjected to stationary, random white noise ground acceleration. The probability density function of spring displacement is determined analytically by means of the Fokker-Planck equation and both r.m.s and mean peak values of spring displacement and mass acceleration are presented for three types of spring nonlinearity: (a) cubic hard spring, (b) cubic soft spring and (c) tangent spring. A method for modelling vehicles as a system of interconnected rigid and flexible bodies is presented in reference [44]. Finite element and component mode substitution techniques are employed to characterize elastic motions of flexible bodies in terms of minimal set of modal co-ordinates. Semi-active control techniques are then used for suppressing vibrations at some desired points, in the chassis, located away from suspension attachments. In references [45-46], a preview control problem of a semi-active suspension was formulated and a truly optimal solution was obtained using the calculus of variations.

Crolla and Abdel-Hady [47] have studied the effects of the following issues in deriving control laws based on a mathematical model of an actively suspended vehicle:

(a) representation of the ground surface as integrated or filtered white noise,

(b) cross-correlation between left and right track inputs,

(c) wheelbase time delay between front and rear inputs.

In reference [48], the basic functions which suspensions must perform are described and categories of controllable suspensions based on the required amount of control power are defined. The kinds of devices which can be used in controllable suspensions are discussed as well as several basic philosophies. Finally, fundamental theoretical and practical limitations in suspension performance are indicated. Lin and Willumeit [49] have simulated the dynamics of a vibrator-controlled adaptive damper. Its potential in vehicle isolation improvement is demonstrated by a quarter car model. The problem of deriving control laws which minimize specified performance indices for a vehicle moving on a rough surface with preview of the surface elevation is considered in reference [50]. Bhave [51] has presented an analysis of a vehicle mounted on air springs at the front and rear which are connected through a capillary tube.

Fodor and Redfield [52] have introduced the concept of regenerative damping in vibration control, the storage of energy normally dissipated by a passive viscous damper. A device, called the variable linear transmission, is proposed to accomplish this task. In reference [53], a continuous time control strategy for an active suspension with preview, based on optimal control theory is presented. It has been shown in reference [54] that an electromagnetic rotating damper can be used as a controlled force generator for vibration isolation in vehicles. Moran and Nagai [55] have shown that how neural networks can be used for the forward and inverse identification as well as the optimal control of nonlinear active suspensions. Well trained neuro-vehicle models can identify the dynamics of actual vehicle suspensions and predict their future behaviour.

Narayanan and Raju [56] have investigated an active suspension system to control the non-stationary response of a single-degree-of-freedom (SDOF) vehicle model with variable velocity traverse over a rough road. They considered the design of an active

optimal suspension to control the non-stationary response of a 2-DOF vehicle model traversing a rough road [57, 58]. They have also studied the active control of non-stationary response of a two-degree-of-freedom vehicle model with nonlinear passive suspension elements [59]. The method of equivalent linearization is used to derive an equivalent linear model and optimal control laws are obtained by using stochastic optimal control theory based on full state information. Velocity squared quadratic damping and hysteretic type of stiffness nonlinearities are considered. In reference [60], active control of the time varying response to a stationary random excitation of a two degree-of-freedom (2-DOF) vehicle model with nonlinear passive suspension elements have been considered.

Tamboli and Joshi [61] have obtained the Root Mean Square Acceleration Response (RMSAR) of a vehicle dynamic system subjected to actual random road excitations, so as to account for the effect of the actual power spectral density (psd) of road excitation and the frequent changes in vehicle velocity. A statistical dimensionless ratio, a ratio of excitations at rear and front axles, has been formulated to study the effect of time lag on the response of the vehicle due to wheelbase. The effect of vehicle velocity and wheelbase on the RMSAR has been studied and the RMSAR is found proportional to the vehicle velocity and inversely proportional to the wheelbase.

Ariaratnam and Wei-Chau Xie [62] have presented various methods to investigate the almost-sure asymptotic stability of nonlinear coupled oscillators under external random excitation. In reference [63], an asymptotic expansion for the maximal Lyapunov exponent, the exponential growth rate of solutions to a linear stochastic system, and the moment Lyapunov exponent, the asymptotic growth rate of the moments of the response, have been obtained for systems driven by a small intensity real noise process. The results obtained are applied to a thin rectangular beam under the action of a stochastic follower force and a model of a vehicle traveling over a rough road.

Blevins [64] has reported the analysis to determine the properties of a random process consisting of the sum of a series of sine waves with deterministic amplitudes and independent random phase angles. The probability density of the series, its peaks and envelope have been found for an arbitrary number of sine waves in the series.

Shinozuka [65] has presented the various efficient methods for digital simulation of a general homogeneous process (multidimensional or multivariate or multivariate-multidimensional) as a series of cosine functions with weighted amplitudes, almost evenly spaced frequencies and random phase angles. The approach is also extended to the simulation of a general non-homogeneous oscillators process characterized by an evolutionary power spectrum. Simulation of one-dimensional uni-variate, stationary, Gaussian stochastic processes using the spectral representation method was presented in reference [66]. In reference [67], a stochastic model for general periodic excitations with random disturbance which is constructed by introducing random amplitude and phase disturbances to individual term in the Fourier series of the corresponding deterministic periodic function has been presented. Johnson et. al.[68] compared the performance of Monte Carlo simulation on various platforms, in the context of a four-dimensional linear oscillator and a Duffing oscillator subjected to a band-limited white noise.

Zeldin and Spanos [69] presented the representation and simulation of random fields using wavelet bases. Examples of simulating random fields encountered in engineering applications are discussed. A Haar wavelet based model for probabilistic behaviour of stochastic dynamic systems was presented [70]. A Hamilton's law of varying action based approach was used to obtain a deterministic model. A single degree-of-freedom spring-mass-damper system subjected to a random forcing function was considered to show the feasibility and the effectiveness of the formulation. In reference [71] a new hierarchical method for the Monte Carlo simulation of random fields called the

Fourier-wavelet method is developed and applied to isotropic Gaussian random fields with power law spectral density functions. This technique is based upon the orthogonal decomposition of the Fourier stochastic integral representation of the field using wavelets.

1.3 Objectives and Organization of the Present Work

The primary objective of the present thesis is to study the effect of nonlinearity in the isolator elements subjected to shock excitation. Both base and force shock excitations have been studied. A simple analytical tool has been developed using perturbation method in conjunction with Laplace transform to determine the transient response of an SDOF system in the presence of nonlinear, dissipative shock isolators. To improve the performance of a shock isolator with base excitation, in the presence of nonlinear cubic damping, four methods namely, Coulomb damped isolator, three element isolator, vibration absorber and two stage isolator have been compared. Next, a 2-DOF (Heave and Pitch) vehicle model moving with constant speed, with a time delay in front and rear wheel inputs, has been studied for shock and random excitations. The organization of the thesis is detailed below.

In chapter 2, a simple technique combining the straightforward perturbation method with Laplace transform has been developed to determine the transient response of a single degree-of-freedom system in the presence of nonlinear, dissipative shock isolators. Analytical results are compared with those obtained by numerical integration using the classical Runge-Kutta method. Three types of input base excitations, namely, the rounded step, the rounded pulse and the oscillatory step are considered. The effects of nonlinear damping on the response are discussed in detail. Both the positive and negative coefficients of the nonlinear damping term have been considered. It has been

shown that a critical value of the positive coefficient maximizes the peak values of relative and absolute displacements. This is true for any power-law damping force with an index greater than 1. On the other hand, the overall performance of a shock isolator improves if the nonlinear damping term is symmetric and quadratic with a negative coefficient as exhibited by elastomers up to a certain value of the amplitude of deformation. It has been established that the nonlinearity in damping predominantly affects the shock isolator response, whereas the effect of nonlinearity in stiffness is insignificant. So, in the subsequent chapters only the damping (and not the stiffness) is taken to be nonlinear.

The performance of the isolator system considered in chapter 2 is re-examined under force shock excitations. These results are included in chapter 3. Unlike with base excitation, the presence of nonlinearity in the damping force is seen to marginally improve the performance of a linear isolator if the system is excited by a shock force on the mass.

In the presence of inherent nonlinear cubic damping in a nonlinear shock isolator with base excitation, four different modifications of the isolator are considered to improve its performance. These modifications are (i) an isolator with a Coulomb damper, (ii) a three element isolator with the nonlinear damper mounted elastically, (iii) an isolator with vibration absorber and (iv) a two stage isolator. Overall, it is seen that the three element and two stage isolators are preferable in the presence of nonlinear cubic damping. These results are presented in chapter 4.

In chapter 5, a 2-DOF model for a vehicle undergoing heave and pitch motions is investigated for shock excitations. It is assumed that the vehicle is moving with a constant speed so that the rear wheels are subjected to the same input as the front wheels but with a time delay. Both coupled and decoupled symmetric systems are considered. It is shown that the decoupled symmetric system gives optimum isolation

performance. Like in SDOF systems, nonlinear damping is detrimental to 2-DOF systems for shock excitation with a two element isolator. A three element isolator nullifies the adverse effect of nonlinear damping in 2-DOF system as well.

The vehicle model considered in chapter 5 is investigated again with random excitation. This study is presented in chapter 6. Here, the front and rear suspensions are subjected to the same filtered white noise but with some time delay governed by the speed of the vehicle. Shinozuka's [66] spectral method is used for generation of the random process. Monte Carlo simulation has been employed to find the response of the vehicle.

In chapter 7, overall conclusions and scope of future work have been presented.

Chapter 2

RESPONSE OF NONLINEAR DISSIPATIVE SHOCK ISOLATORS TO DISPLACEMENT EXCITATION

2.1 Introduction

Nonlinearity is ubiquitous in nature. Linearity is an approximation to reality. In shock and vibration systems, isolators such as air springs, elastomeric dampers, and wire-rope isolators are inherently nonlinear. Assumption of Hookes' law for springs and linear viscous damping for dampers is done just for mathematical simplicity. Sometimes the amplitudes of steady-state vibration are small enough to justify the assumption of linearity. However, the transient displacements may often be sufficiently large when the nonlinearity in springs and dampers cannot be ignored.

Ravindra and Mallik [72-74] have studied the effect of nonlinear damping on the

performance of vibration isolators under harmonic loading. They observed bifurcations, chaos and strange attractors due to the presence of nonlinearity in springs and dampers in vibration isolators. They concluded that a strictly dissipative nonlinear damping may be used as a passive control strategy to suppress various instabilities occurring in nonlinear vibration isolation systems. The major objective of this chapter is to ascertain the effect of nonlinear damping on the response of shock isolators.

Various analytical methods are available in the literature [18-32] for transient analysis of nonlinear systems, namely, Linearization method [19], Ultraspherical polynomial method [20-22], and Lighthill's extension of Poincare's perturbation method [23]. In this chapter, a simple straightforward perturbation method along with Laplace transform is used. This method is applicable for any order of nonlinearity, both in the restoring and damping forces, expressed in the form of polynomials. A cubic nonlinearity in the restoring force is assumed, whereas various forms of nonlinearities so far as the damping force is concerned have been included. For example, a cubic type nonlinearity over and above the common linear viscous damping, as exhibited by fluid-dampers at high velocities has been given special attention. Numerical results are included for a typical elastomeric damper which can be modelled up to a certain amplitude of deformation, by a combination of linear viscous damping and a dissipative quadratic damping with a negative coefficient[75].

Three types of base excitations, namely, the rounded step, the rounded pulse and the oscillatory step given in reference [5] are considered. Analytical results obtained by the present method are compared with those obtained by direct numerical integration. For the quadratic damping case, results are obtained by numerical integration alone since the symmetric dissipative quadratic damping can not be expressed in polynomial form. The effects of nonlinear damping on the response of various models of shock isolators are discussed in detail.

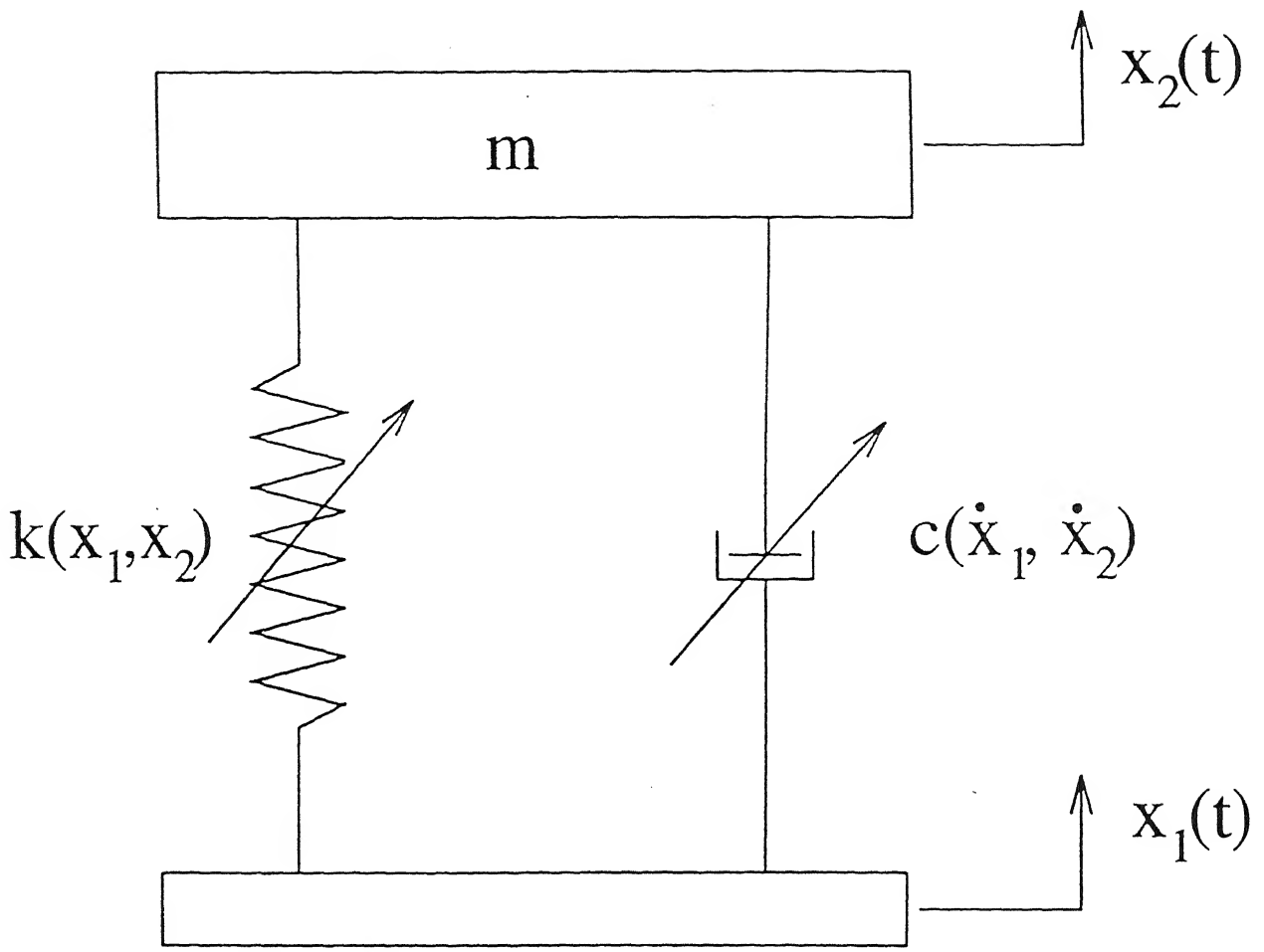

Figure 2.1: Non-linear base excited system

2.2 Equations of Motion

A single degree-of-freedom (SDOF) shock isolator system is shown in Figure 2.1, where the base is subjected to a shock displacement. The spring and the damper elements of the isolator are taken to be nonlinear with a cubic nonlinearity superimposed on a linear term. The equation of motion for the mass m, to be isolated, is

$$m\ddot{x}_2 + c_0(\dot{x}_2 - \dot{x}_1) + c_1(\dot{x}_2 - \dot{x}_1)^3 + k_0(x_2 - x_1) + k_1(x_2 - x_1)^3 = 0 \qquad (2.1)$$

where x_1 and x_2 are the absolute displacements of the base and the mass m, respectively, and the dots denote derivatives with respect to time t, k_0 and k_1 are linear and nonlinear stiffness constants, and c_0 and c_1 are linear and nonlinear damping coefficients. The initial conditions on x_2 are taken to be zero, i.e., $x_2 = \dot{x}_2 = 0$ at $t = 0$. This equation is written in the non-dimensional form as

$$\Delta'' + 2\zeta\Delta' + \delta^*(\Delta')^3 + \Delta + \epsilon^*\Delta^3 = f(T) \qquad (2.2)$$

where, $\Delta = (x_2 - x_1)/x_{1max}$ is the relative displacement, between the mass m and the base, non-dimensionalised with respect to the maximum base displacement x_{1max}, T is the non-dimensionalised time $T = \omega_0 t$, where $\omega_0 = \sqrt{\frac{k_0}{m}}$, is the linear natural frequency, the primes denote derivatives with respect to T, and the other non-dimensional parameters are

$$\zeta = \frac{c_0}{2m\omega_0}, \quad \delta^* = \frac{c_1\omega_0(x_{1max})^2}{m}, \quad \epsilon^* = \frac{k_1(x_{1max})^2}{k_0}, \quad \text{and}$$

$$f(T) = -\frac{x_1''}{x_{1max}}. \qquad (2.3)$$

2.3 Types of Input Displacements of The Base

Three different input displacements [4, 5] considered in this study are defined in the following section. These inputs are chosen to be physically realistic in that they describe

the translation of the foundation through a finite distance in a finite time with finite acceleration and deceleration. These inputs are defined by the following equations:

Case (a) Rounded displacement step:

This type of base excitation is shown in Figure 2.2 and is described as

$$\begin{aligned} x_1(t) &= 0 \qquad\qquad \text{when} \quad t < 0, \\ x_1(t) &= x_{1max}\left[1 - (1 + \gamma\omega_0 t)\, e^{(-\gamma\omega_0 t)}\right] \quad \text{for} \;\; t \geq 0 \end{aligned} \tag{2.4}$$

with γ as the severity parameter. The severity parameter (γ) describes the finite rise time, τ, of the step in terms of the half-period of natural vibration $T_p/2$ of the isolator system; thus

$$\gamma = T_p/(2\tau) = \pi/(\omega_0\tau). \tag{2.5}$$

The rise time τ of the rounded displacement step is defined as the time required for the displacement to reach 82% of its final value.

Case (b) Unidirectional rounded displacement pulse:

This type of pulse excitation is shown in Figure 2.3 and is described as

$$\begin{aligned} x_1(t) &= 0 \qquad\qquad \text{when} \quad t < 0, \\ x_1(t) &= x_{1max}(e^2/4)\,(\gamma\omega_0 t)^2\, e^{(-\gamma\omega_0 t)} \quad \text{for} \quad t \geq 0. \end{aligned} \tag{2.6}$$

Again, the severity parameter (γ) is defined by equation (2.5). Here, the duration τ of the displacement pulse is defined as the length of an equivalent rectangular pulse that has the same area ($\frac{x_{1max}e^2}{2\gamma\omega_0}$) as that of the rounded pulse, but with a height 17.6% higher than x_{1max}.

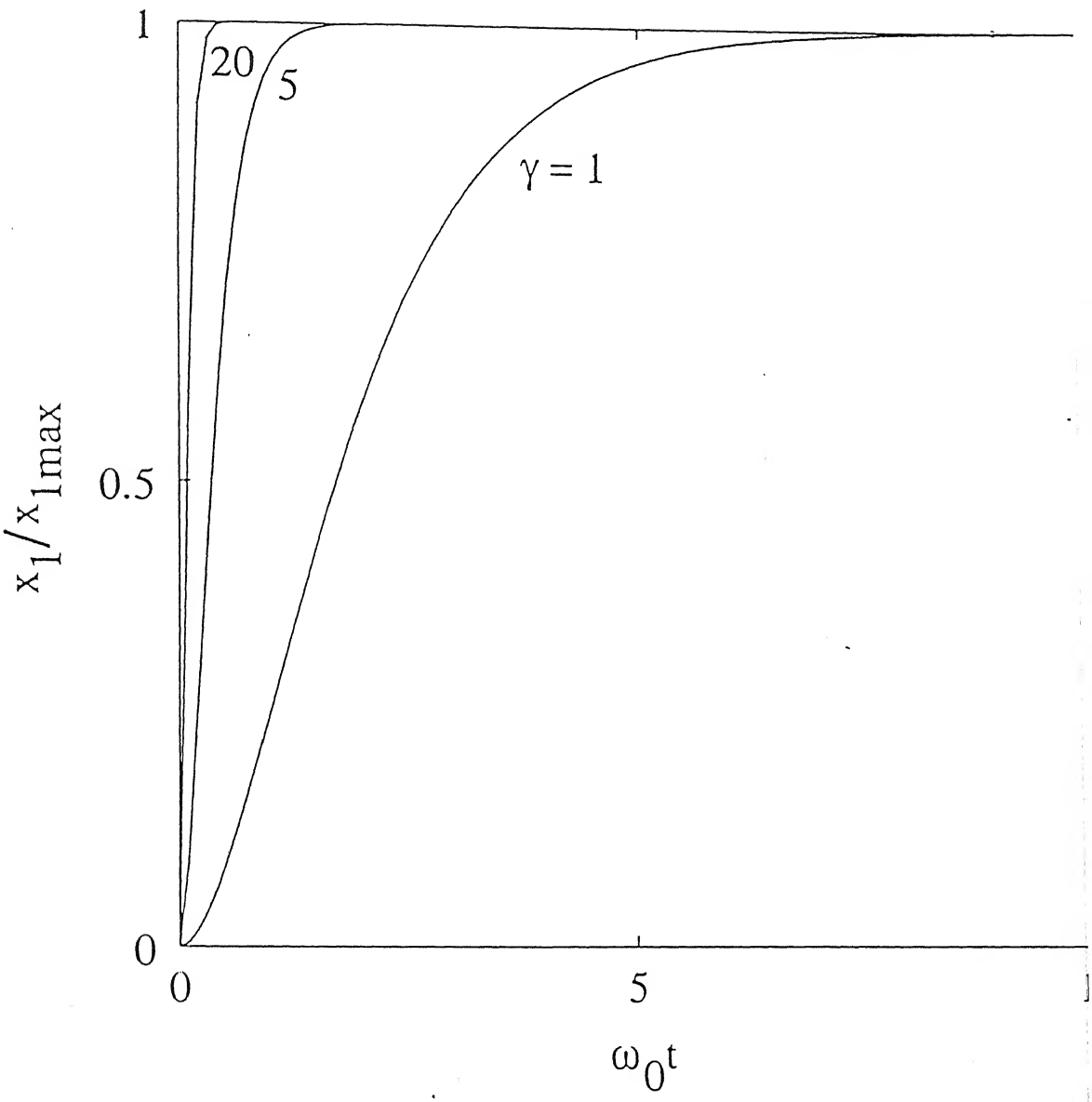

Figure 2.2: The rounded step displacement.

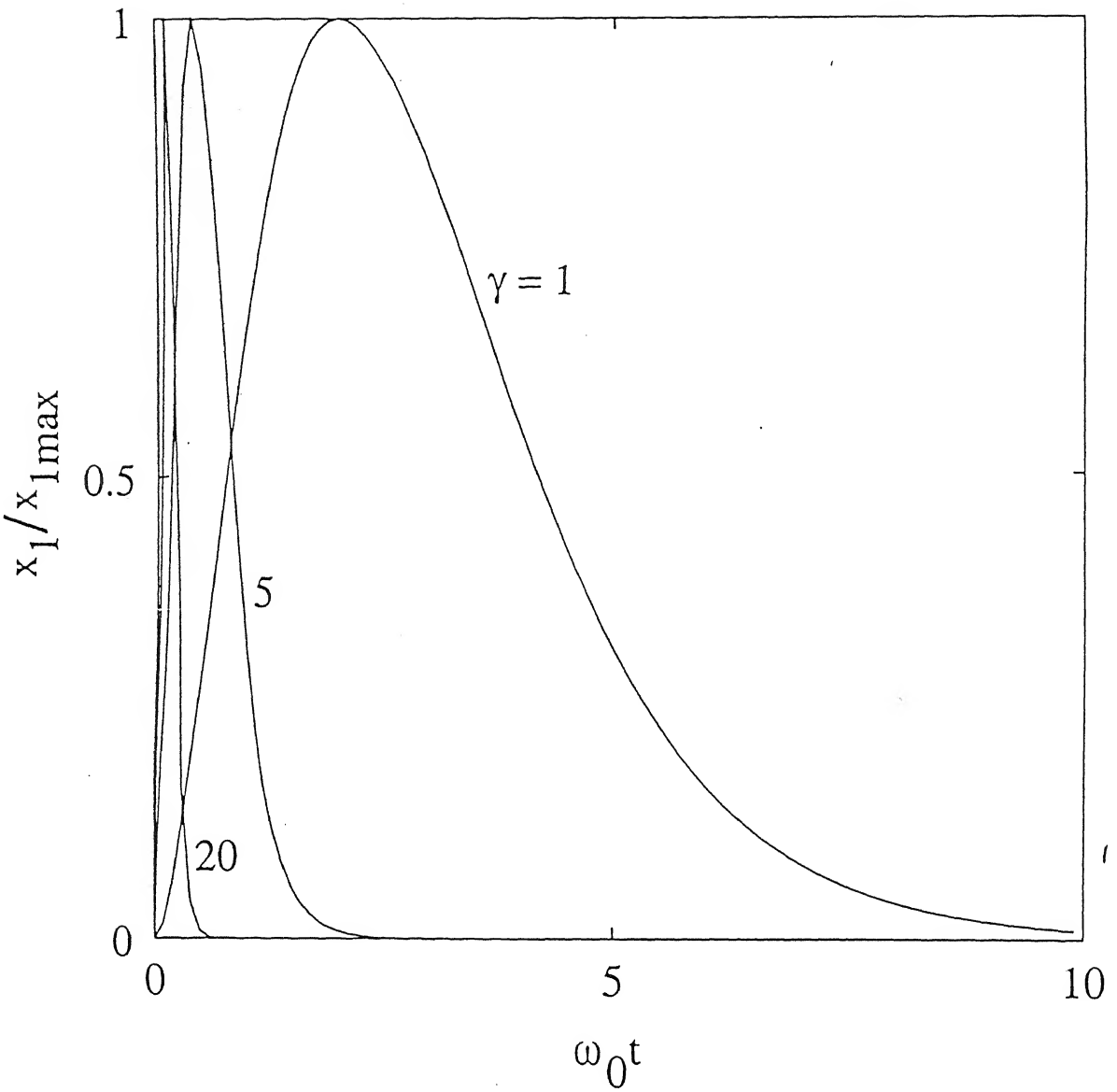

Figure 2.3: The rounded pulse displacement.

Case (c) Oscillatory displacement step:

This type of base excitation is shown in Figure 2.4 and is described as

$$\begin{aligned} x_1(t) &= 0 \qquad\qquad \text{when} \quad t < 0, \\ x_1(t) &= x_{1max}(0.68684)\left[1 - \{\cos(\gamma\omega_0 t) + 0.25\sin(\gamma\omega_0 t)\}e^{(-0.25\gamma\omega_0 t)}\right] \qquad (2.7) \\ &\qquad\qquad\qquad\qquad\qquad\qquad\qquad\qquad\qquad\qquad \text{for } t \geq 0. \end{aligned}$$

Once again, the severity parameter (γ) is defined by equation (2.5), but here, the rise time τ of the oscillatory displacement step is exactly the time required for the displacement to reach its maximum value x_{1max}.

The method of selecting the input displacement by equation (2.7) is explained in reference [5]. For the sake of completeness, the method is presented below. This input represents the character of an abrupt transient disturbance after it had passed through and had been 'filtered' by the foundation structure that supports the mounting system under consideration.

The base of an SDOF system is subjected to a step displacement $x(t) = x_0$, the resultant displacement x_1 of the system mass is given in reference [4] by the equation

$$x_1 = x_0[1 + e^{(-\zeta_F\omega_F t)}\{(\zeta_F\omega_F/\omega_d)\sin(\omega_d t) - \cos(\omega_d t)\}] \qquad (2.8)$$

where ω_F is the natural frequency of the filtered system, ζ_F is its damping ratio, and $\omega_d = \omega_F\sqrt{1-\zeta_F^2}$.

This input displacement x_1 in equation (2.8) is not physically realistic because its velocity is discontinuous and its acceleration is infinite at the time origin. However, if the sine term in equation (2.8) is reversed in sign, then velocity is zero and acceleration remains finite at the time origin. Further, for all but large values of ζ_F, the equation may be simplified as follows:

$$x_1 = x_0[1 - e^{(-\zeta_F\omega_F t)}\{(\zeta_F)\sin(\omega_F t) + \cos(\omega_F t)\}]. \qquad (2.9)$$

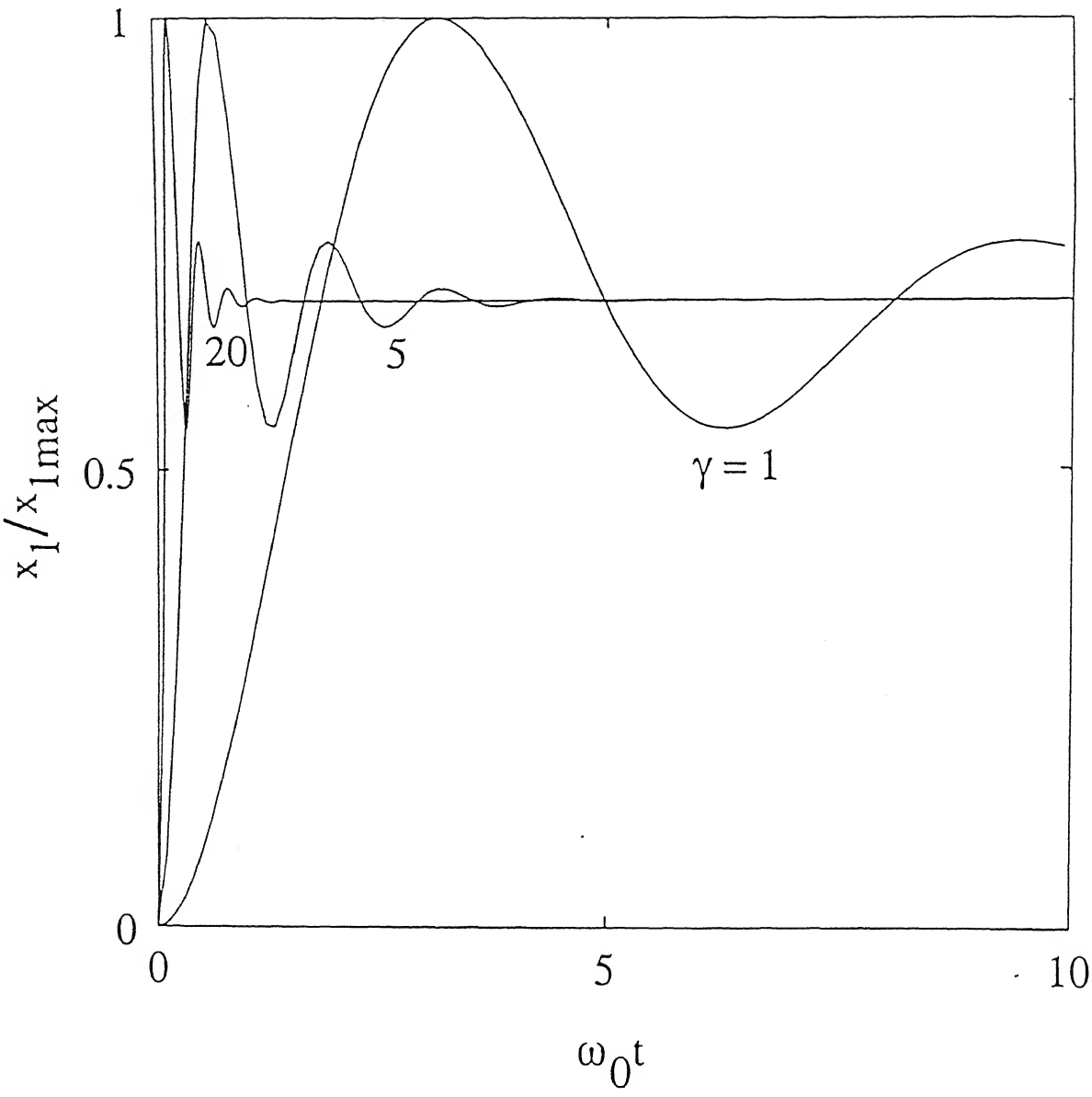

Figure 2.4: The oscillatory displacement step.

This displacement takes a maximum value

$$x_{1max} = x_0[1 + e^{(-\zeta_F \pi)}] \tag{2.10}$$

when

$$\omega_F t = \pi \tag{2.11}$$

this equation directly specifies the rise time of the step. Consequently, from equation (2.5) it is possible to write that

$$\gamma = \frac{\pi}{\omega_0 \pi / \omega_F} = \omega_F / \omega_0 \tag{2.12}$$

and, from equation (2.9) one can write

$$x_1 = x_{1max}[1 - e^{(-\zeta_F \gamma \omega_0 t)}\{\zeta_F \sin(\gamma \omega_0 t) + \cos(\gamma \omega_0 t)\}]/[1 + e^{(-\zeta_F \pi)}]. \tag{2.13}$$

The oscillatory displacement step of equation (2.7) is obtained by substituting $\zeta_f = 0.25$ in equation (2.13).

The maximum values attained by the velocity and acceleration of the above three input displacements of equations (2.4), (2.6) and (2.7) are listed here, because these values will be referred in subsequent chapters when the various performance indices of shock isolators are evaluated.

For rounded step

$$\dot{x}_{1max} = 0.36788 \gamma \omega_0 x_{1max}, \tag{2.14}$$

$$\ddot{x}_{1max} = \gamma^2 \omega_0^2 x_{1max}, \tag{2.15}$$

for rounded pulse

$$\dot{x}_{1max} = 0.85188 \gamma \omega_0 x_{1max}, \tag{2.16}$$

$$\ddot{x}_{1max} = 3.69453 \gamma^2 \omega_0^2 x_{1max} \tag{2.17}$$

and for oscillatory step

$$\dot{x}_{1max} = 0.50825\gamma\omega_0 x_{1max}, \tag{2.18}$$

$$\ddot{x}_{1max} = 0.72977\gamma^2\omega_0^2 x_{1max}. \tag{2.19}$$

2.4 Closed Form Solutions

It is desirable to have an analytical solution of equation (2.2). This would facilitate calculating transients at any given instant directly from the closed form solution rather than integrating numerically equation (2.2) from $T = 0$. To this end, perturbation method [23-32] has been used to separate the terms of the same order and then the solutions of differential equations are obtained through Laplace transformation.

The parameters δ^* and ϵ^* in equation (2.2) are taken to be small and of the same order, so that equation (2.2) can be rewritten as

$$\Delta'' + 2\zeta\Delta' + \Delta + \epsilon[\delta_1(\Delta')^3 + \epsilon_1\Delta^3] = f(T) \tag{2.20}$$

where $\epsilon \ll 1$.

The form of equation (2.20) is useful in that, by putting ϵ_1 and δ_1 equal to zero or one, the effect of nonlinearity, in only stiffness or in only damping or in both stiffness and damping, can be studied. The solution of equation (2.20) is perturbed in small parameter $\epsilon(\ll 1)$ as

$$\Delta(T) = \sum_{i=0}^{\infty} \epsilon^i \Delta_i(T). \tag{2.21}$$

Substitution of equation (2.21) in equation (2.20) and collection of like power terms of ϵ yields

$$\Delta_0'' + 2\zeta\Delta_0' + \Delta_0 = f(T) \quad \text{for} \quad i = 0 \tag{2.22}$$

and

$$\Delta_i'' + 2\zeta\Delta_i' + \Delta_i = -\epsilon_1 \left[\sum_{j=0}^{i-1}\sum_{n=0}^{j} \Delta_{i-j-1}\Delta_{j-n}\Delta_n\right] - \delta_1 \left[\sum_{j=0}^{i-1}\sum_{n=0}^{j} \Delta'_{i-j-1}\Delta'_{j-n}\Delta'_n\right] \quad (2.23)$$

for $i \geq 1$,

with $\Delta_i = \Delta_i' = 0$ at $T = 0 \ \forall \ i > 0$.

Convergence

The series in equation (2.21) is a Cauchy product of $\sum_{i=0}^{\infty} \epsilon^i$ and $\sum_{i=0}^{\infty} \Delta_i(T)$. For $\epsilon \ll 1$, $\sum_{i=0}^{\infty} \epsilon^i$ is a convergent geometric series and $\sum_{i=0}^{\infty} \Delta_i(T)$ is bounded for $\zeta > 0, \gamma > 0$ since the solution of equations (2.22) and (2.23) contain exponential terms with negative indices, which are bounded. Therefore, the series $\sum_{i=0}^{\infty} \epsilon^i \Delta_i(T)$ is convergent [76]. It is to be noted here that the damping term is retained in equation (2.22) in order to avoid secular terms and thereby ensuring bounded solutions [25].

The focus here is on transients alone and that too over a short time duration. It was observed that the three term solution of equation (2.20) (i.e., up to $i = 2$, in equation (2.21)) give good convergence. Hence the solution of equation (2.20) are given below up to second order (i.e., $i = 2$ in equation (2.21)) only.

2.4.1 Zeroth Order Solution

With the initial conditions $\Delta = \Delta' = 0$ at $T = 0$, the solutions of equation (2.22), for the three input functions in equations (2.4),(2.6) and (2.7), are obtained using Laplace transformation and are listed below:

Case (a) Rounded displacement step:

Substitution of equation(2.4) in equation (2.3) yields

$$f(T) = -\gamma^2 (1 - \gamma T) e^{(-\gamma T)} \quad \text{for} \quad T \geq 0. \tag{2.24}$$

The equation (2.24) may be rewritten as

$$f(T) = e^{aT} \left(\sum_{m=0}^{N} A_m T^m \right) e^{(-\gamma T)} \quad \text{for} \quad T \geq 0 \tag{2.25}$$

where, $a = -\gamma, N = 1, A_0 = -\gamma^2, A_1 = \gamma^3$.

The solution of equation (2.22) for $f(T)$ given in equation (2.25) is obtained by using the formulae listed in Case (i) of Appendix A. Therefore, the zeroth order solution may be written as

$$\Delta_0(T) = \Delta_{01}(T) + \Delta_{02}(T) \tag{2.26}$$

where,

$$\Delta_{01}(T) = e^{(-\zeta T)}[P_1 \cos(\beta T) + Q_1 \sin(\beta T)]/\beta; \tag{2.27}$$

$$\Delta_{02}(T) = e^{(aT)}\left[B_1 + B_2 T\right]; \tag{2.28}$$

$$\beta = \sqrt{(1 - \zeta^2)}; \tag{2.29}$$

$$Q_1 + iP_1 = \frac{A_1 + A_0(\alpha - a)}{(\alpha - a)^2}; \tag{2.30}$$

$$\alpha = -\zeta + i\beta; \tag{2.31}$$

$$i = \sqrt{(-1)}; \tag{2.32}$$

$$B_1 = \left[A_0 - 2(\zeta - \gamma)B_2\right]/\Gamma; \tag{2.33}$$

$$B_2 = A_1/\Gamma; \tag{2.34}$$

$$\Gamma = \gamma^2 - 2\gamma\zeta + 1. \tag{2.35}$$

Case (b) Unidirectional rounded displacement pulse:

By substituting equation(2.6) in equation (2.3), $f(T)$ is obtained as

$$f(T) = -(e^2\gamma^2/4)\left(2 - 4\gamma T + \gamma^2 T^2\right) e^{(-\gamma T)} \quad \text{for} \quad T \geq 0. \tag{2.36}$$

The equation (2.36) may be rewritten succinctly as

$$f(T) = e^{aT}\left(\sum_{m=0}^{N} A_m T^m\right) e^{(-\gamma T)} \quad \text{for} \quad T \geq 0 \tag{2.37}$$

where, $a = -\gamma, N = 2, A_0 = -e^2\gamma^2/2, A_1 = e^2\gamma^3, A_2 = -e^2\gamma^4/4.$

The solution of equation (2.22) for $f(T)$ given in equation (2.37) is obtained by using again the formulae listed in Case (i) of Appendix A. Therefore, the zeroth order solution may be written as

$$\Delta_0(T) = \Delta_{01}(T) + \Delta_{02}(T) \tag{2.38}$$

where,

$$\Delta_{01}(T) = e^{(-\zeta T)}[P_1\cos(\beta T) + Q_1\sin(\beta T)]/\beta; \tag{2.39}$$

$$\Delta_{02}(T) = e^{(aT)}\left[B_1 + B_2 T + B_3 T^2/2\right]; \tag{2.40}$$

$$\beta = \sqrt{(1-\zeta^2)}; \tag{2.41}$$

$$Q_1 + iP_1 = \frac{2A_2 + A_1(\alpha - a) + A_0(\alpha - a)^2}{(\alpha - a)^3}; \tag{2.42}$$

$$\alpha = -\zeta + i\beta; \tag{2.43}$$

$$i = \sqrt{(-1)}; \tag{2.44}$$

$$B_1 = [A_0 - 2(\zeta - \gamma)B_2 - B_3]/\Gamma; \tag{2.45}$$

$$B_2 = [A_1 - 2(\zeta - \gamma)B_3]/\Gamma; \tag{2.46}$$

$$B_3 = A_2/\Gamma; \tag{2.47}$$

$$\Gamma = \gamma^2 - 2\gamma\zeta + 1. \tag{2.48}$$

Case (c) Oscillatory displacement step:

Substitution of equation(2.7) in equation (2.3) yields

$$f(T) = -(17/16)(0.68684)\gamma^2[\cos(\gamma T) - 0.25\sin(\gamma T)]e^{(-0.25\gamma T)} \tag{2.49}$$

for $T \geq 0$.

The solution of equation (2.22) for $f(T)$ given in equation (2.49) is obtained by using the formulae listed in Case (ii) of Appendix A. Therefore, the zeroth order solution may be written as

$$\Delta_0(T) = \Delta_{01}(T) + \Delta_{02}(T) \tag{2.50}$$

where,
$$\Delta_{01}(T) = e^{(-\zeta T)}[P_2\cos(\beta T) + Q_2\sin(\beta T)]/\beta; \tag{2.51}$$

and
$$\Delta_{02}(T) = e^{(aT)}[R_1\cos(\omega_1 T) + S_1\sin(\omega_1 T)]; \tag{2.52}$$

$$\beta = \sqrt{(1-\zeta^2)}; \tag{2.53}$$

$$\alpha = -\zeta + i\beta; \tag{2.54}$$

$$i = \sqrt{(-1)}; \tag{2.55}$$

$$Q_2 + iP_2 = \frac{C_1(\alpha - a) + D_1\omega_1}{(\alpha - a)^2 + \omega_1^2} \tag{2.56}$$

$$\alpha_1 = a + i\omega_1; \tag{2.57}$$

$$S_1 + iR_1 = \frac{D_1 + iC_1}{\alpha_1^2 + 2\zeta\alpha_1 + 1}. \tag{2.58}$$

$$C_1 = -(17/16)(0.68684)\gamma^2; \tag{2.59}$$

$$D_1 = (17/16)(0.68684)\gamma^2/4; \tag{2.60}$$

$$a = -\gamma/4; \tag{2.61}$$

$$\omega_1 = -\gamma/4. \tag{2.62}$$

2.4.2 First Order Solution

For $i = 1$, equation (2.23) yields

$$\Delta_1'' + 2\zeta\Delta_1' + \Delta_1 = -\left[\epsilon_1(\Delta_0)^3 + \delta_1(\Delta_0')^3\right]. \tag{2.63}$$

Case(a) Rounded displacement step:

From equation (2.26), the non-homogeneous term Δ_0^3 in equation (2.63) may be expressed as

$$\Delta_0^3(T) = \Delta_{01}^3(T) + \Delta_{02}^3(T) + 3\Delta_{01}^2(T)\Delta_{02}(T) + 3\Delta_{01}(T)\Delta_{02}^2(T). \tag{2.64}$$

From equation (2.27), $\Delta_{01}^3(T)$ in equation (2.64) may be written concisely as

$$\Delta_{01}^3(T) = e^{a_1 T}\left[\sum_{m=1}^{N}\{C_m\cos(\omega_m T) + D_m\sin(\omega_m T)\}\right] \tag{2.65}$$

where, $a_1 = -3\zeta$; $\omega_1 = \beta$; $\omega_2 = 3\beta$; $N = 2$; $C_1 = 3P_1(P_1^2 + Q_1^2)/4\beta^3$;
$D_1 = 3Q_1(P_1^2 + Q_1^2)/4\beta^3$; $C_2 = P_1(P_1^2 - 3Q_1^2)/4\beta^3$; and $D_2 = -Q_1(Q_1^2 - 3P_1^2)/4\beta^3$.

From equation (2.28), the second term in the right-hand-side of equation (2.64) may be written in simplified form as

$$\Delta_{02}^3(T) = e^{a_2 T}\left[\sum_{m=1}^{N} A_m T^m\right] \tag{2.66}$$

where, $a_2 = -3\gamma$; $N = 3$; $A_0 = B_1^3$; $A_1 = 3B_1^2B_2$; $A_2 = 3B_1B_2^2$ and $A_3 = B_2^3$.

From equations (2.27) and (2.28), the third and the fourth terms in the right-hand-side of equation (2.64) are expressed in succinct form as

$$3\Delta_{01}^2\Delta_{02} = e^{a_3 T}\left[C + E\cos(\Omega T) + F\sin(\Omega T)\right]\left[\sum_{m=0}^{N} A_m T^m\right] \tag{2.67}$$

where, $a_3 = -(2\zeta + \gamma)$; $C = (P_1^2 + Q_1^2)/2$; $E = (P_1^2 - Q_1^2)/2$; $F = P_1Q_1$;
$\Omega = 2\beta$; $N = 1$; $A_0 = 3CB_1/\beta^2$ and $A_1 = 3CB_2/\beta^2$

and

$$3\Delta_{01}\Delta_{02}^2 = e^{a_4 T}\left[E\cos(\Omega T) + F\sin(\Omega T)\right]\left[\sum_{m=0}^{N} A_m T^m\right] \tag{2.68}$$

where, $a_4 = -(\zeta+2\gamma); E = P_1; F = Q_1; \Omega = \beta; N = 2; A_0 = B_1^2; A_1 = 2B_1B_2$ and $A_2 = B_2^2$.

The sum of the all four terms in the right-hand-side of equation (2.64) can be expressed as the sum of the following three generalized functions with appropriate values of coefficients and indices

$$e^{aT}\left[\sum_{m=0}^{N} A_m T^m\right], \tag{2.69}$$

$$e^{aT}\left[\sum_{m=0}^{N}\{C_m\cos(\omega_m T) + D_m\sin(\omega_m T)\}\right] \tag{2.70}$$

and

$$e^{aT}\left[E\cos(\Omega T) + F\sin(\Omega T)\right]\left[\sum_{m=0}^{N} A_m T^m\right]. \tag{2.71}$$

Similarly, the second non-homogeneous term in equation(2.63) can also be expressed as the summation of three generalized functions given by equations (2.69), (2.70) and (2.71).

The solution of equation (2.63) is obtained by using the formulae listed in Appendix A cases (i), (ii) and (iii), corresponding to the terms in equations (2.69), (2.70) and (2.71) respectively.

Case(b) Unidirectional rounded displacement pulse:

In this case also, the non-homogeneous term in equation (2.63) can be expressed as the summation of the three generalized functions given by equations (2.69), (2.70) and (2.71). Again the solution of equation (2.63) is obtained by using the formulae listed in Appendix A.

Case(c) Oscillatory displacement step:

In this case, the non-homogeneous term in equation (2.63) can be expressed as the generalized function given by equation (2.70). The solution of equation (2.63) is obtained by using the formulae listed in case(ii) of Appendix A.

2.4.3 Second Order Solution

For $i = 2$, equation (2.23) yields

$$\Delta_2'' + 2\zeta\Delta_2' + \Delta_2 = -3\left[\epsilon_1(\Delta_0)^2\Delta_1 + \delta_1(\Delta_0')^2\Delta_1'\right]. \tag{2.72}$$

Cases (a) and (b): In these two cases, the non-homogeneous term in the equation (2.72) can be expressed as the summation of three generalized functions given in equations (2.69), (2.70) and (2.71). Once again, the solutions of equation (2.72) are obtained by using the formulae given in Appendix A.

Case (c): In this case, the non-homogeneous term in the equation (2.72) again turns out to be only the second generalized function given by equation (2.70). The solution of equation (2.72) is obtained by using the formulae listed in case(ii) of Appendix A.

2.5 Results and Discussions

The results are presented in two parts: the first one to validate the accuracy of the closed form solutions and the second part to highlight the effects of nonlinearity in isolator elements. The linear damping ratio ζ is taken to be 0.1 in all the results.

2.5.1 Validation of Closed Form Solutions

The closed form solutions of equation (2.2), obtained through Laplace transformation of equations (2.22) and (2.23), were checked against the numerically integrated solutions of equation (2.20). Numerical integration was carried out by using classical fourth order Runge-Kutta method. For classical fourth order Runge-Kutta method, 'rk4' routine in Numerical Recipes [78] has been used with a step siz of 0·001. These numerical results are compared with NAG routin with the same step size and tolerance 0·000001. It was observe that both routines generated the same numerical values.

First the nonlinearity in stiffness alone is considered by taking $\epsilon = 0.01$, $\epsilon_1 = 1$ and $\delta_1 = 0$ in equation (2.20). Figure 2.5 shows the comparative results for the three types of excitation, where curves (a), (b) and (c) correspond to three different excitations, described by equations (2.4), (2.6) and (2.7) respectively. It was observed that for the lower values of $\gamma < 20$ the effect of nonlinearity is not predominant both in the nonlinear damping and nonlinear stiffness cases, but for higher values of $\gamma > 20$ nonlinear damping effect is very high. So, the severity parameter of the shock displacement, γ, is taken to be equal to 20 for all these results. It is clear from these curves that even the zeroth order solutions given by equations (2.26), (2.38) and (2.50) are very close to the exact numerical solutions. This indicates that the effect of nonlinearity in stiffness of the isolator is negligible. The same behaviour was observed for a large range of the severity parameter γ up to 100.

The closed form solutions for isolator with nonlinearity in damping alone are presented for three types of base excitation in Figures 2.6, 2.7 and 2.8, with $\epsilon = 0.01, \epsilon_1 = 0, \delta_1 = 1$ and $\gamma = 20$. It is evident from these figures that the nonlinearity in damping does affect the response, especially for rounded pulse and oscillatory step inputs (Figures 2.7 and 2.8). Further, as more terms are included in equation(2.21), the result progressively converges to the numerically integrated solution. It is evident from Figures 2.6 and 2.7, that first order solution is good enough for case (a), but second order solution is needed for case (b) to match well with the numerical solution. Similar results were obtained over a large range of γ up to 100. On the other hand, for case(c) as seen from Figure 2.8 the two terms solution is still far away from the numerically integrated results. While varying γ for this case, it was observed that only when the value of γ is around 10 the closed form solution matched closely with the numerical solution. For a value of γ around 10 the effect of nonlinear damping is not very much pronounced. The closed form solution again does not yield good result if the severity

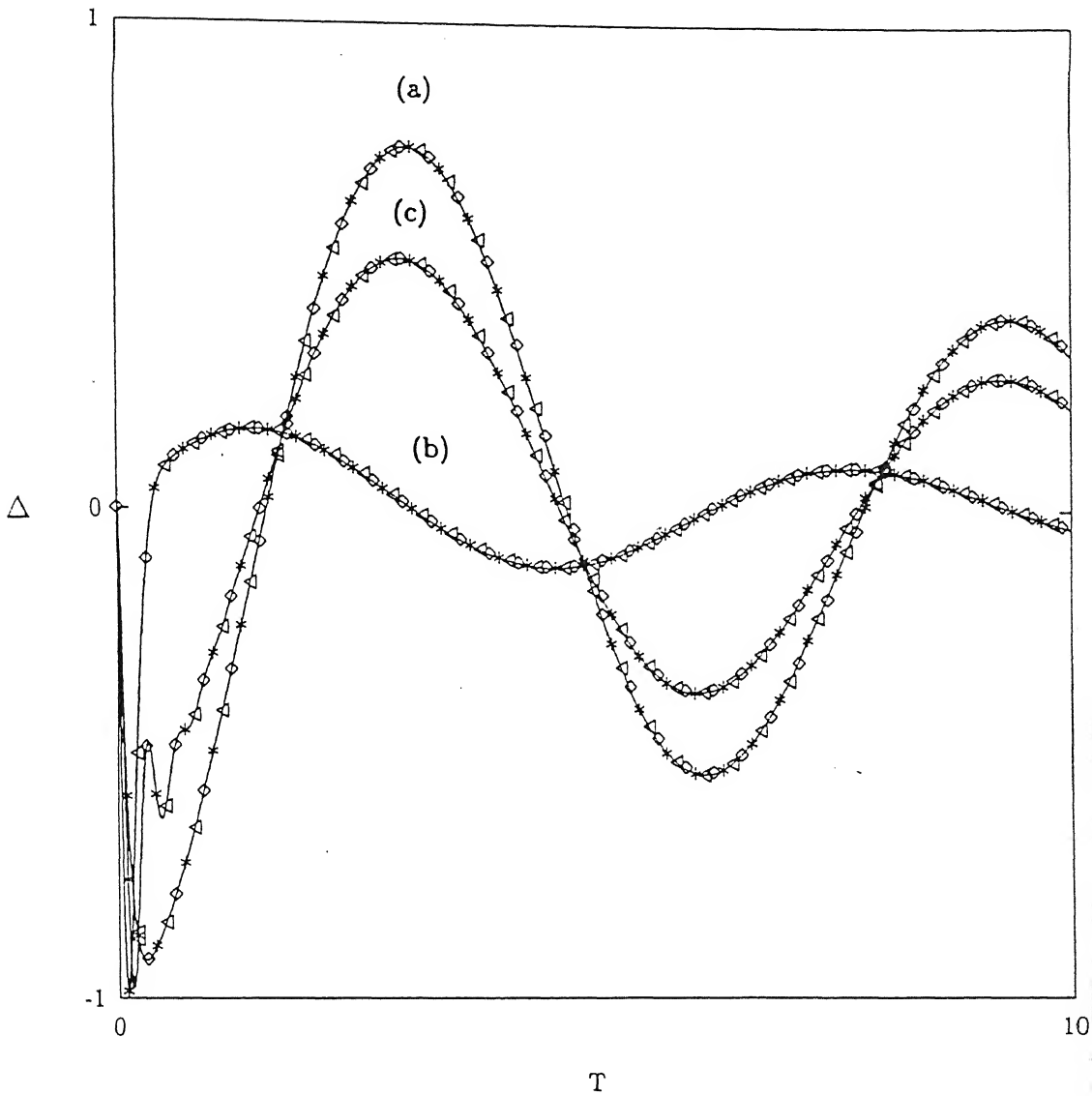

Figure 2.5: Comparison of analytical and numerical results for the cubic nonlinearity in stiffness only. $\zeta = 0.1, \gamma = 20, \epsilon = 0.01, \epsilon_1 = 1, \delta_1 = 0$. $\diamond$ zeroth order, $*$ first order, $\triangleright$ second order, —— numerical. Curve (a): the rounded step displacement; curve (b): the rounded pulse displacement; curve (c): the oscillatory displacement step.

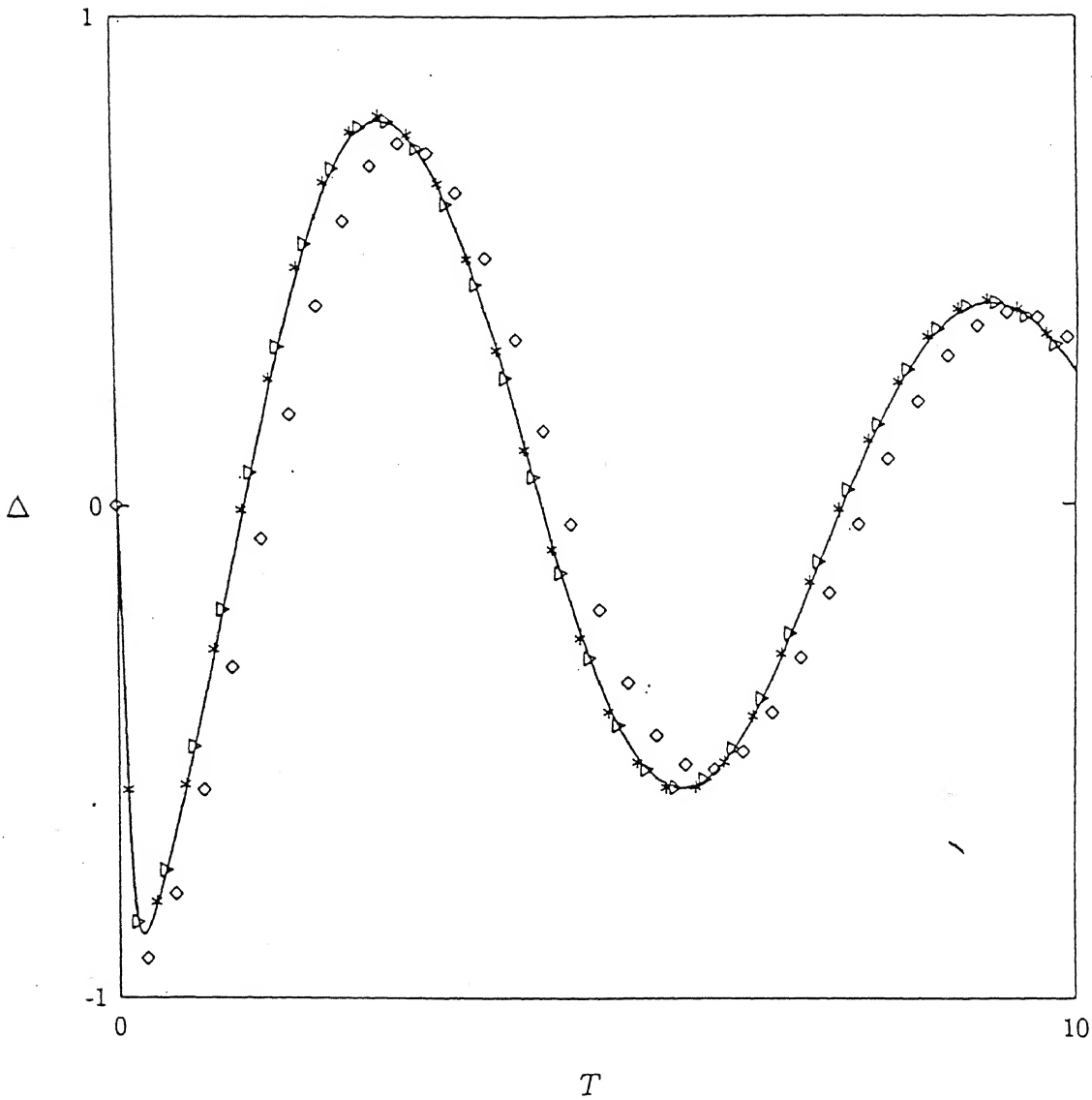

Figure 2.6: Comparison of analytical and numerical results for the cubic nonlinearity in damping only for the rounded step displacement. $\zeta = 0.1$, $\epsilon = 0.01$, $\epsilon_1 = 0$, $\delta_1 = 1$ $\gamma = 20$ $\diamond$ zeroth order, $*$ first order, $\triangleright$ second order, —— numerical.

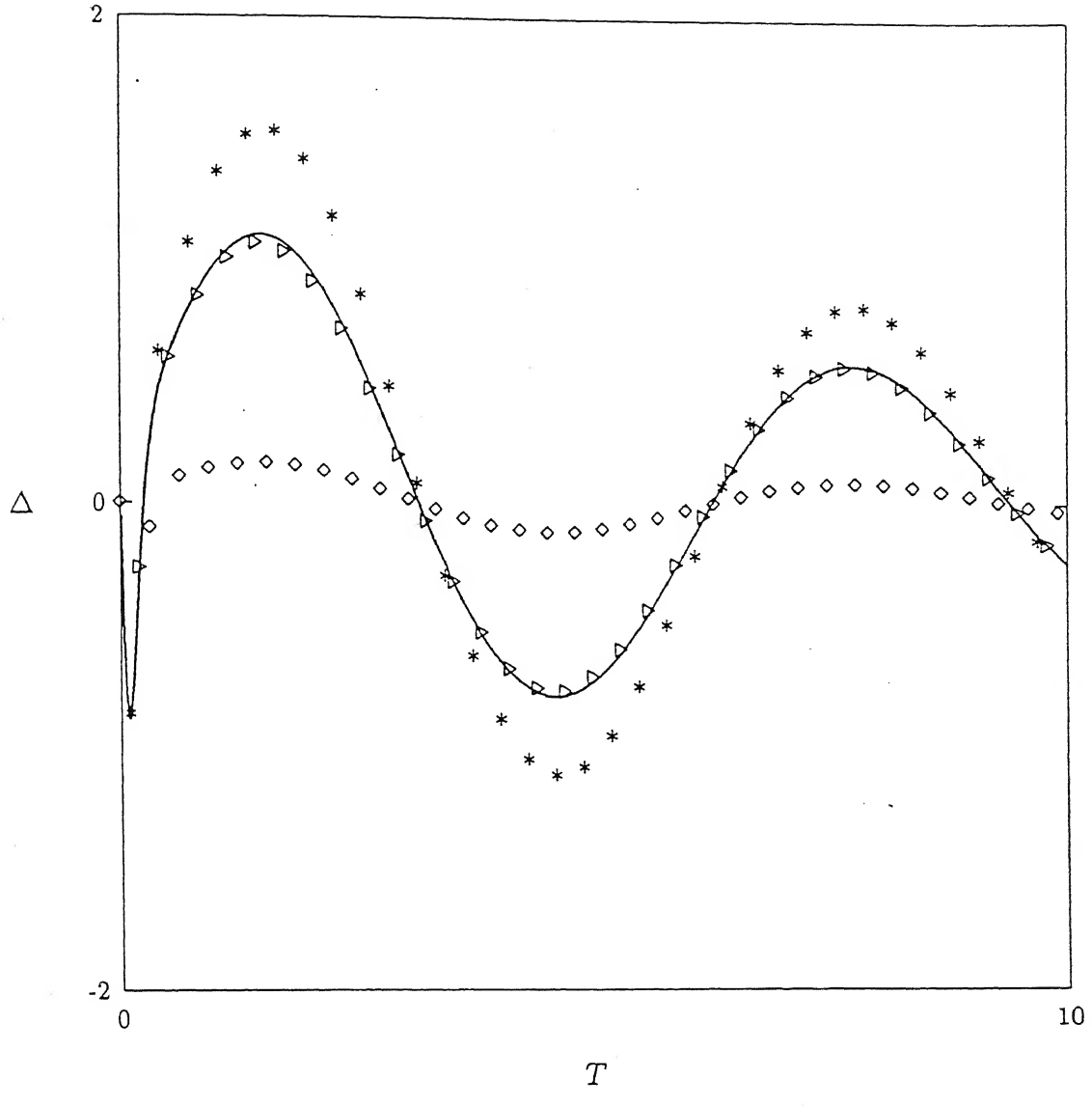

Figure 2.7: Comparison of analytical and numerical results for the cubic nonlinearity i
damping only for the rounded pulse displacement. $\zeta = 0.1$, $\epsilon = 0.01$, $\epsilon_1 = 0$, $\delta_1 =$
$\gamma = 20$ $\diamond$ zeroth order, $*$ first order, $\triangleright$ second order, —— numerical

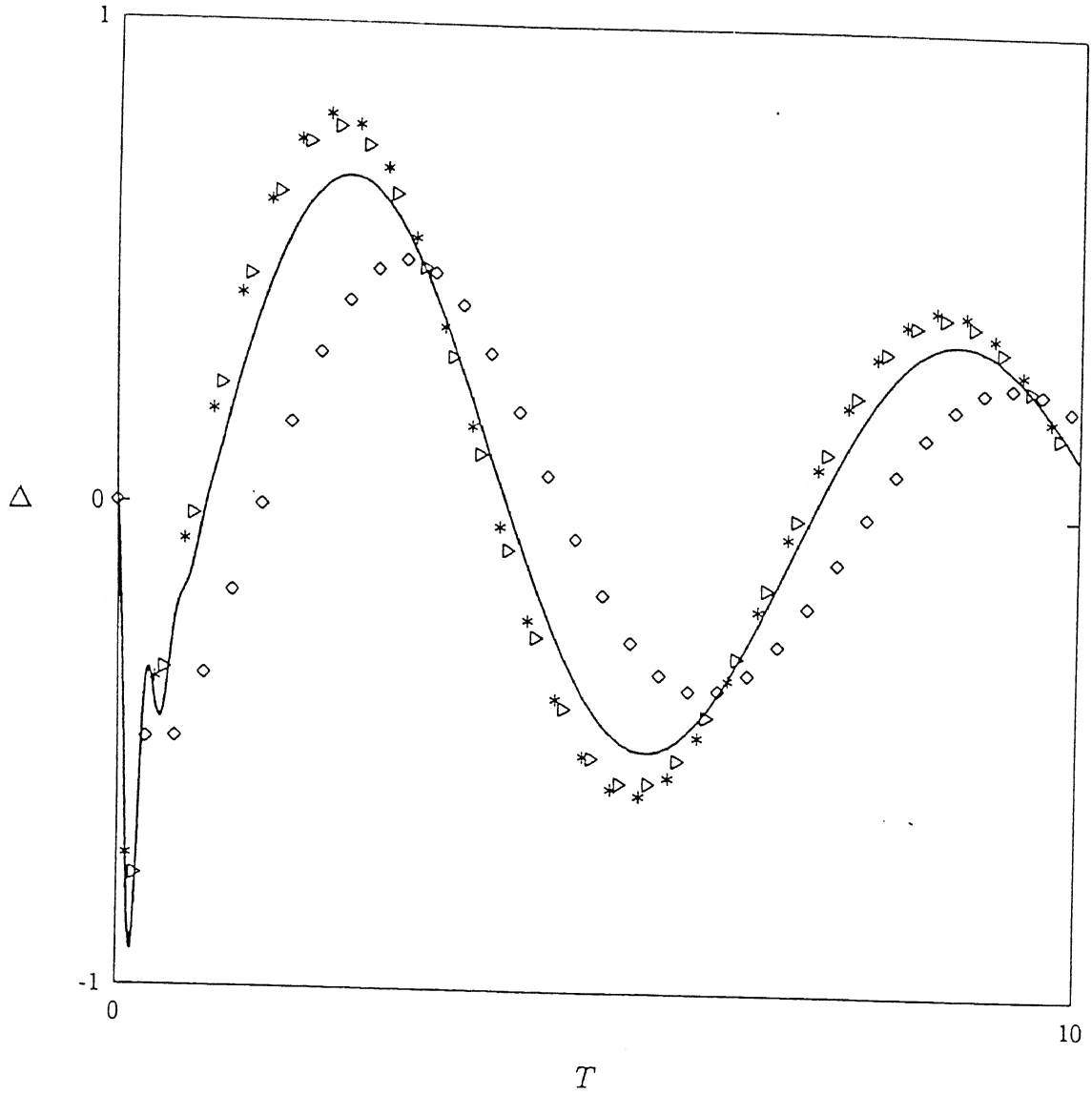

Figure 2.8: Comparison of analytical and numerical results for the cubic nonlinearity in damping only for the oscillatory displacement step. $\zeta = 0.1$, $\epsilon = 0.01$, $\epsilon_1 = 0$, $\delta_1 = 1$ $\gamma = 20$ $\diamond$ zeroth order, $*$ first order, $\triangleright$ second order, —— numerical.

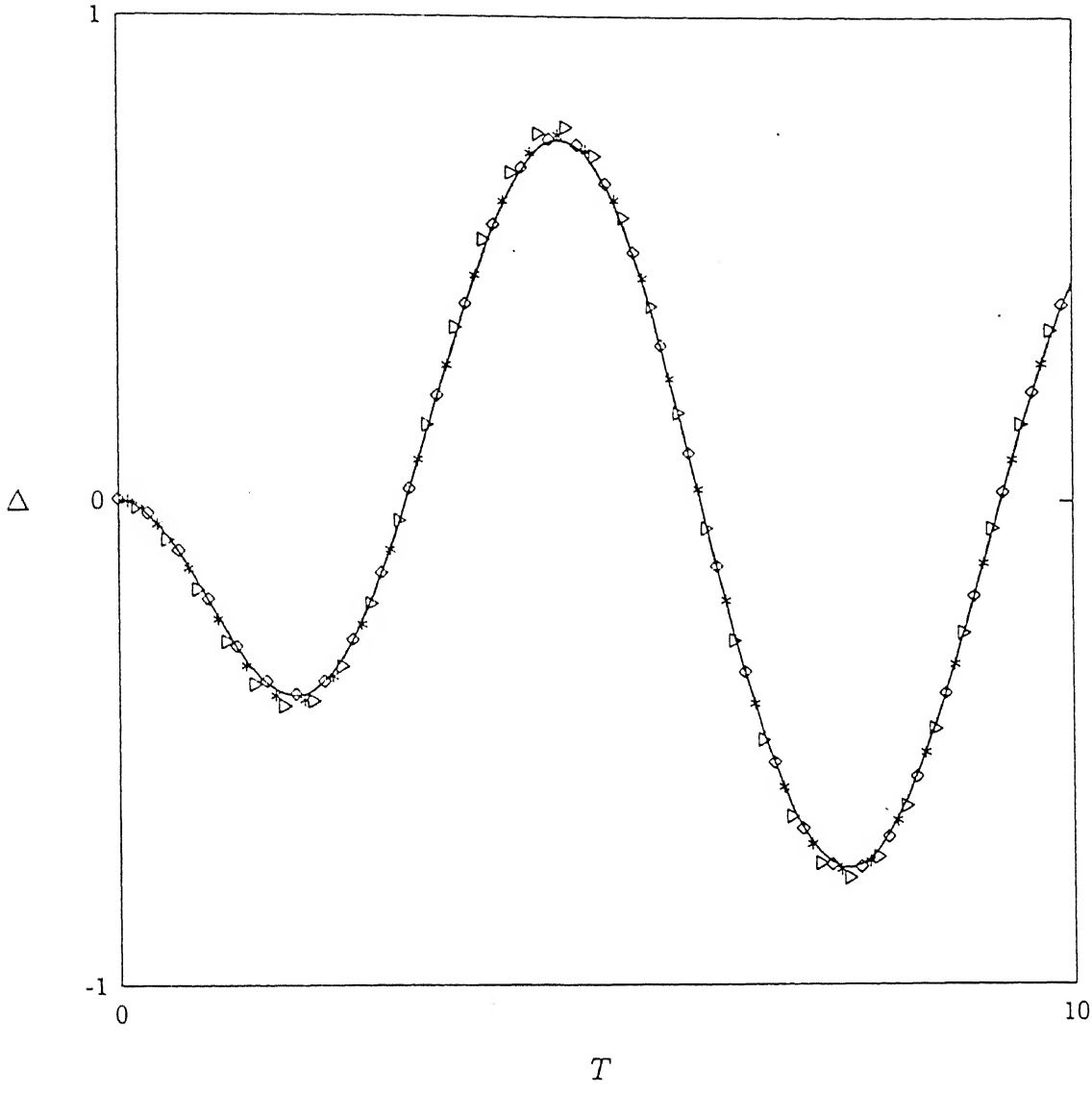

Figure 2.9: Comparison of analytical and numerical results for the cubic nonlinearity in damping only for the oscillatory displacement step. $\zeta = 0.1$, $\epsilon = 0.01$, $\epsilon_1 = 0$, $\delta_1 = 1$ $\gamma = 1$ $\diamond$ zeroth order, $*$ first order, $\triangleright$ second order, —— numerical.

parameter γ is around 1; in fact, as shown in Figure 2.9, the solution diverges as more number of terms are taken in the closed form solution. This is expected near $\gamma = 1$ with the oscillatory input (see equations (2.10) and (2.22)), because the oscillations in the input are at the linear natural frequency of the isolator which in turn gives rise to secular terms in the perturbed solutions (see equations (2.23), (2.30) and (2.34)).

2.5.2 Effect of Nonlinear Damping

The nonlinear damping term makes the isolator response differ appreciably from the response of a linearly damped isolator (e.g., see Figure 2.6). This difference increases as the severity parameter γ is increased. The effect of nonlinear damping on the response (relative displacement) to the rounded step input is highlighted in Figure 2.10.

These results for various values of δ^* have been obtained through numerical integration of equation (2.22) with $\epsilon^* = 0$. With increasing values of δ^*, the peak response values increase up to $\delta^* \approx 0.05$, thereafter an increase in δ^* reduces the peak value. However, the peak values are always higher for $\delta^* > 0$ than that for $\delta^* = 0$. Similar trends were also observed for other types of inputs, namely, inputs of cases (b) and (c). In fact this trend was also observed for any power-law damping forces with the exponent greater than one.

Other Performance Variables

The relative displacement of the mass is only one of the measures of the isolator performance and it is important when the rattle space is the design criteria. Other performance criteria of a shock isolator are indicated by the absolute displacement (x_2/x_{1max}), the relative velocity (Δ'), the absolute velocity (x_2'/x_{1max}) and acceleration (x_2''/x_{1max}) of the mass. The absolute displacement exhibits features similar to those

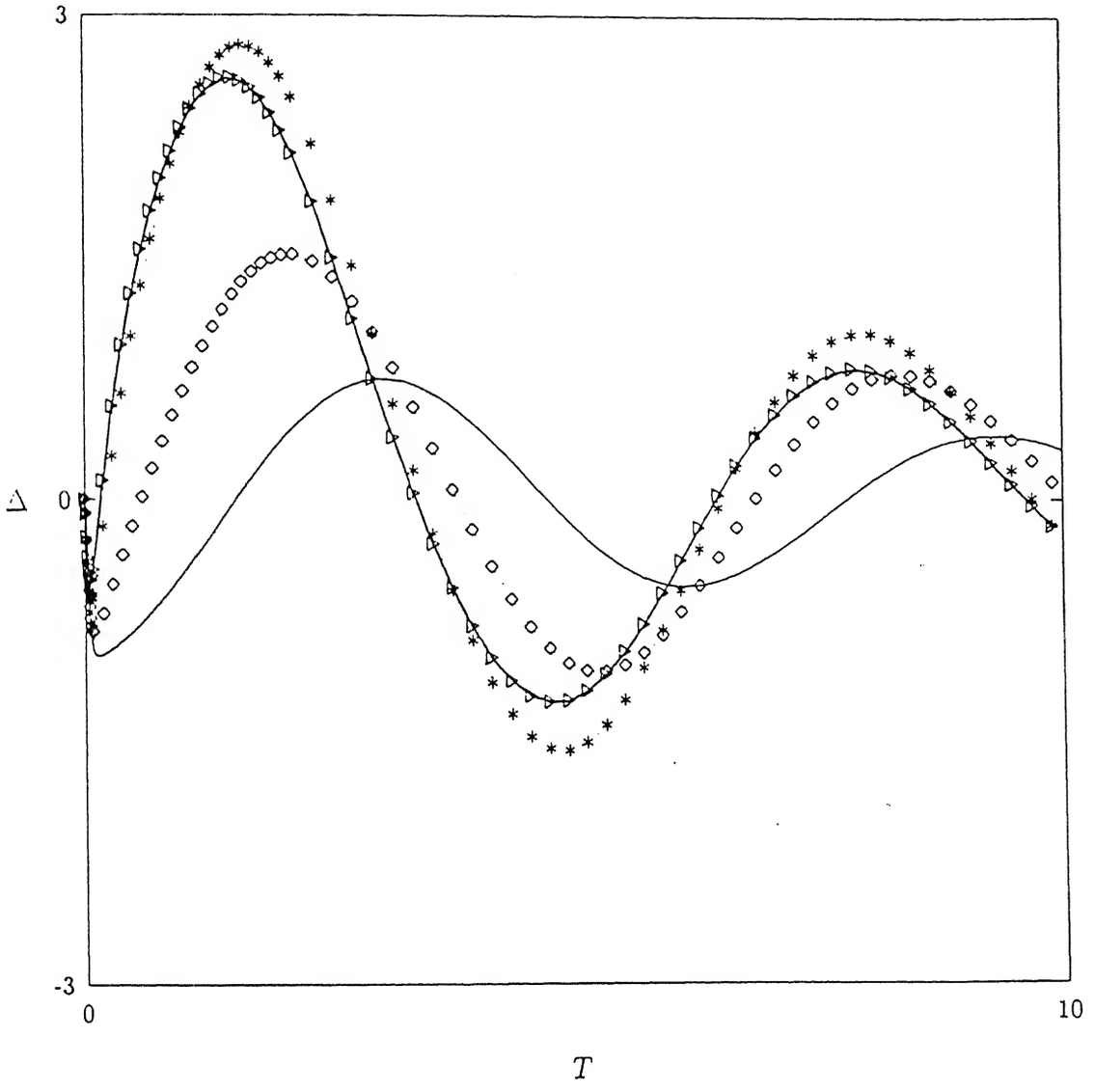

Figure 2.10: The effect of nonlinear cubic damping on the relative displacement for the rounded displacement step. $\gamma = 50$, $\zeta = 0.1$, $\epsilon^* = 0$. —— $\delta^* = 0$, $\diamond$ $\delta^* = 0.01$, $*$ $\delta^* = 0.05$, $\rightarrow$ $\delta^* = 0.1$

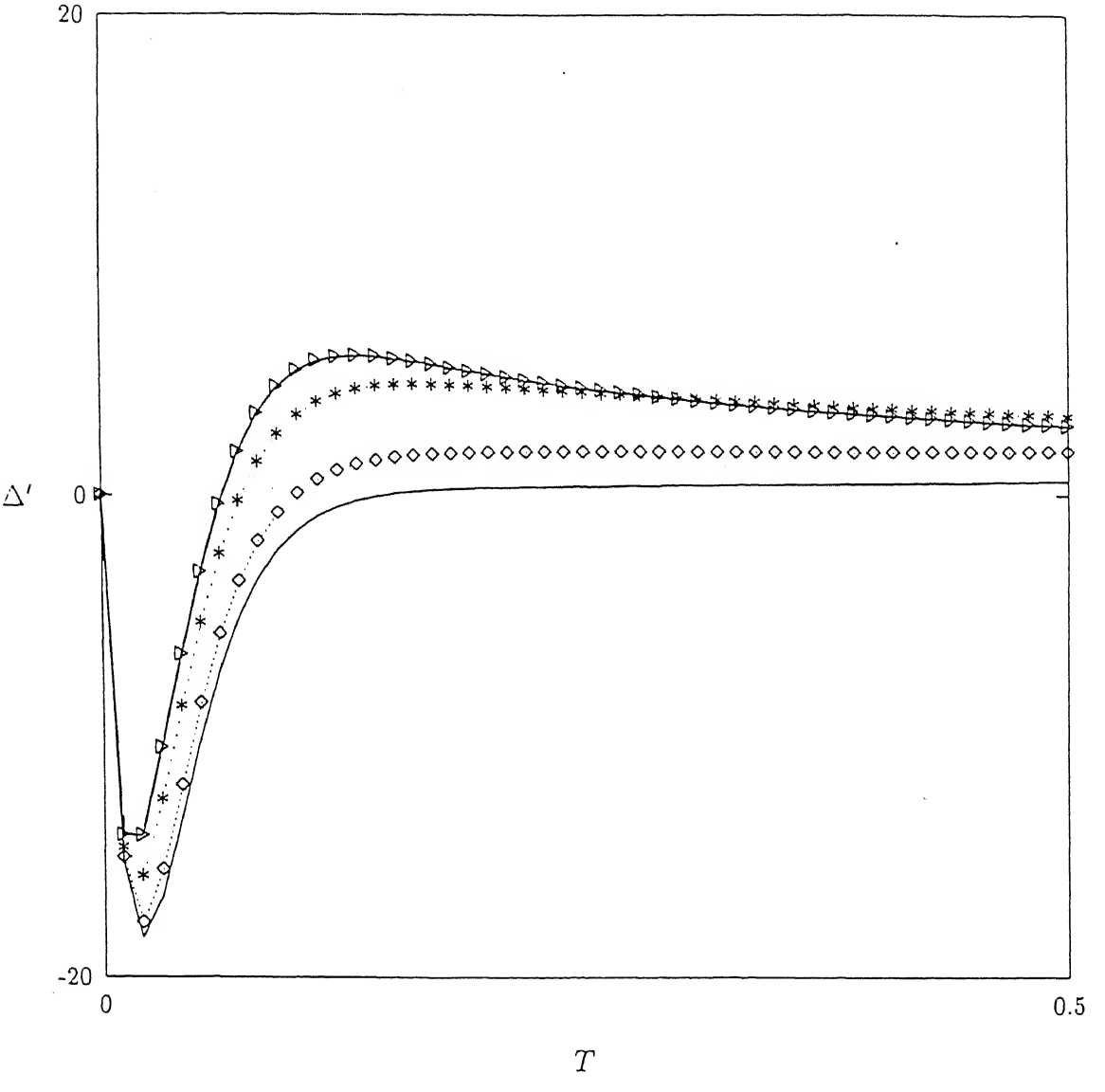

Figure 2.11: The effect of nonlinear cubic damping on the relative velocity for the rounded displacement step. $\gamma = 50$, $\zeta = 0.1$, $\epsilon^* = 0$. · —— $\delta^* = 0$, ◇ $\delta^* = 0.01$, ∗ $\delta^* = 0.05$, —▷— $\delta^* = 0.1$

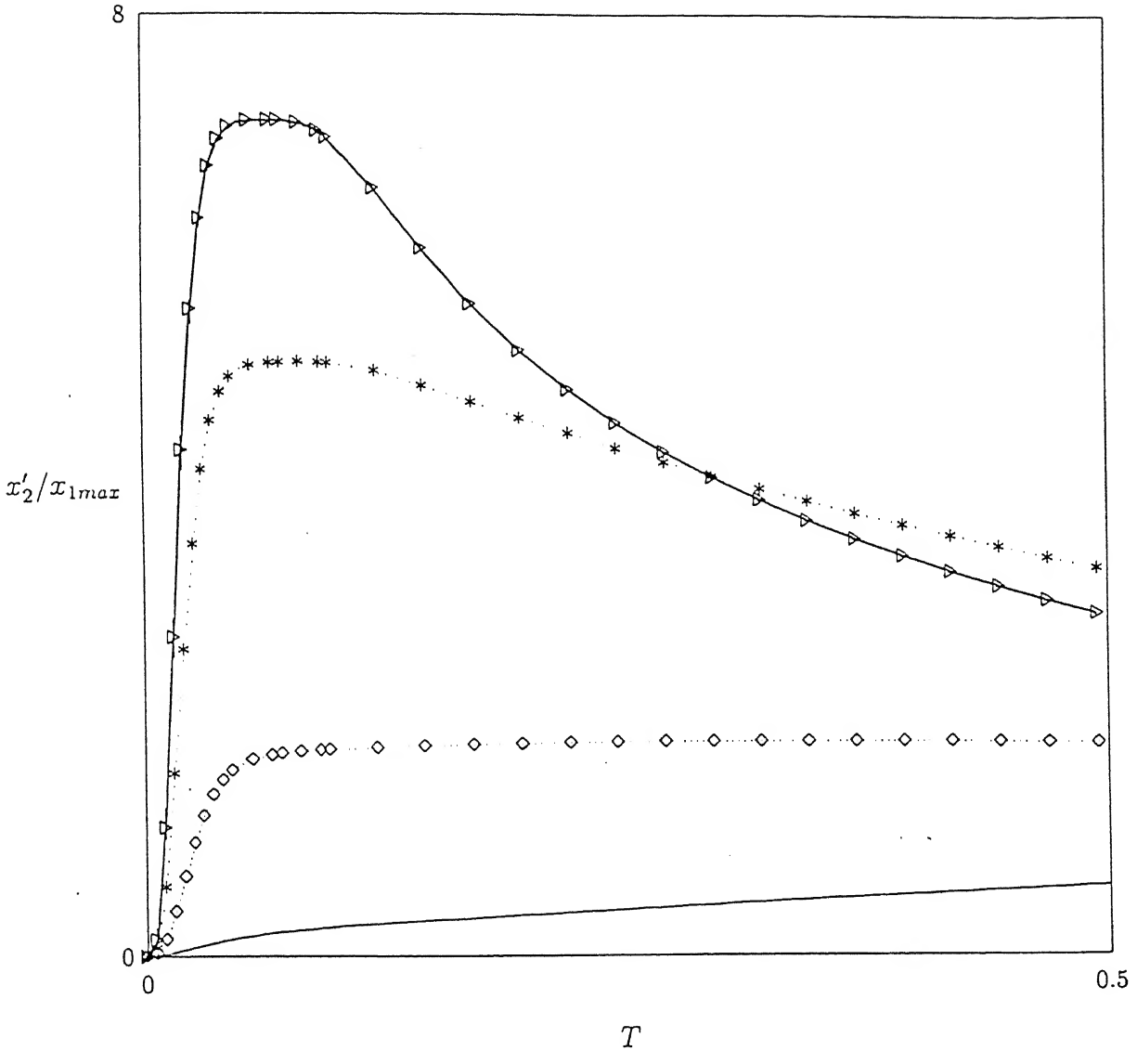

Figure 2.12: The effect of nonlinear cubic damping on the velocity for the rounded displacement step. $\gamma = 50$, $\zeta = 0.1$, $\epsilon^* = 0$. —— $\delta^* = 0$, $\diamond$ $\delta^* = 0.01$, $*$ $\delta^* = 0.05$, $\rightarrow$ $\delta^* = 0.1$

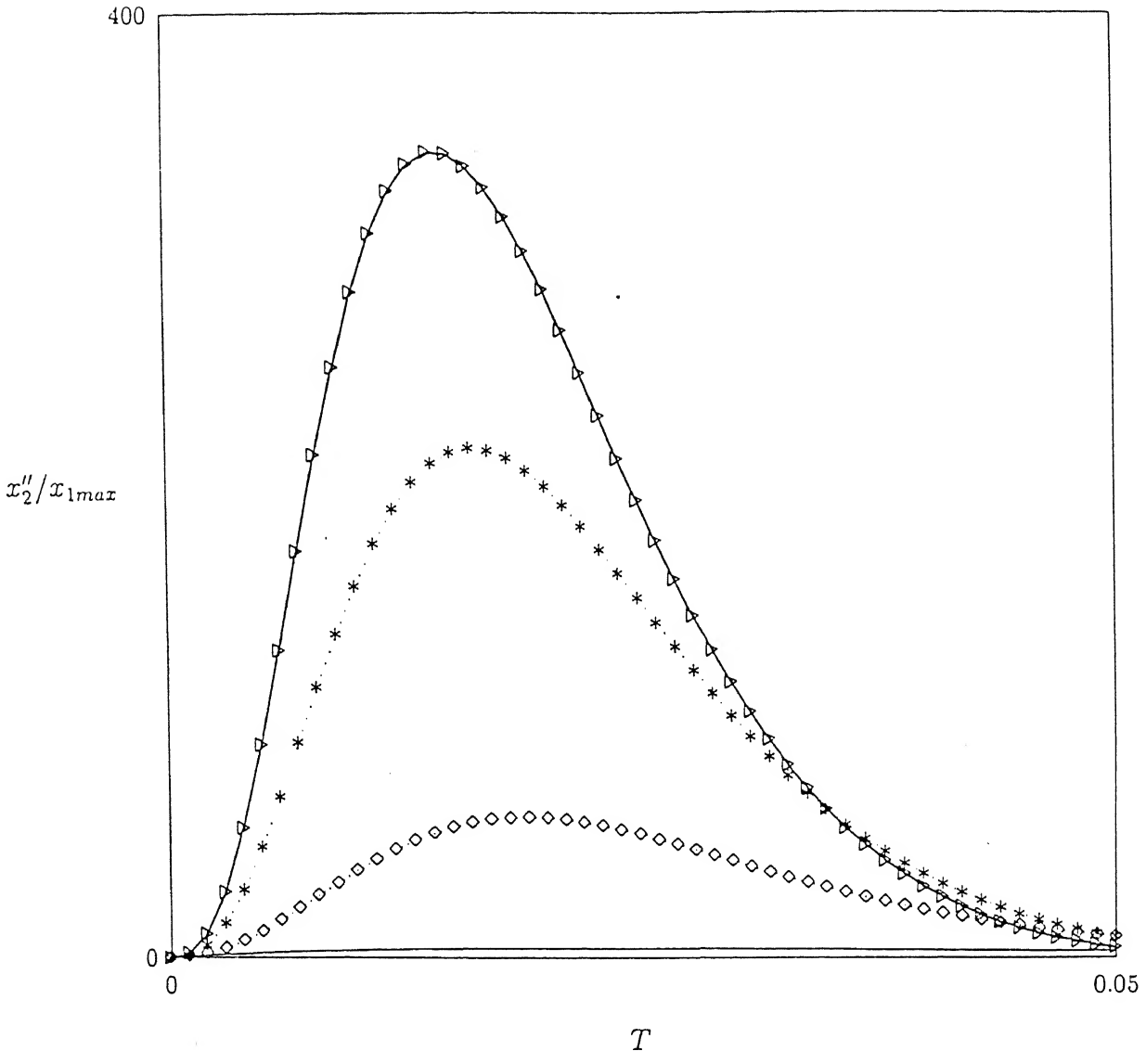

Figure 2.13: The effect of nonlinear cubic damping on the acceleration for the rounded displacement step. $\gamma = 50$, $\zeta = 0.1$, $\epsilon^* = 0$. —— $\delta^* = 0$, $\diamond$ $\delta^* = 0.01$, $*$ $\delta^* = 0.05$, $\triangleright$ $\delta^* = 0.1$

shown in Figure 2.10 (for the relative displacement) and is not shown again. The effect of nonlinear damping on the other three criteria are depicted in Figures 2.11, 2.12 and 2.13. Figure 2.11 shows that the peak value of the relative velocity is reduced by increasing the coefficient of the nonlinear, cubic damping term. However, Figures 2.12 and 2.13 clearly indicate that an increase in the same coefficient results in higher peaks in both the absolute velocity and the acceleration of the isolated mass.

With a shock displacement to the base, the initial velocity across the damping element is quite large. The cubic nonlinearity in damping then causes a large excitation to the mass which in turn accounts for the high value of its response.

Quadratic Damping

Fluid dampers, in certain range of velocity across them, can be better modelled by including a quadratic damping term [75]. Some elastomeric isolators are also modelled by a combination of linear and quadratic damping forces. In the first case the coefficient of the quadratic term is positive, whereas in the latter, this coefficient is a small (compared to that of the linear term) negative number. Both these types of damping can be incorporated in equation (2.2) if the term $\delta^*(\Delta')^3$ is replaced by $\delta^* \mid \Delta' \mid \Delta'$ with δ^* positive or negative as the case may be. Then the equation of motion for the quadratic damping may be written as

$$\Delta'' + 2\zeta\Delta' + \delta^* \mid \Delta' \mid \Delta' + \Delta + \epsilon^*\Delta^3 = f(T) \tag{2.73}$$

Equation (2.73) was numerically integrated for various combination of parameters. It was seen that the effects of such quadratic damping with a negative δ^* are negligible so far as the relative and absolute displacements are concerned. However, the absolute acceleration do get effected by the quadratic damping. Figure 2.14 shows that the peak value of the absolute acceleration can be very effectively controlled with a negative δ^*.

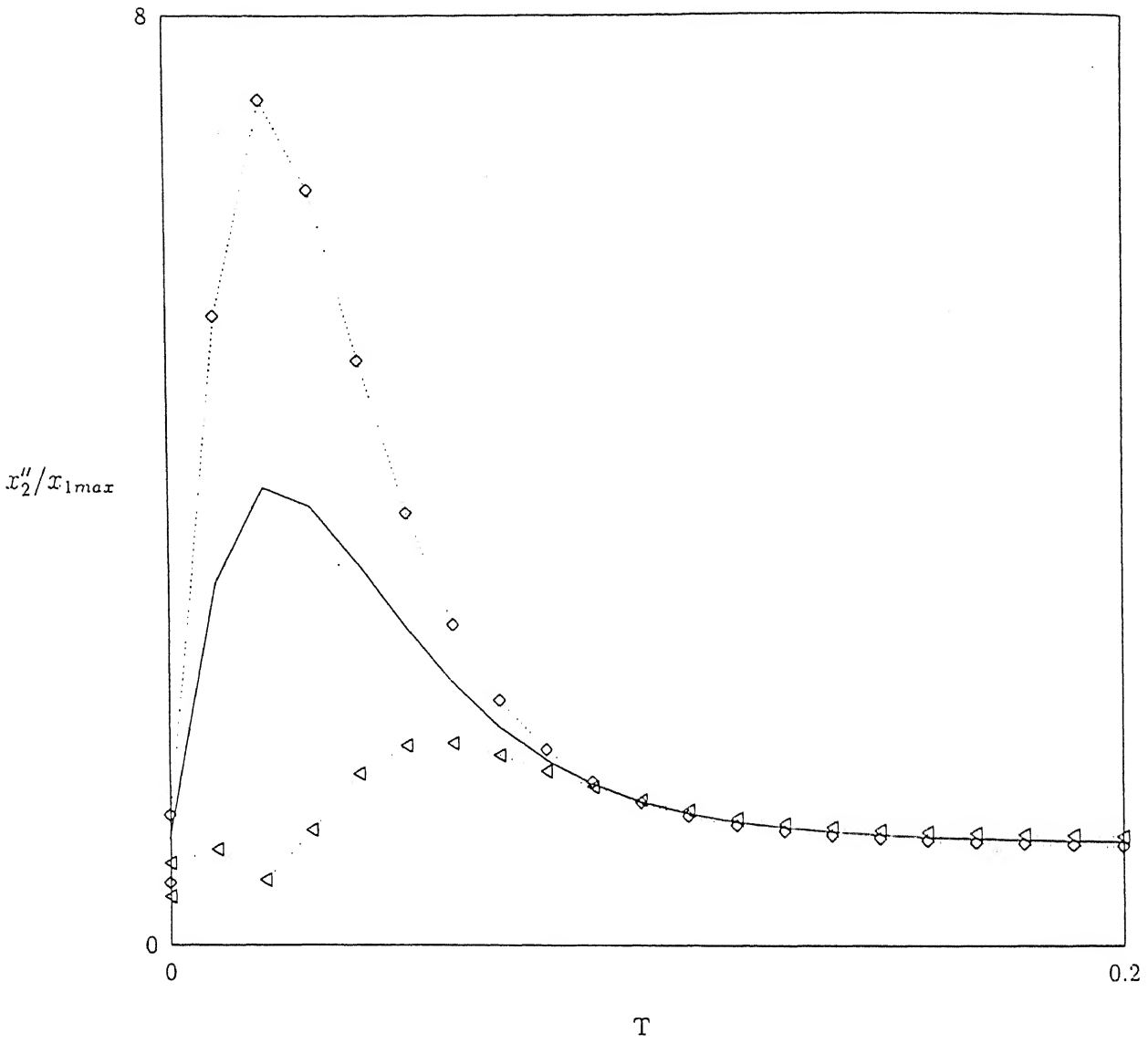

Figure 2.14: The effect of nonlinear quadratic damping on the acceleration for the rounded step. $\gamma = 50$, $\zeta = 0.1$, $\epsilon^* = 0$. —— $\delta^* = 0$, ◇ $\delta^* = 0.01$, ▷ $\delta^* = -0.01$

Chapter 3

RESPONSE OF NONLINEAR DISSIPATIVE SHOCK ISOLATORS TO FORCE EXCITATION

3.1 Introduction

In the previous chapter the effect of nonlinear damping on shock isolators has been studied for base excitation. In this chapter the effect of nonlinear cubic damping on shock isolators is presented for force excitation. Two types of force excitations, namely rounded step and rounded pulse, have been considered. Any sudden increment of the force may be considered as a rounded step excitation whereas a sharp rise followed by a gradual decline can be modelled as a rounded pulse excitation. The anvil of a drop forging machine is subjected to the second type of excitation.

Unlike for the base excitation of nonlinear shock isolators, it was found that for the

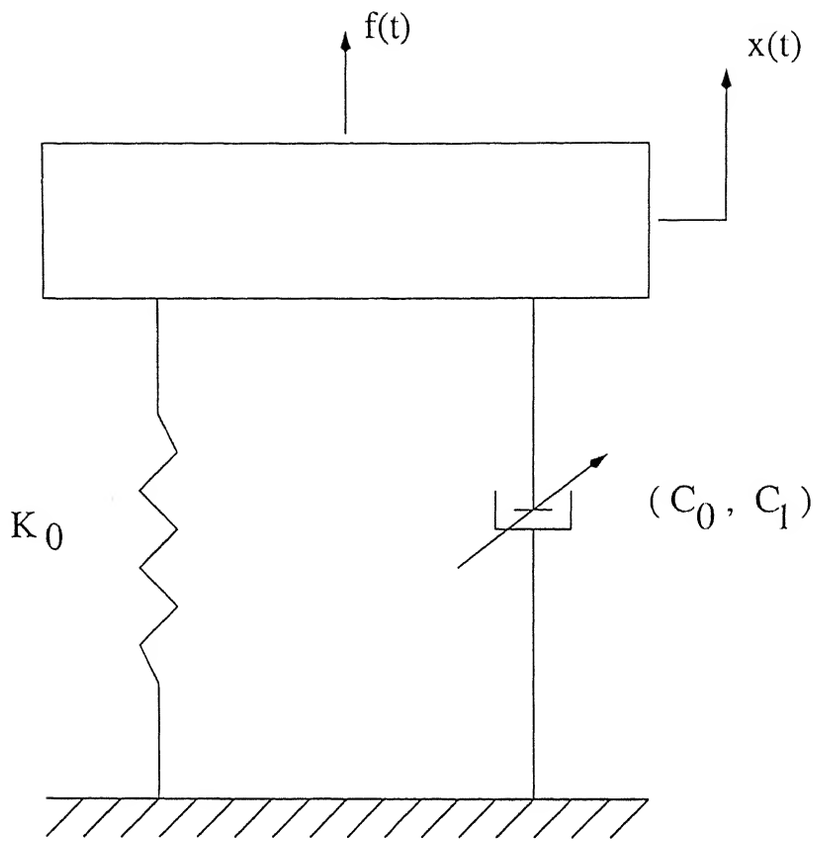

Figure 3.1: Non-linear force excited system

force excitation, the nonlinear damping does not deteriorate the isolator performance for both rounded step and rounded pulse force excitations.

3.2 Equations of Motion

A single degree-of-freedom shock isolator system is shown in Figure 3.1, where the mass is subjected to a shock force. The spring is considered as linear and the the damper of the isolator is taken to be nonlinear with a cubic nonlinearity superimposed on a

linear term. The equation of motion for the mass m, to be isolated, is

$$m\ddot{x} + c_0\dot{x} + c_1\dot{x}^3 + k_0x = f(t) \tag{3.1}$$

where x is the absolute displacement of the mass m, and the dots denote derivatives with respect to time t; k_0 is the linear spring constant. c_0 and c_1 are the linear and nonlinear damping coefficients and $f(t)$ is the shock force excitation. The initial conditions on x are taken to be zero, i.e., $x = \dot{x} = 0$ at $t = 0$. Equation (3.1) is written in the non-dimensional form as

$$X'' + 2\zeta X' + \delta^*(X')^3 + X = F(T) \tag{3.2}$$

where, $X = x/x_{max}$ is the non-dimensionalised displacement of the mass m;
$x_{max} = f_{max}/k_0$, f_{max} is the maximum shock force applied to the mass m, the non-dimensionalised time $T = \omega_0 t$ with $\omega_0 = \sqrt{\frac{k_0}{m}}$, the primes denote derivatives with respect to T, and the other non-dimensional parameters are

$\zeta = \frac{c_0}{2m\omega_0}$, $\delta^* = \frac{c_1\omega_0(x_{max})^2}{m}$, and

$$F(T) = \frac{f(t)}{f_{max}}. \tag{3.3}$$

Types of Input Shock Forces

Two types of shock forces, rounded step and rounded pulse, have been considered. The functional form of these forces are similar to the functional form of the base excitations discussed in the previous chapter. These functional forms are continuous and differentiable at the time origin. The rounded step shock force represents any sudden increment in the force applied to the isolator mass m. The rounded pulse shock force represents a sudden increment in the force followed by a gradual decline. These forces are described mathematically as given below:

Case (a) Rounded step shock force:

This type of force excitation, shown in Figure 3.2, is expressed as

$$f(t) = f_{max}\left[1 - (1 + \gamma\omega_0 t)\, e^{(-\gamma\omega_0 t)}\right] \quad \text{for} \quad t \geq 0 \tag{3.4}$$

with γ as the severity parameter.

Case (b) Unidirectional rounded pulse shock force:

This type of force excitation is shown in Figure 3.3 and is written as

$$f(t) = f_{max}(e^2/4)\,(\gamma\omega_0 t)^2\, e^{(-\gamma\omega_0 t)} \quad \text{for} \quad t \geq 0. \tag{3.5}$$

Solution Procedure

Equation (3.2) can be solved by using the perturbation method explained in the previous chapter. The non-homogeneous term $F(T)$ in equation (3.2) may be expressed in generalized form using equations (3.3), (3.4) and (3.5) as given below:

$$F(T) = C + e^{aT}\left[\sum_{m=0}^{N} A_m T^m\right], \tag{3.6}$$

where, $C = 1$, $a = -\gamma$, $N = 1$, $A_0 = -1$ and $A_1 = -\gamma$ for rounded step and $C = 0$, $a = -\gamma$, $N = 2$, $A_0 = 0$, $A_1 = 0$ and $A_2 = e^2\gamma^2/4$ for rounded pulse.

3.3 Results and Discussions

The effect of nonlinear damping for rounded step and rounded pulse types of shock forces are discussed below. The linear damping coefficient $\zeta = 0.1$ and the nonlinear damping coefficient $\delta^* = 0.05$ have been considered. It was observed that the effect of nonlinear damping is discernible at high severity parameters for rounded step force excitation. But, for the rounded pulse force excitation, the nonlinear damping effect is appreciable at low severity parameters, particularly at $\gamma = 1$. So, $\gamma = 50$ for the rounded step excitation and the $\gamma = 1$ for the rounded pulse force excitation have been used in all the results.

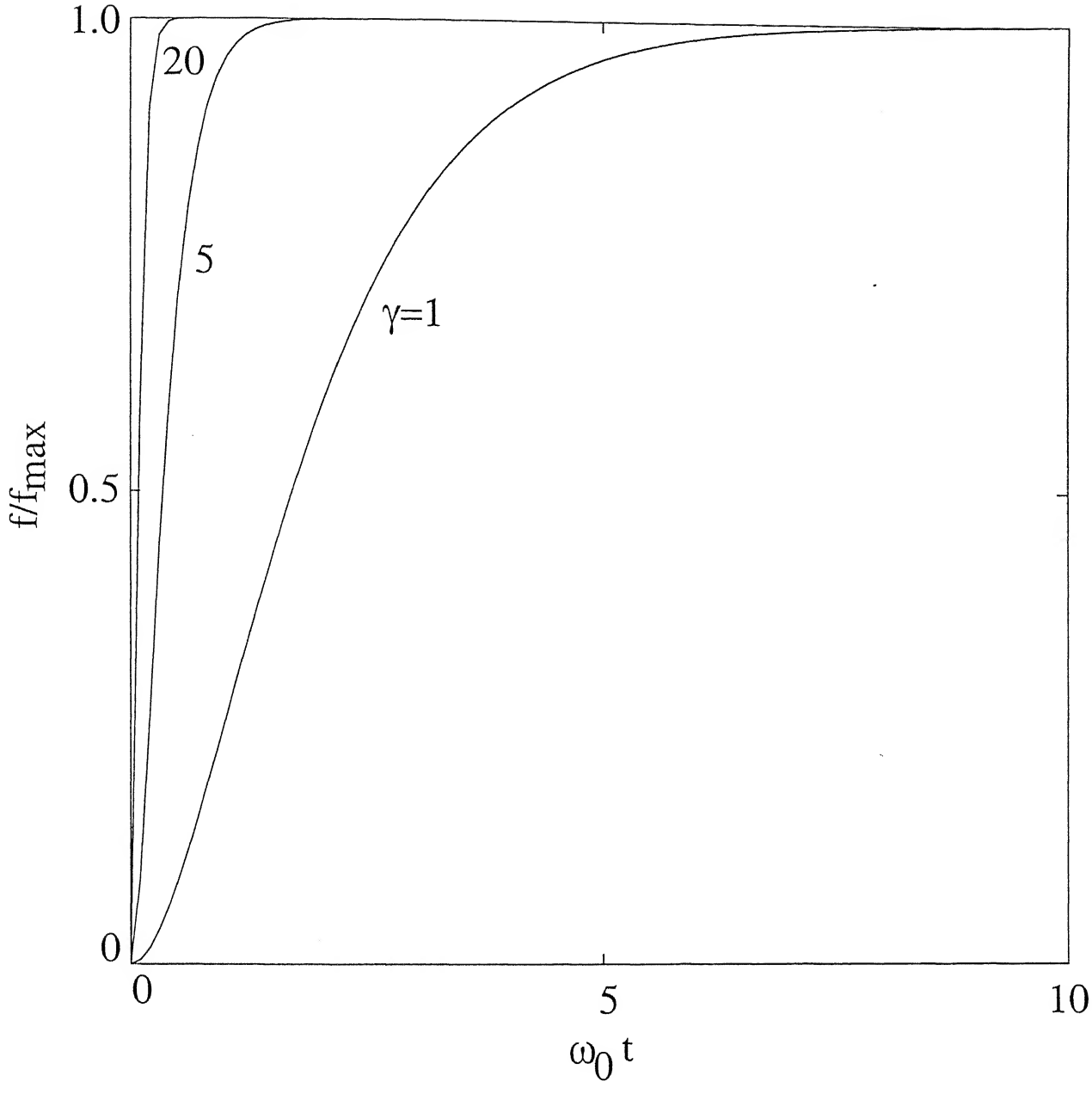

Figure 3.2: The rounded step force excitation.

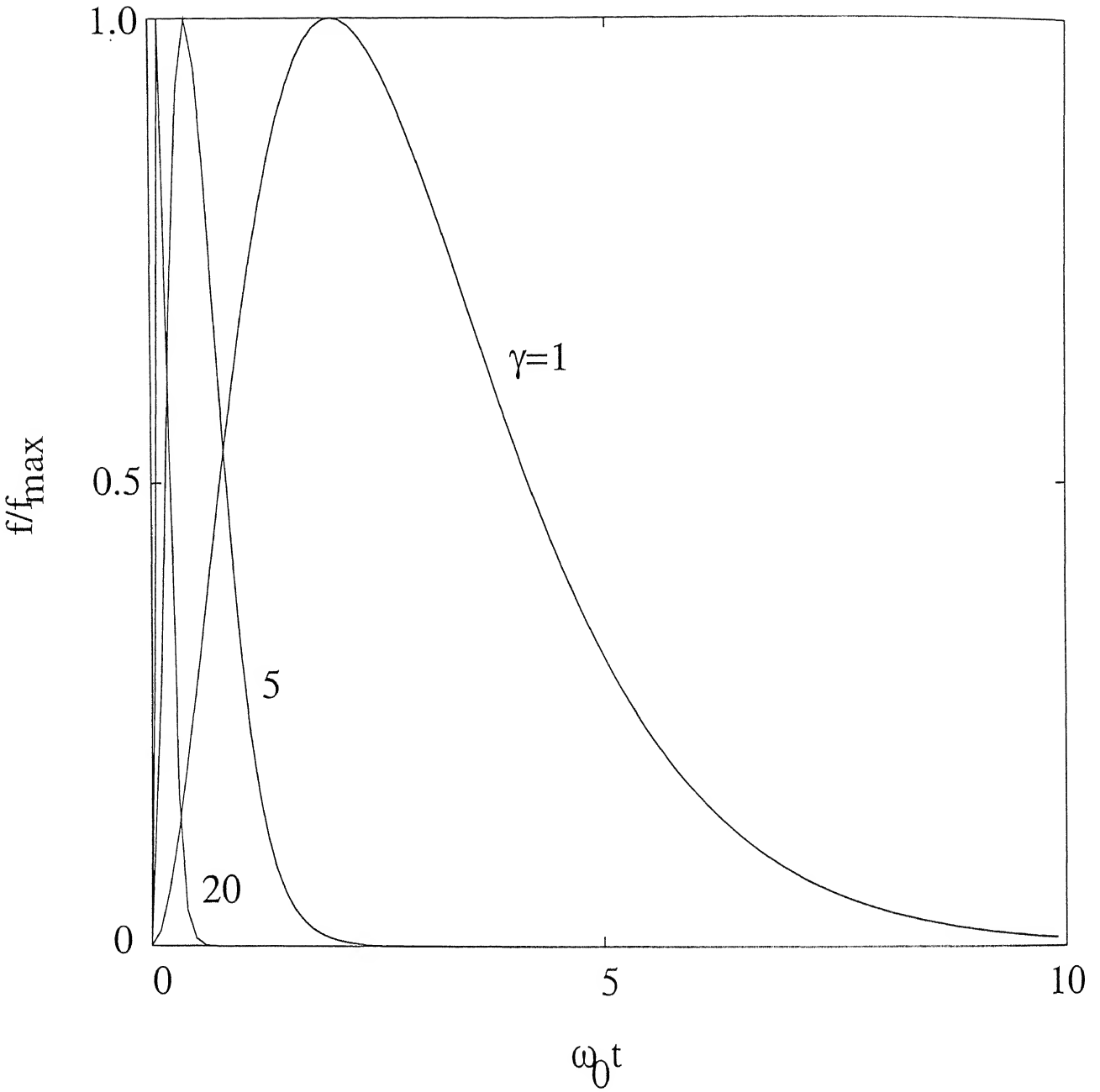

Figure 3.3: The rounded pulse force excitation.

3.3.1 Effect of Nonlinear Damping

Rounded Step Force Excitation

The effect of nonlinear damping on displacement, velocity and acceleration for rounded step force excitation are shown in Figures 3.4, 3.5 and 3.6 respectively. These results are obtained by numerical integration. Unlike in rounded step displacement base excitation (see Figures 2.9-2.13), nonlinear damping in rounded step force excitation reduces displacement, velocity and accelerations peaks simultaneously. Similar to rounded step base excitation, nonlinear damping effect is appreciable when severity parameter is very high. At low severity parameters, the effect of nonlinear damping for rounded step force excitation is negligible and it is not shown here.

Rounded Pulse Force Excitation

The effect of nonlinear damping on displacement, velocity and acceleration for rounded pulse force excitation are presented in Figures 3.7, 3.8 and 3.9 respectively. Unlike in rounded pulse displacement base excitation, nonlinear damping effect on various response variables is insignificant at high severity parameters for rounded pulse force excitation. But, at low severity parameters, the nonlinear damping effect is appreciable on various response variables for rounded pulse force excitation. The nonlinear damping reduces the peaks of displacement, velocity and acceleration simultaneously for rounded pulse force excitation at low severity parameter ($\gamma = 1$).

In overall, the presence of nonlinearity in damping does not deteriorate the performance of isolator in shock force excitation. Assumption of linearity in shock force excitation gives conservative estimate of the isolator performance, which is contrary to the base shock displacement excitation. So, in forthcoming chapters, force shock excitation is not considered.

CENTRAL LIBRARY
I. I. T., KANPUR
No. A 131094

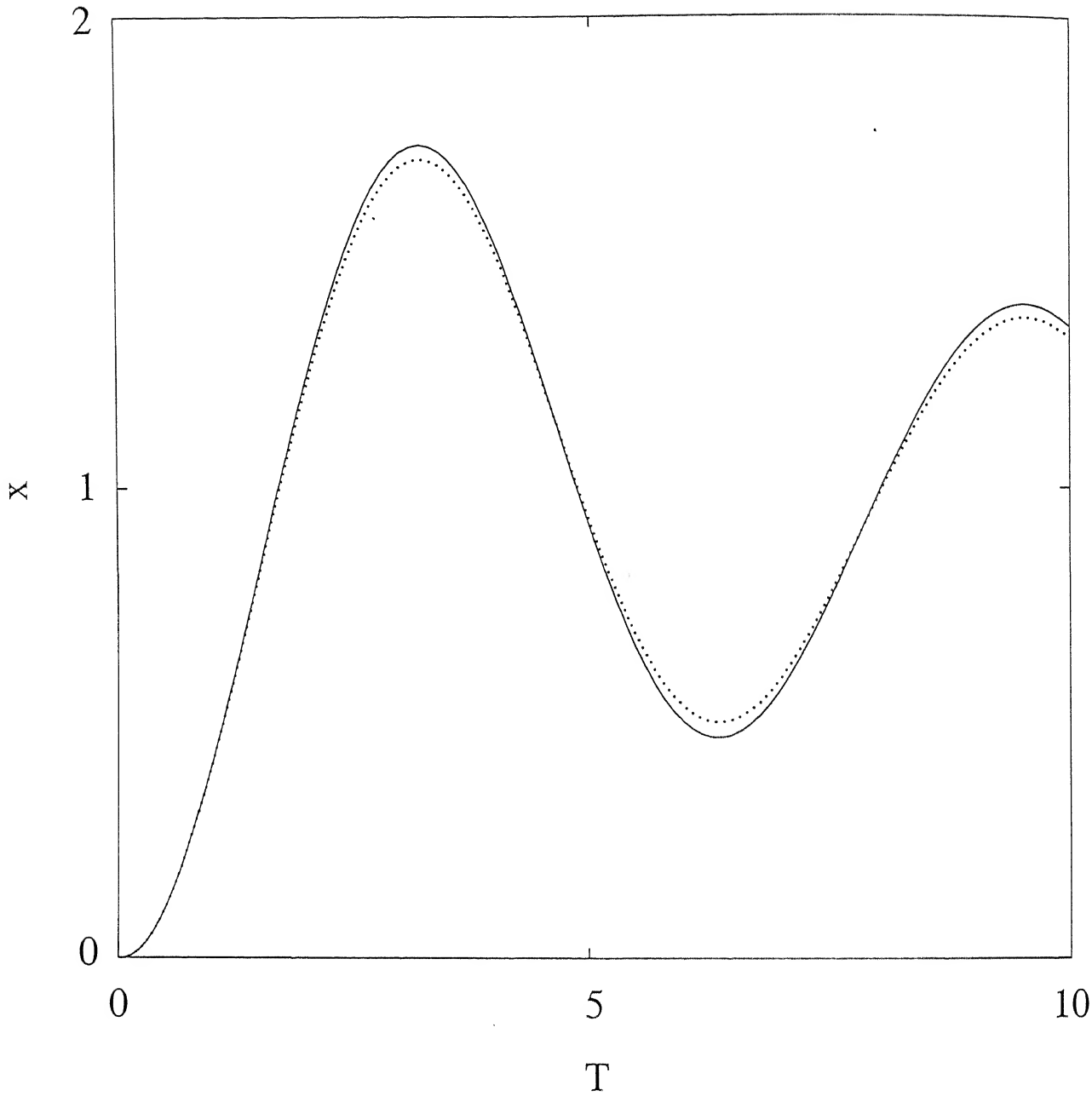

Figure 3.4: The effect of nonlinear cubic damping on the displacement for the rounded step force excitation. $\gamma = 50, \quad \zeta = 0.1.$ ——— : $\delta^* = 0, \quad$ .... : $\delta^* = 0.05$

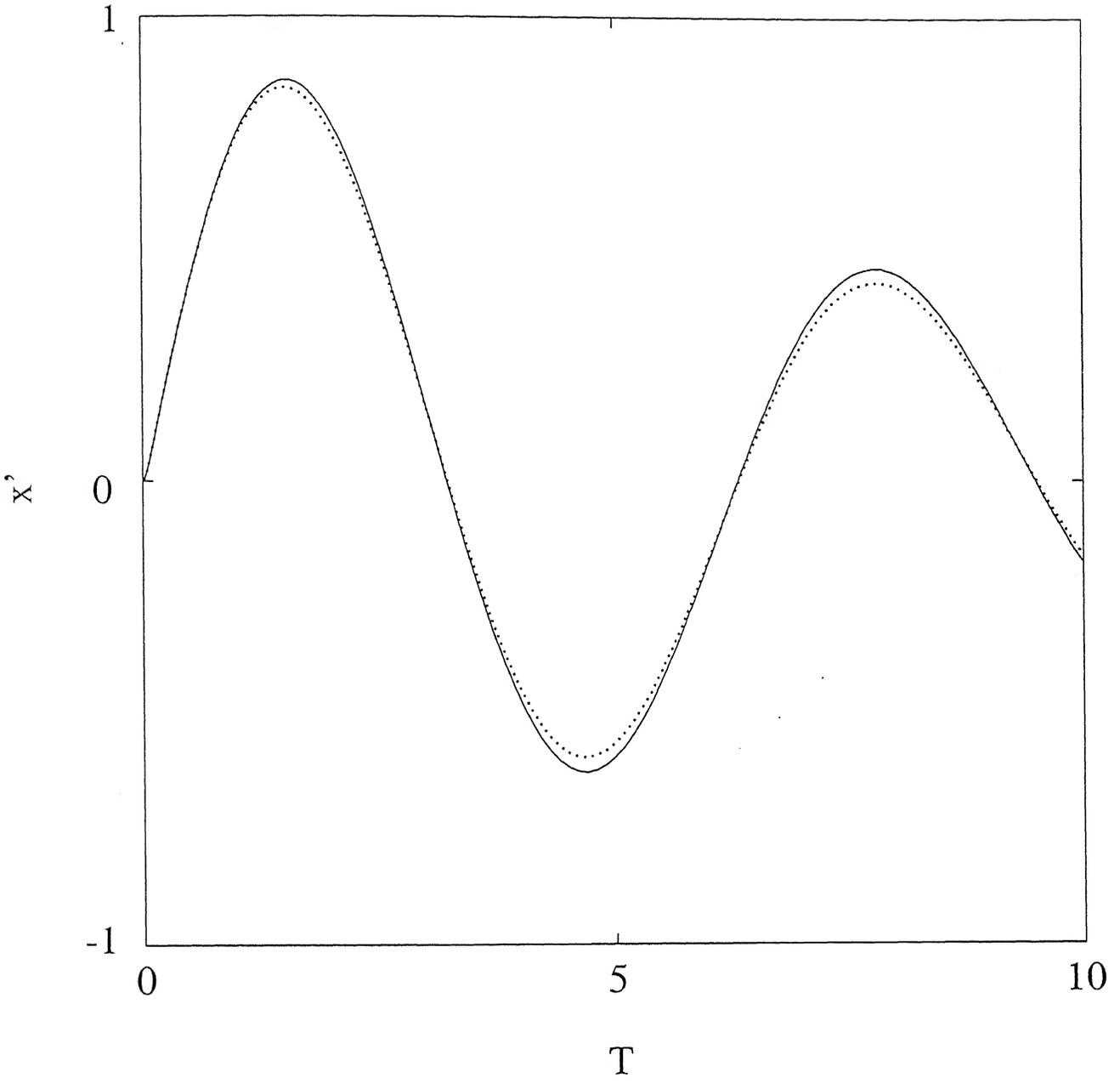

Figure 3.5: The effect of nonlinear cubic damping on the velocity for the rounded step force excitation. $\gamma = 50, \quad \zeta = 0.1.$ —— : $\delta^* = 0, \quad$ .... : $\quad \delta^* = 0.05$

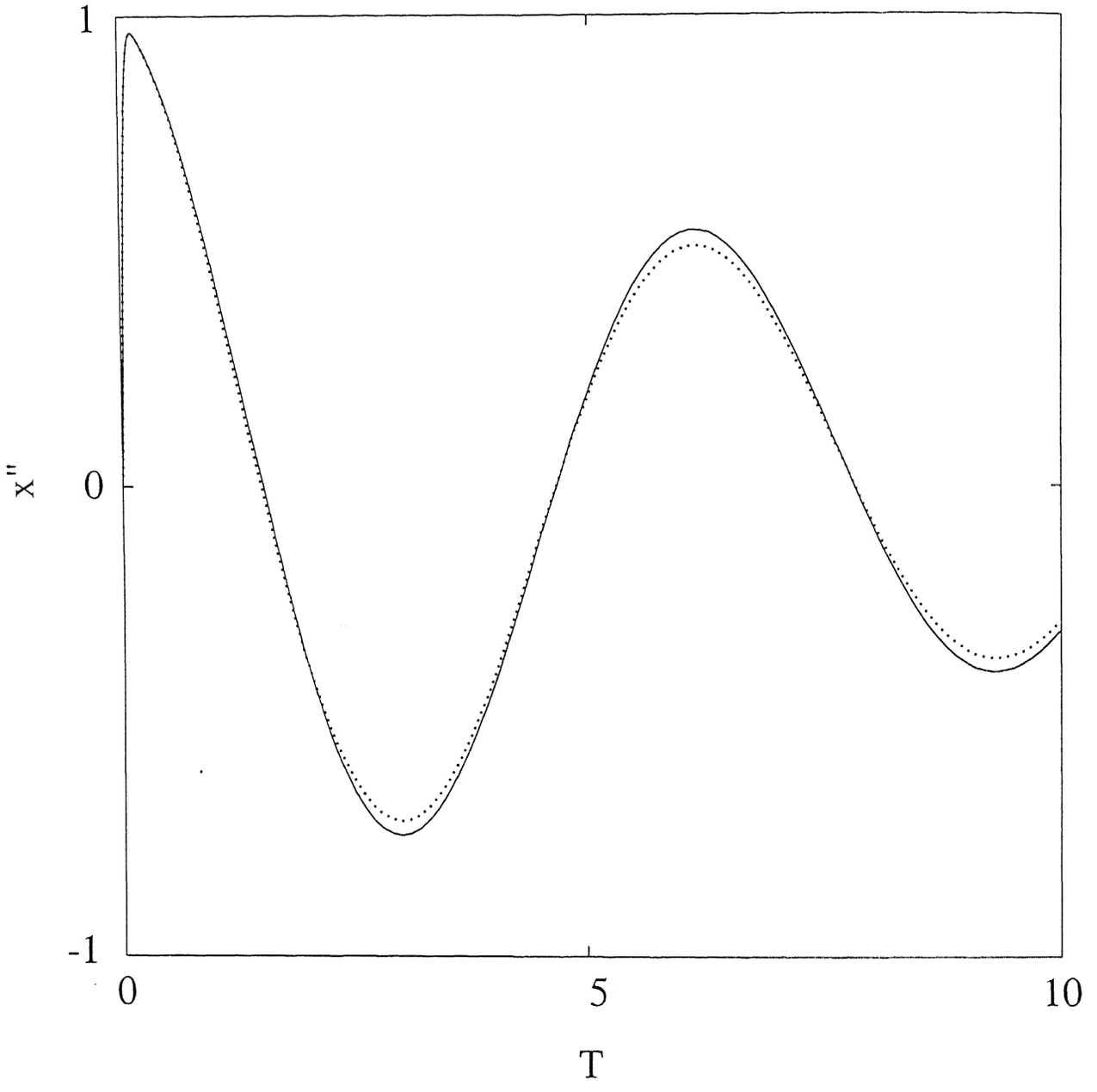

Figure 3.6: The effect of nonlinear cubic damping on the acceleration for the rounded step force excitation. $\gamma = 50, \quad \zeta = 0.1.$ —— : $\delta^* = 0, \quad$ .... : $\delta^* = 0.05$

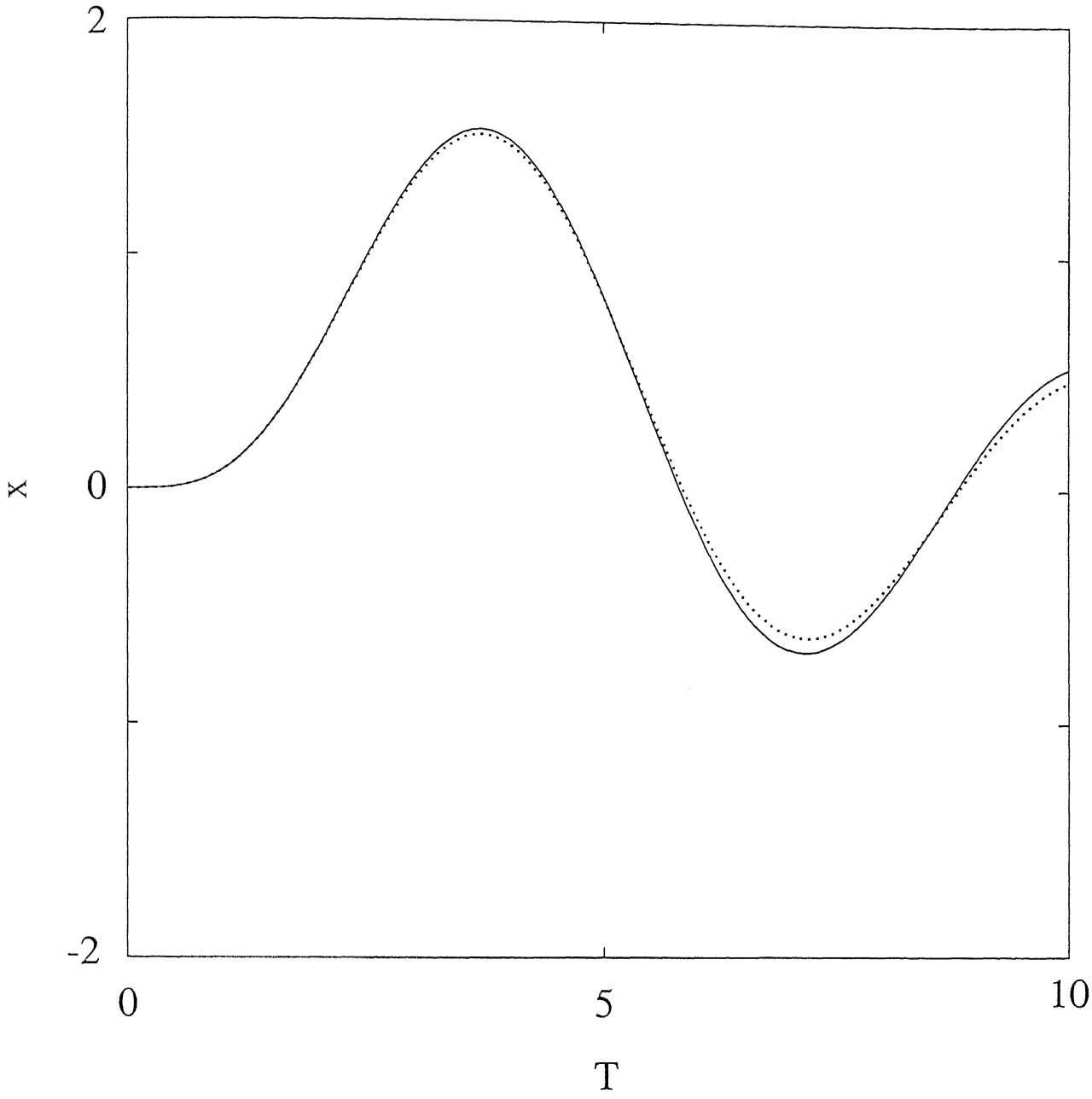

Figure 3.7: The effect of nonlinear cubic damping on the displacement for the rounded pulse force excitation. $\gamma = 1, \quad \zeta = 0.1.$ —— : $\delta^* = 0, \quad$ .... : $\delta^* = 0.05$

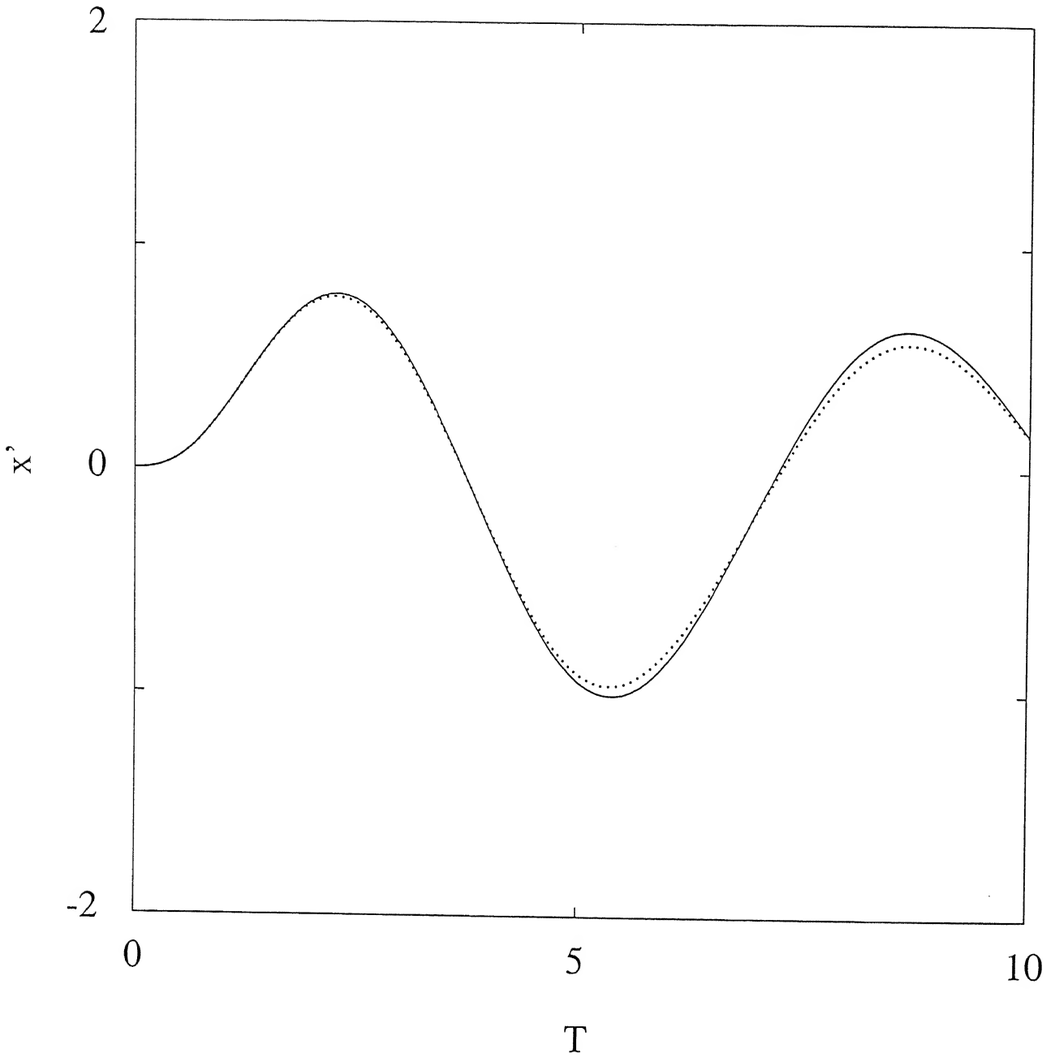

Figure 3.8: The effect of nonlinear cubic damping on the velocity for the rounded pulse force excitation. $\gamma = 1, \quad \zeta = 0.1.$ —— : $\delta^* = 0, \quad$ .... : $\delta^* = 0.05$

Chapter 4

PERFORMANCE OF NONLINEAR ISOLATORS AND ABSORBERS TO SHOCK EXCITATIONS

4.1 Introduction

Insertion of a vibration isolator between the source and receiver of vibration, and an attachment of a vibration absorber (a secondary system) to the main vibratory system are two very common methods of vibration control [1-3]. Under steady-state excitations, both the isolator and absorber are modelled as linear systems. However, for a shock loading on the system, the nonlinear characteristics present in the stiffness and damping properties of these systems, viz., air springs, elastomeric dampers and wire-rope isolators [4], come into play. In the second chapter, a single-stage shock isolator comprising of a parallel combination of a nonlinear spring and a nonlinear

damper has been considered. It was shown that the nonlinearity in the damping rather than that in the stiffness has more pronounced effect on different indices expressing the performance of a shock isolator. The presence of a nonlinear velocity dependent damping term with a positive coefficient was found to have detrimental effects on the isolator performance.

In this chapter, different alternatives are considered for improving the performance of an isolator having a nonlinear cubic damping over and above the usual viscous damping. Since the nonlinearity in the isolator restoring force does not have any appreciable effect in its performance [32], the stiffness of the isolator is assumed to be constant in this chapter. The following four different alternatives are being considered and compared [77] :

(i) inclusion of a Coulomb damper in parallel to the original nonlinear isolator,

(ii) a three element isolator where the nonlinear damper is elastically (rather than rigidly) connected,

(iii) attachment of a secondary system through a linear spring and a nonlinear damper,

(iv) a two stage isolator, where each stage comprises of a linear spring and a nonlinear damper.

Three different types of shock inputs are considered as the base motion to be isolated. Three different indices are used to judge the overall performance characteristics of the isolator. Overall, it is seen that the three-element and two-stage isolators are preferable in the presence of nonlinear cubic damping.

4.2 Equations of Motion

In this section, equations of motion for the four systems described above are derived in non-dimensionalized form.

4.2.1 Type 1 Isolator : Shock Isolator with a Coulomb Damper

Let a rigid mass m be isolated from the base excitation, $x_1(t)$, by using three elements in parallel viz., a linear spring, a nonlinear velocity-dependent damper and a Coulomb damper as shown in Figure 4.1. The equation of motion for the mass m, is

$$m\ddot{x}_2 + c_0(\dot{x}_2 - \dot{x}_1) + c_1(\dot{x}_2 - \dot{x}_1)^3 + c_f sgn(\dot{x}_2 - \dot{x}_1) + k_0(x_2 - x_1) = 0 \qquad (4.1)$$

where x_1 and x_2 are the absolute displacements of the base and the mass m, respectively, and the dots denote derivatives with respect to time t. c_f is the coulomb damper coefficient. The initial conditions on x_2 are taken to be zero, i.e., $x_2 = \dot{x}_2 = 0$ at $t = 0$. Equation (4.1) can be written in the non-dimensional form

$$\Delta'' + 2\zeta\Delta' + \delta^*(\Delta')^3 + \delta_f sgn(\Delta') + \Delta = f(T) \qquad (4.2)$$

where, $\Delta = (x_2 - x_1)/x_{1max}$ is the non-dimensionalized relative displacement between the mass m and the base; the non-dimensionalized time $T = \omega_0 t$ with $\omega_0 = \sqrt{\frac{k_0}{m}}$; the primes denote derivatives with respect to T, and the other non-dimensional parameters are $\zeta = \frac{c_0}{2m\omega_0}$, $\delta^* = \frac{c_1\omega_0(x_{1max})^2}{m}$, $\delta_f = \frac{c_f}{mx_{1max}\omega_0^2}$, and $f(T) = -\frac{x_1''}{x_{1max}}$.

4.2.2 Type 2 Isolator : Three Element Shock Isolator

A three element mounting comprised of two springs and a nonlinear damper is shown in Figure 4.2, where an elastically connected nonlinear damper is put in parallel to another spring.

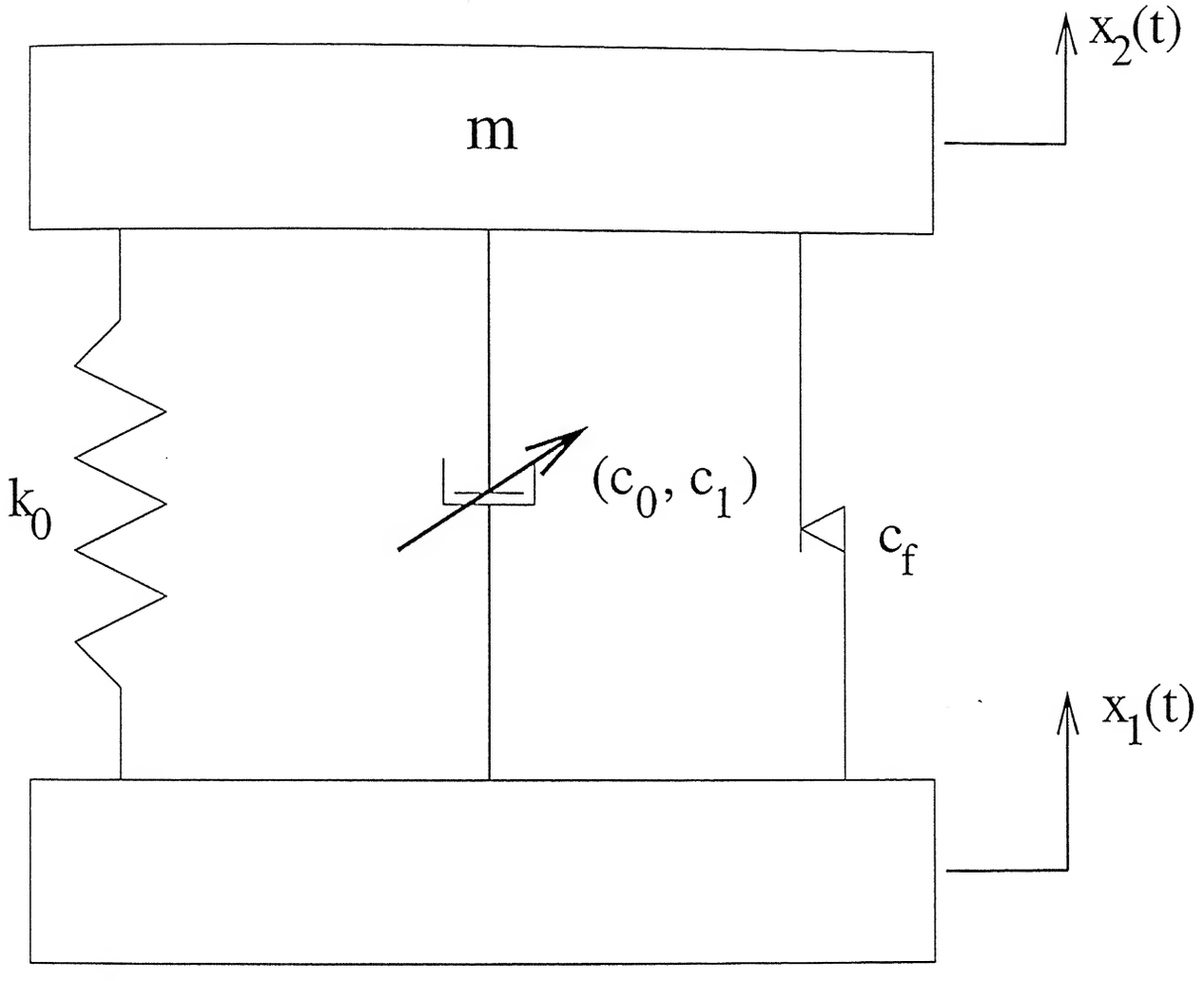

Figure 4.1: Type 1 Isolator

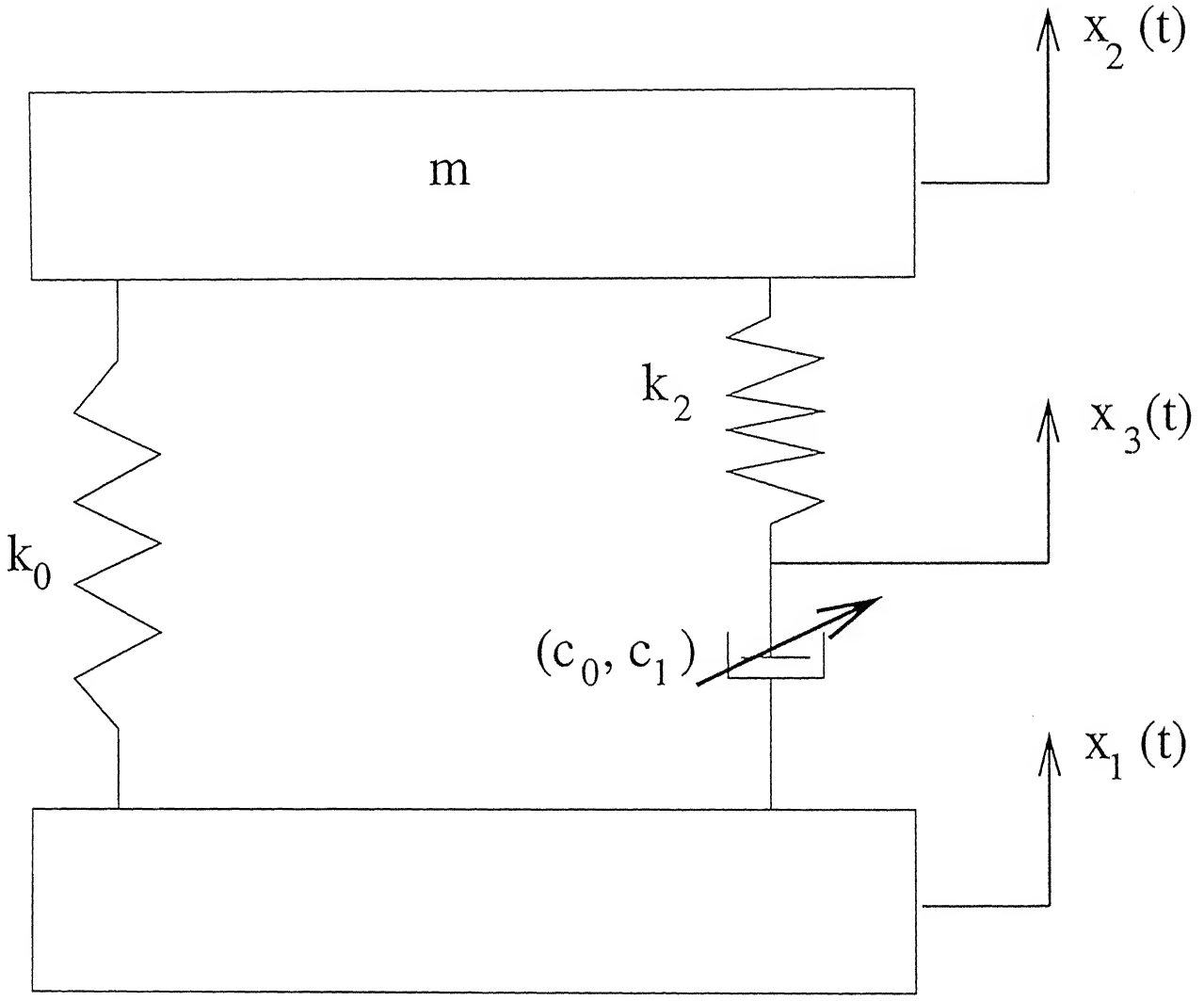

Figure 4.2: Type 2 Isolator

The equation of motion for the rigid mass m may be written as

$$m\ddot{x}_2 + k_0(x_2 - x_1) + k_2(x_2 - x_3) = 0. \tag{4.3}$$

Further, because the dashpot and the spring experience the same transient force,

$$k_2(x_3 - x_2) = c_0(\dot{x}_1 - \dot{x}_3) + c_1(\dot{x}_1 - \dot{x}_3)^3. \tag{4.4}$$

The initial conditions on x_2 and x_3 are taken to be zero, i.e., $x_2 = x_3 = \dot{x}_2 = \dot{x}_3 = 0$ at $t = 0$. Equations (4.3) and (4.4) are written in the non-dimensional forms as

$$\Delta'' + \Delta + n(\Delta - Z) = f(T) \tag{4.5}$$

and

$$n(Z - \Delta) + 2\zeta Z' + \delta^* Z'^3 = 0 \tag{4.6}$$

where, $Z = (x_3 - x_1)/x_{1max}$, $n = k_2/k_0$, and the other parameters are already defined in section 4.2.1.

4.2.3 Type 3 Isolator : Transient Vibration Absorber

Let a secondary system be connected to the primary mass m which is being isolated from the base subjected to a shock excitation. The secondary system (transient vibration absorber) consists of a rigid mass m_2 connected to m, through a linear spring and a nonlinear damper as shown in Figure 4.3. The equations of motion for the masses m and m_2 are

$$\begin{aligned} m\ddot{x}_2 + c_0(\dot{x}_2 - \dot{x}_1) + c_1(\dot{x}_2 - \dot{x}_1)^3 + k_0(x_2 - x_1) + c_2(\dot{x}_2 - \dot{x}_3) & \\ +c_3(\dot{x}_2 - \dot{x}_3)^3 + k_2(x_2 - x_3) &= 0 \end{aligned} \tag{4.7}$$

and

$$m_2\ddot{x}_3 + c_2(\dot{x}_3 - \dot{x}_2) + c_3(\dot{x}_3 - \dot{x}_2)^3 + k_2(x_3 - x_2) = 0 \tag{4.8}$$

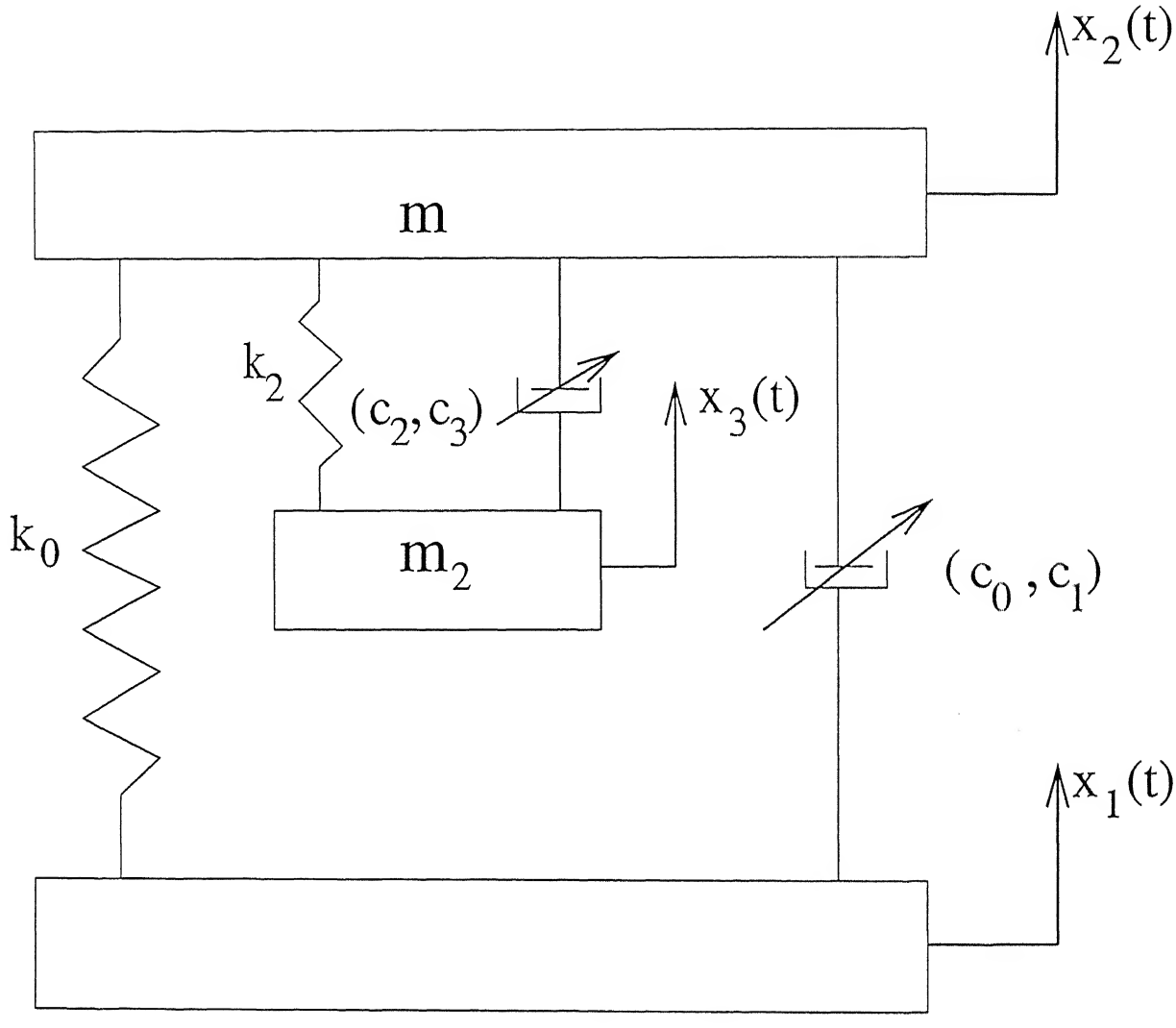

Figure 4.3: Type 3 Isolator

where, x_1, x_2 and x_3 are the absolute displacements of the base, the isolated mass m and the absorber mass m_2, respectively. The initial conditions on x_2 and x_3 are taken to be zero, i.e., $x_2 = x_3 = \dot{x}_2 = \dot{x}_3 = 0$ at $t = 0$. Equations (4.7) and (4.8) may be written in the non-dimensional forms as

$$\Delta'' + 2\zeta\Delta' + \delta^*(\Delta')^3 + \Delta - [nY + 2\zeta_2\sqrt{n\mu}Y' + \delta_2\mu\sqrt{\mu/n}Y'^3] = f(T) \tag{4.9}$$

and

$$Z'' + (n/\mu)Y + 2\zeta_2\sqrt{n/\mu}Y' + \delta_2\sqrt{\mu/n}Y'^3 = f(T) \tag{4.10}$$

where, $Y = (x_3 - x_2)/x_{1max}$, $\mu = m_2/m$, $\omega_2 = \sqrt{k_2/m_2}$, $\zeta_2 = \frac{c_2}{2m_2\omega_2}$, $\delta_2 = \frac{c_3\omega_2(x_{1max})^2}{m_2}$, and the other parameters have already been defined.

4.2.4 Type 4 Isolator : Two Stage Shock Isolator

A two stage isolator system is shown in Figure 4.4, where the main mass m (to be isolated) is connected to an intermediate mass m_2 (called the first stage), which, in turn, is then connected to the base (referred to as the second stage). In both the primary and secondary stages the spring elements are linear whereas the dampers are nonlinear. The equations of motion for the mass m and m_2 are

$$m\ddot{x}_2 + c_0(\dot{x}_2 - \dot{x}_3) + c_1(\dot{x}_2 - \dot{x}_3)^3 + k_0(x_2 - x_3) = 0 \tag{4.11}$$

and

$$\begin{aligned} m_2\ddot{x}_3 + c_0(\dot{x}_3 - \dot{x}_2) + c_1(\dot{x}_3 - \dot{x}_2)^3 + k_0(x_3 - x_2) + c_2(\dot{x}_3 - \dot{x}_1) \\ +c_3(\dot{x}_3 - \dot{x}_1)^3 + k_2(x_3 - x_1) \;=\; 0 \end{aligned} \tag{4.12}$$

where, x_1, x_2 and x_3 are the absolute displacements of the base, the mass m and the mass m_2, respectively. The initial conditions on x_2 and x_3 are taken to be zero, i.e.,

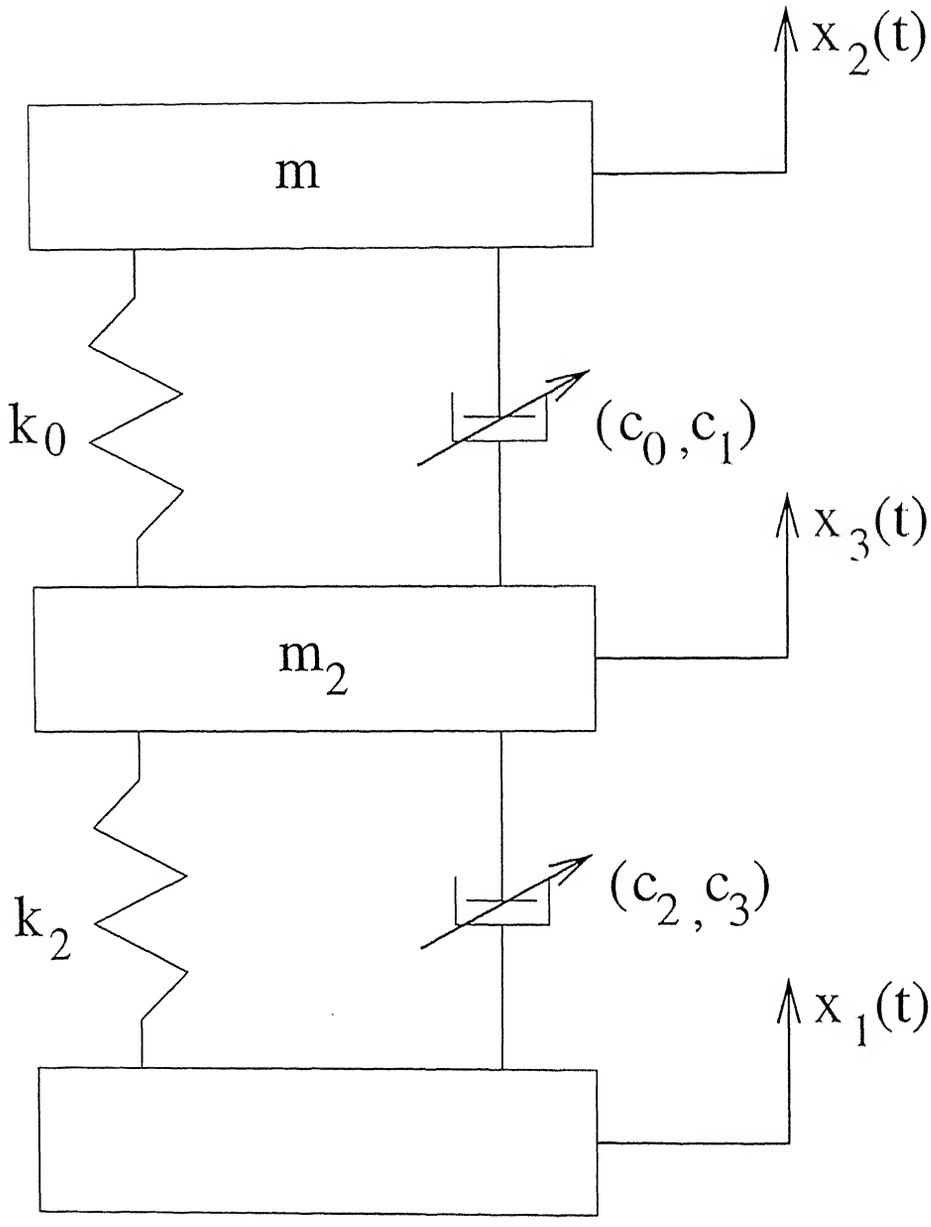

Figure 4.4: Type 4 Isolator

$x_2 = x_3 = \dot{x}_2 = \dot{x}_3 = 0$ at $t = 0$. Using the non-dimensional parameters defined earlier, equations (4.11) and (4.12) may be written as

$$\Delta'' - [Y + 2\zeta Y' + \delta^* Y'^3] = f(T) \tag{4.13}$$

and

$$Z'' + (n/\mu)Z + 2\zeta_2\sqrt{n/\mu}Z' + \delta_2\sqrt{\mu/n}Z'^3 + [Y + 2\zeta Y' + \delta^* Y'^3]/\mu = f(T). \tag{4.14}$$

Types of Shock Displacements of The Base

The three commonly considered shock displacements of the base, taken as input $x_1(t)$, for all the above four types of isolators are already discussed in chapter 2.

4.3 Results and Discussions

In this section, the performance of each of the four types of shock isolator (discussed in previous section) systems are evaluated using the following three indices:

Relative Displacement Ratio (RDR) = $\mid \Delta \mid_{max}$;

Shock Displacement Ratio (SDR) = $\frac{|x_2|_{max}}{x_{1max}}$;

Shock Acceleration Ratio (SAR) = $\frac{|x_2''|_{max}}{x_{1max}''}$.

The last index is expressed in dB scale by rewriting SAR = $20 \log_{10} \frac{|x_2''|_{max}}{x_{1max}''}$.

These indices are obtained for each type of isolator by numerically integrating the corresponding equation of motion. The Runge-Kutta Cash-Karp routine [78] has been used for numerical integration. In all the cases considered for the original isolator, the linear damping coefficient is taken as $\zeta = 0.1$ and the nonlinear cubic damping coefficient is taken as $\delta^* = 0.01$.

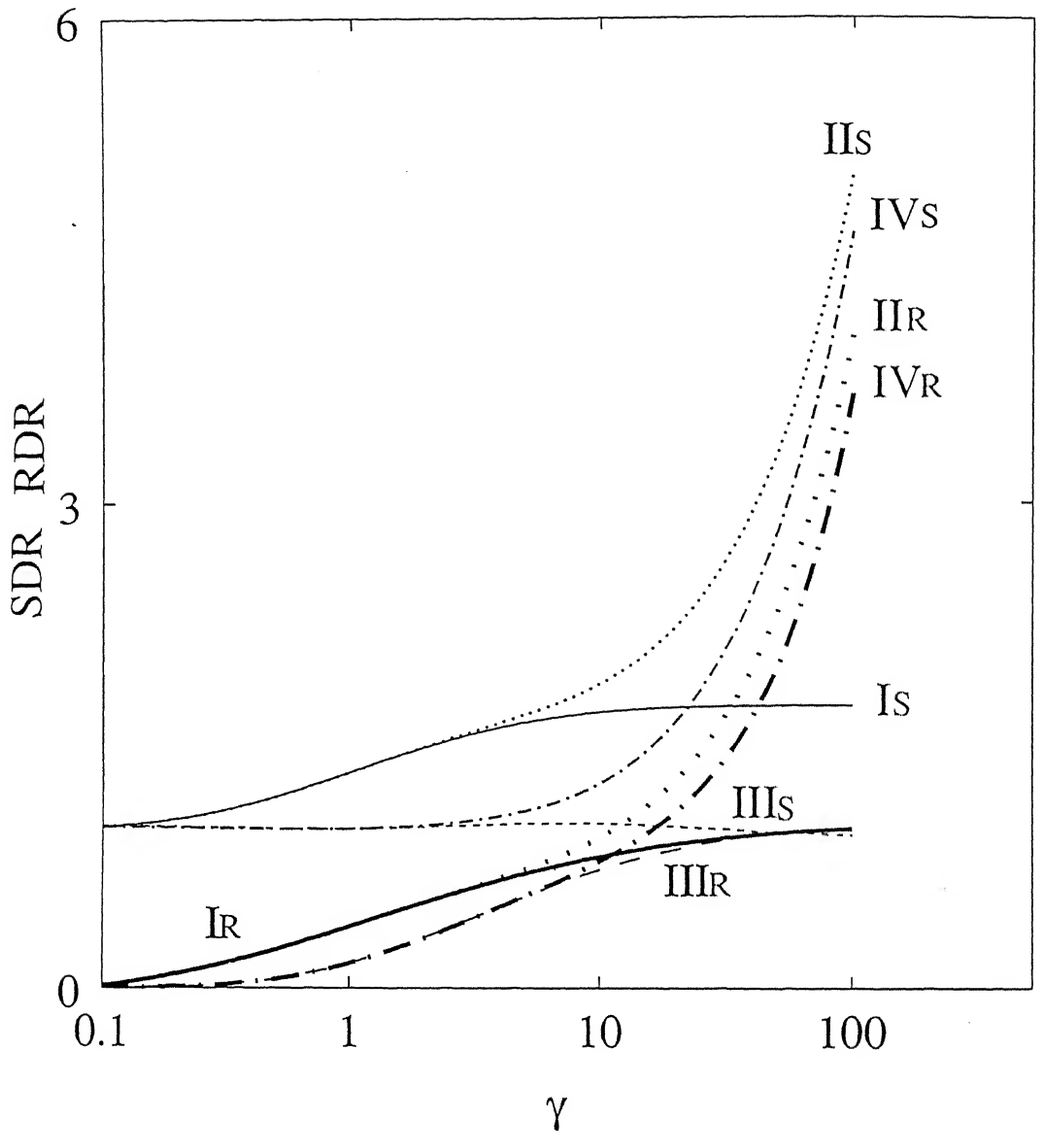

Figure 4.5: SDR and RDR curves for type 1 isolator as a function of γ for the rounded step displacement. I. linear damping $\zeta = 0.1$, II. linear + cubic damping $\zeta = 0.1, \delta^* = 0.01$, III. linear + Coulomb damping $\zeta = 0.1, \delta_f = 0.5$ and IV. linear + cubic + Coulomb damping $\zeta = 0.1, \delta^* = 0.01, \delta_f = 0.5$ (suffix S for SDR and R for RDR).

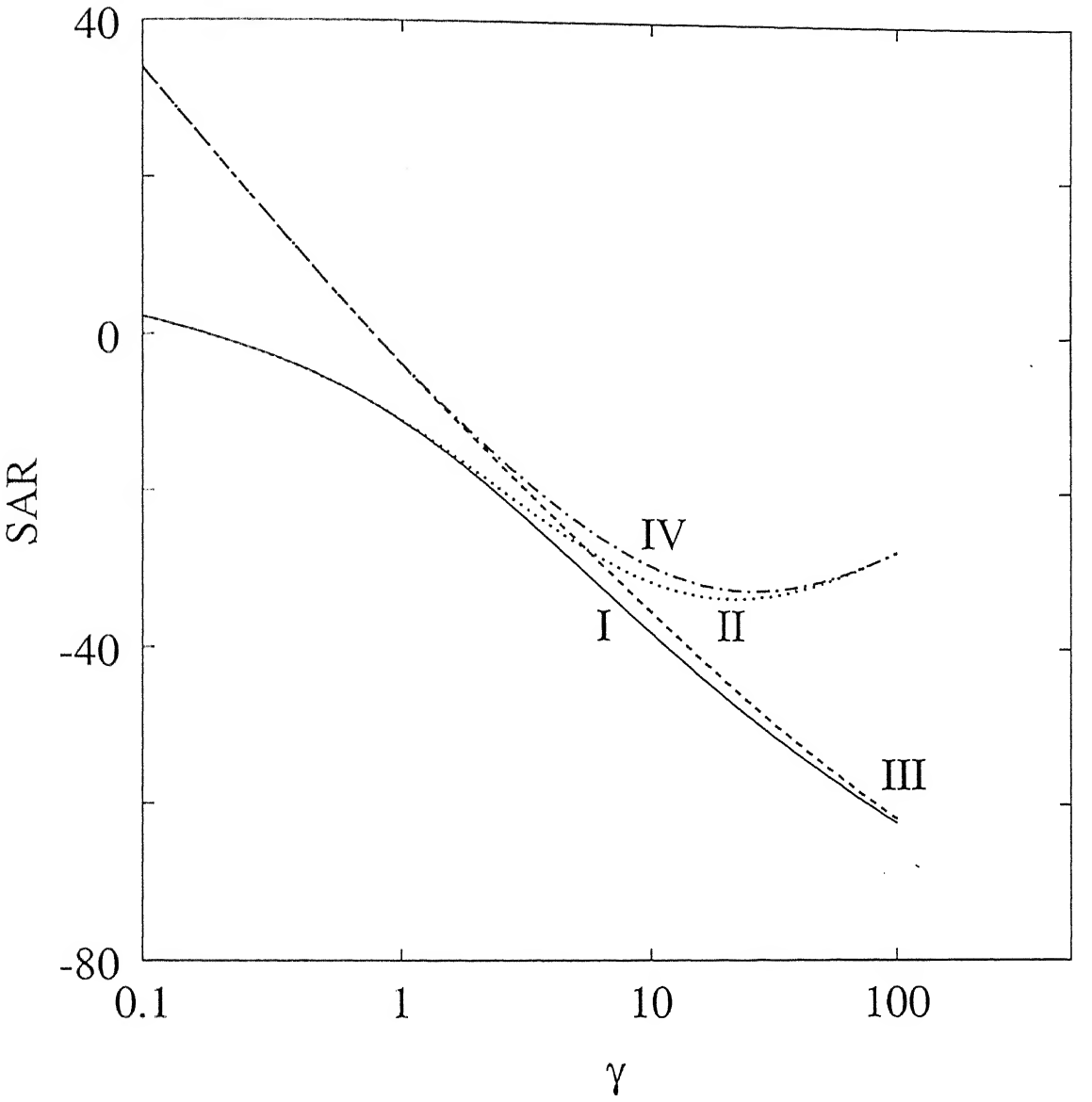

Figure 4.6: SAR curves in dB for type 1 isolator as a function of γ for the rounded step displacement. I. linear damping $\zeta = 0.1$, II. linear + cubic damping $\zeta = 0.1, \delta^* = 0.01$, III. linear + Coulomb damping $\zeta = 0.1, \delta_f = 0.5$ and IV. linear + cubic + Coulomb damping $\zeta = 0.1, \delta^* = 0.01, \delta_f = 0.5$

4.3.1 Type 1 Isolator

In this section, the effect of the Coulomb damping on the performance of a shock isolator system (equation (4.2)) is discussed. For the rounded step base excitation given by equation (2.4), the SDR, RDR and SAR curves are shown in Figures 4.5 and 4.6, as a function of the severity parameter γ.

It is evident by comparing curves I (linear damping) and II (linear + cubic damping) in Figures 4.5 and 4.6, that even for a reasonable severity parameter ($\gamma > 5$), the cubic damping is always detrimental to the isolator system. If a Coulomb damper is added in parallel to the linear viscous damper, then both the SDR and RDR are reduced as is evident by comparing the cases I and III in Figure 4.5. The SAR curve in Figure 4.6 shows somewhat worse response for low γ, i.e., the SAR values (case III) are high for small γ in the presence of Coulomb damping. This is due to the combination of a high value of the Coulomb damping coefficient ($\delta_f = 0.5$) and a low excitation level for small γ. With the inclusion of a Coulomb damper to a (linear + cubic) damped isolator, the SDR and RDR values (curve IV) asymptotically approach those without the Coulomb damper from below with increasing γ (Figure 4.5). However, in the case of SAR, the values without the Coulomb damper are approached from above when the Coulomb damper is incorporated (Figure 4.6). This is due to the high relative velocities at high severity parameters, which give rise to a high cubic damping force as compared to the constant Coulomb damping force.

In Figure 4.5, for the cases I, II and IV, SDR $\approx$ 1 + RDR, but for case III, SDR $\approx$ RDR with increasing γ. This is due to the fact that in the presence of Coulomb damping, the system comes to a rest before completing the first half cycle and the peaks of the relative and absolute displacements are approximately equal.

It is obvious from the above discussion, that if SDR is the design criterion for

a shock isolator system, then the inclusion of a Coulomb damper is helpful. It was observed that if the severity parameter is indeed high, then increasing the Coulomb damping reduces the SDR values. For example, for $\gamma = 50$, the parameter combination $\zeta = 0.1, \delta^* = 0.01, \delta_f = 0.5$ yields SDR = 1.994, whereas with $\zeta = 0.1, \delta^* = 0.01, \delta_f = 1.0$ the SDR value is reduced to 1.598.

The response results with the other two types of inputs, given by equations (2.6) and (2.7) are qualitatively similar to what has been just discussed and therefore, are not repeated.

The normal stick-slip phenomenon in the presence of Coulomb damping was not observed with these transient excitations. Once the system sticks, it does not slip again.

4.3.2 Type 2 Isolator

Snowdon[4] has studied a three element isolator with linear elements and concluded that its performance is better than that of a two element isolator. This is specially so at high values of the severity parameter. In this section, the performance of a three element isolator in the presence of cubic damping is discussed. Figures 4.7 and 4.8 show the SDR, the RDR and the SAR curves as a function of the severity parameter γ for the rounded step excitation. In these Figures, the curve V refers to the three element isolator, for $n = 1$, with all other parameter values same as in the previous section. It may be noted that, a three element isolator reduces the SDR and the RDR values close to those with the linear two-element isolator, even in the presence of cubic damping. This is true for all values of the severity parameter.

Figure 4.8 reveals that for $\gamma > 10$, the SAR values with the three element isolator are much lower than those with the linear two element isolator. The effect of the spring-ratio parameter, n, on the SDR is shown in Figure 4.9 for $\gamma = 50$. It is clear from

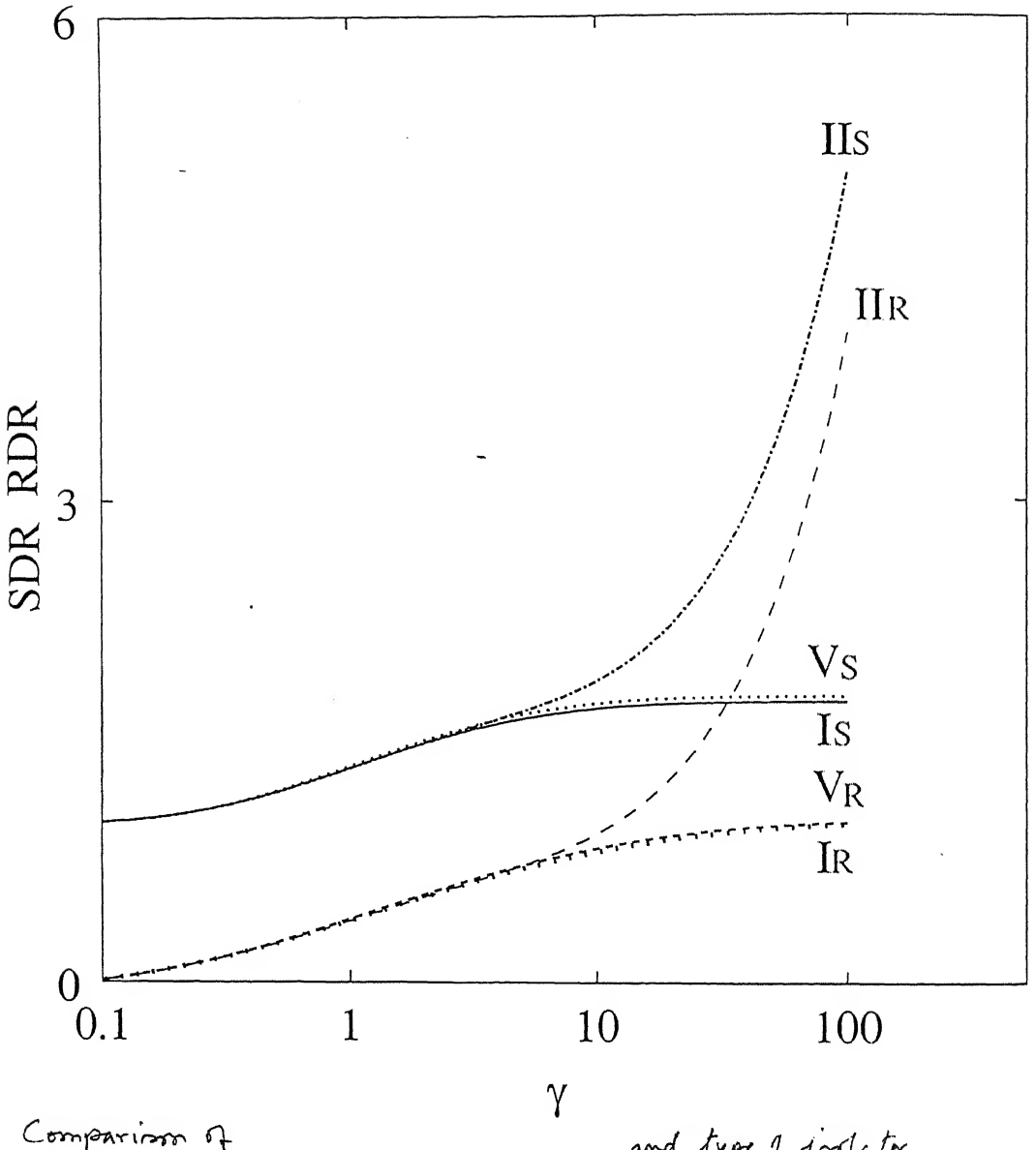

Comparison of and type 1 isolator

Figure 4.7: SDR and RDR curves for type 2 isolator as a function of γ for the rounded step displacement. I. linear damping $\zeta = 0.1$, II. linear + cubic damping $\zeta = 0.1, \delta^* = 0.01$, V. type 2 isolator $\zeta = 0.1, \delta^* = 0.01, n = 1$ (suffix S for SDR and R for RDR).

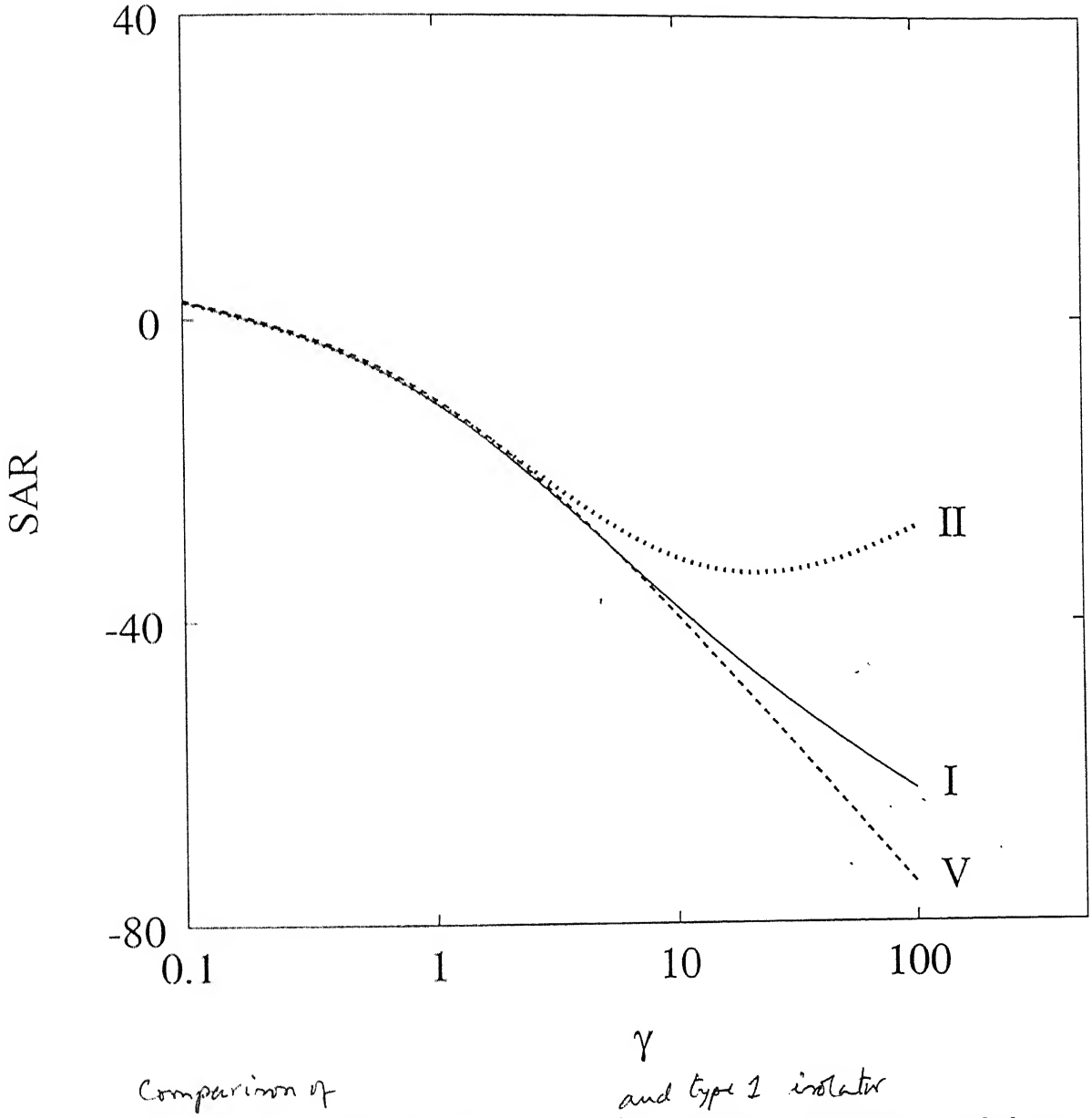

Figure 4.8: SAR curves in dB for type 2 isolator as a function of γ for the rounded step displacement. I. linear damping $\zeta = 0.1$, II. linear + cubic damping $\zeta = 0.1, \delta^* = 0.01$, V. type 2 isolator $\zeta = 0.1, \delta^* = 0.01, n = 1$.

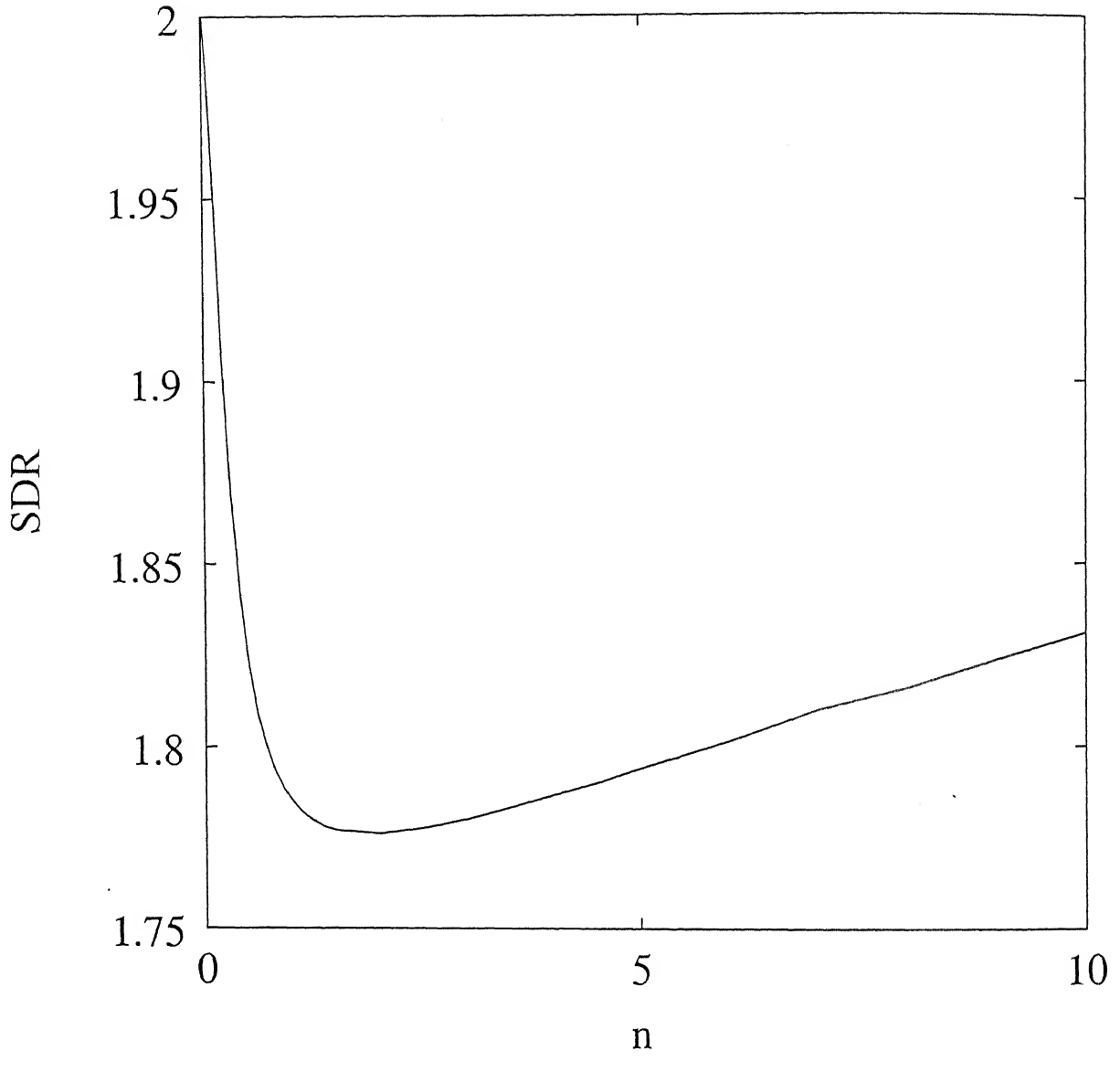

Figure 4.9: The effect of stiffness ratio (n) on the SDR in type 2 isolator for the rounded step displacement at $\gamma = 50$ ($\zeta = 0.1, \delta^* = 0.01$)

this Figure, that the optimum value of n is near 1. Furthermore, the value of n can be somewhat larger than this $n_{optimum}$ without much appreciable effect but reducing n from $n_{optimum}$ is undesirable.

Comparison of Figures 4.5 and 4.6 with Figures 4.7 and 4.8, respectively, reveals that, at high severity parameters, the performance of a three element isolator is better than that of the type 1 isolator. Therefore, to nullify the cubic damping effect, it is better to mount the cubic damper elastically for a single-stage shock isolator.

Similar trends were observed for all types of excitations.

4.3.3 Type 3 Isolator

Snowdon [4] has also studied a transient vibration absorber attached to an isolator with linear elements and concluded that when the absorber is of optimum design, the motion of the mounted item decays very rapidly with time. He also concluded that the maximum acceleration of the mounted item is considerably reduced by the dynamic absorber when γ is large. In this section, the effects of attaching a vibration absorber over and above the nonlinear isolator are discussed. Figures 4.10 to 4.13 show the SDR and the SAR curves as a function of the severity parameter γ for different types of excitation. In these Figures, curve VI corresponds to a transient vibration absorber, for $\mu = 0.5$, $\zeta_2 = 0.1$ and $\delta_2 = 0.01$, with all other parameter values same as in the previous section.

As shown in Figure 4.10, the vibration absorber does reduce the SDR values for a rounded step displacement excitation (compared to that for the linear plus cubic damped isolator) at high values of the severity parameter ($\gamma > 10$). This reduction is large at high severity parameters, but the SDR values are still much higher than those with the linearly damped isolator. However, for the oscillatory step excitation (Figure 4.11)), the SDR values are lower than even that with the linearly damped isolator at

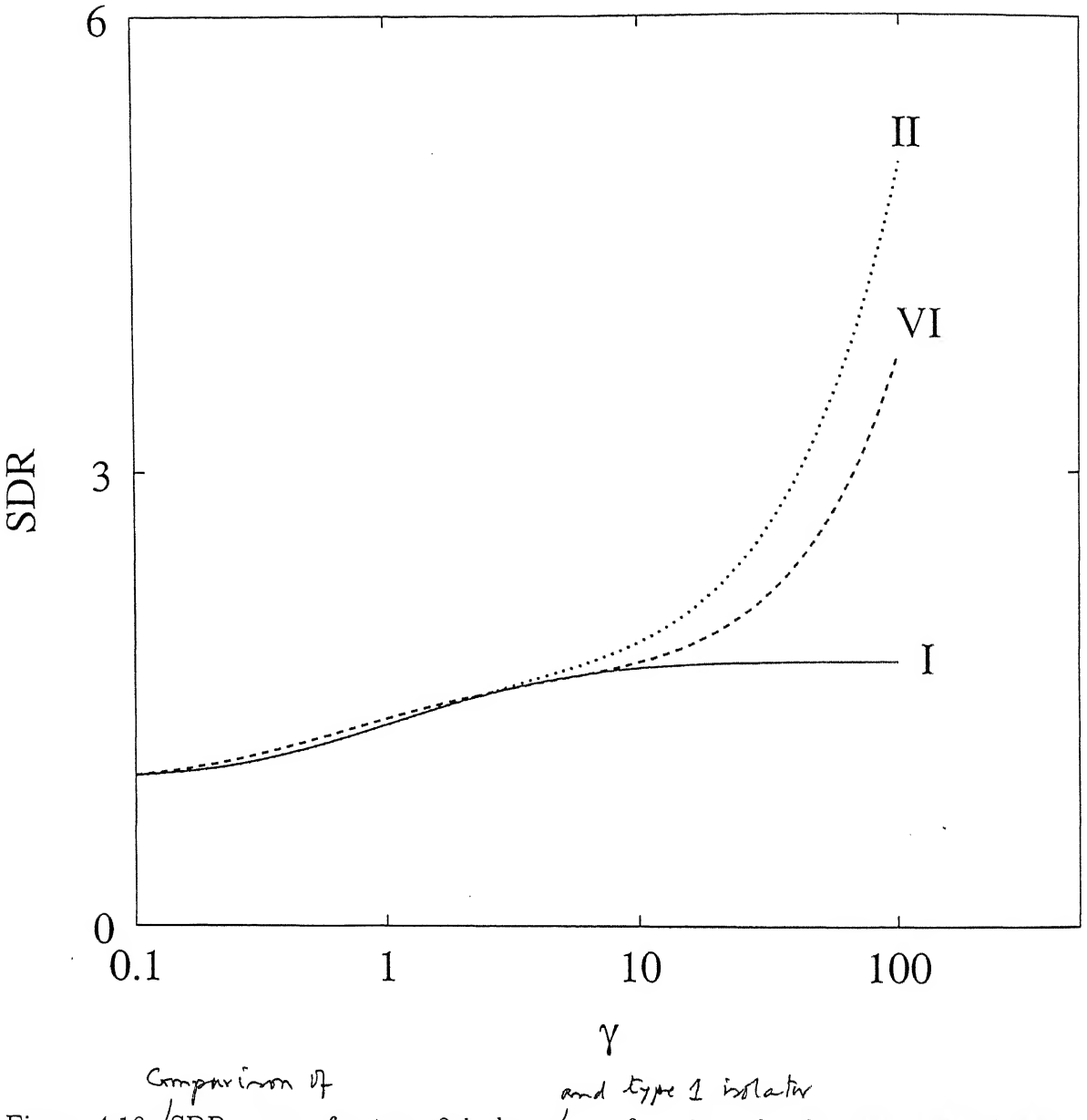

Figure 4.10: SDR curves for type 3 isolator as a function of γ for the rounded step displacement. I. linear damping $\zeta = 0.1$, II. linear + cubic damping $\zeta = 0.1, \delta^* = 0.01$, VI. type 3 isolator $\zeta = 0.1, \delta^* = 0.01, n = 1, \delta_2 = 0.01, \mu = 0.5$

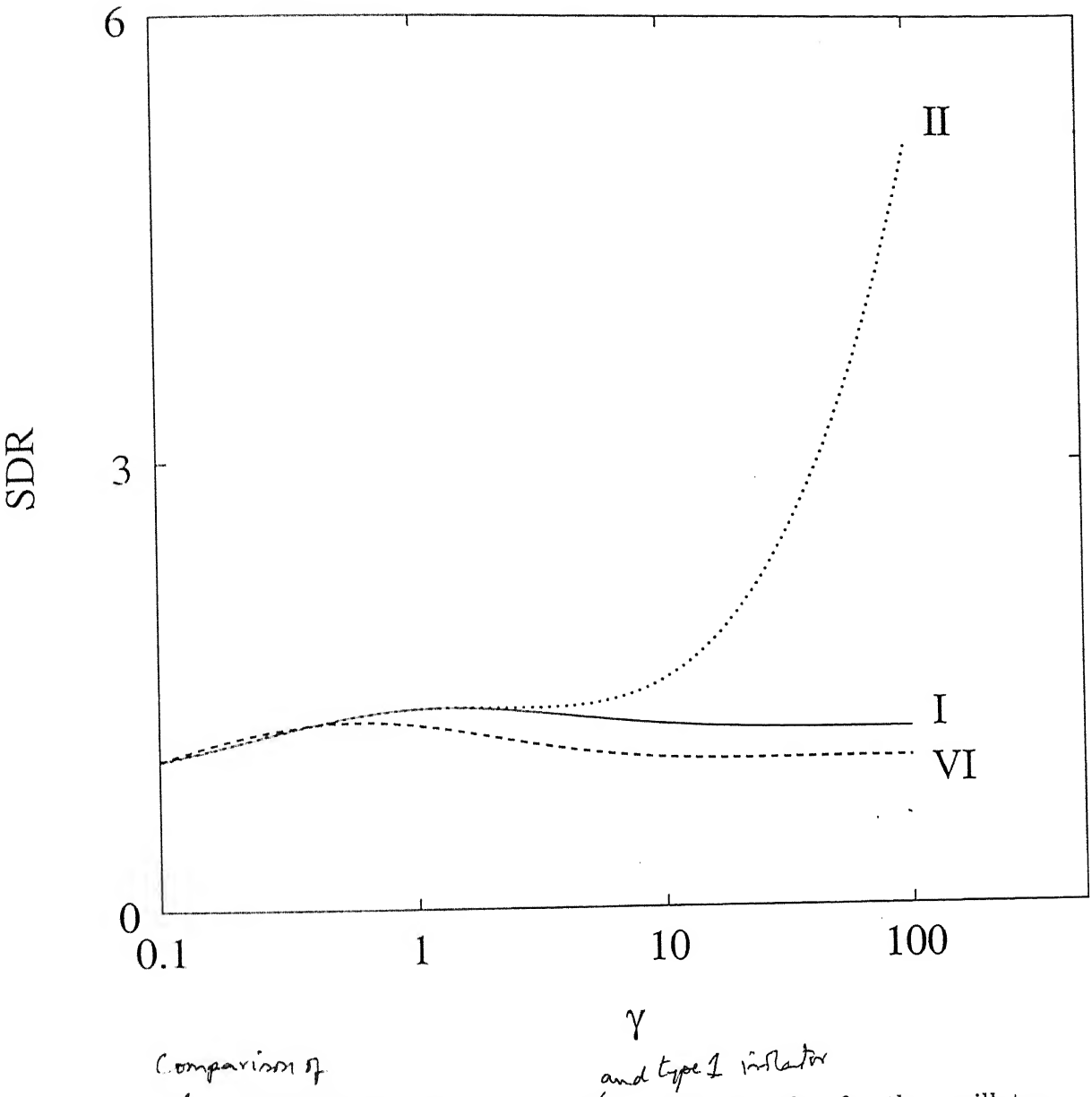

Figure 4.11: SDR curves for type 3 isolator as a function of γ for the oscillatory displacement step. I. linear damping $\zeta = 0.1$, II. linear + cubic damping $\zeta = 0.1, \delta^* = 0.01$, VI. type 3 isolator $\zeta = 0.1, \delta^* = 0.01, n = 1, \delta_2 = 0.01, \mu = 0.5$

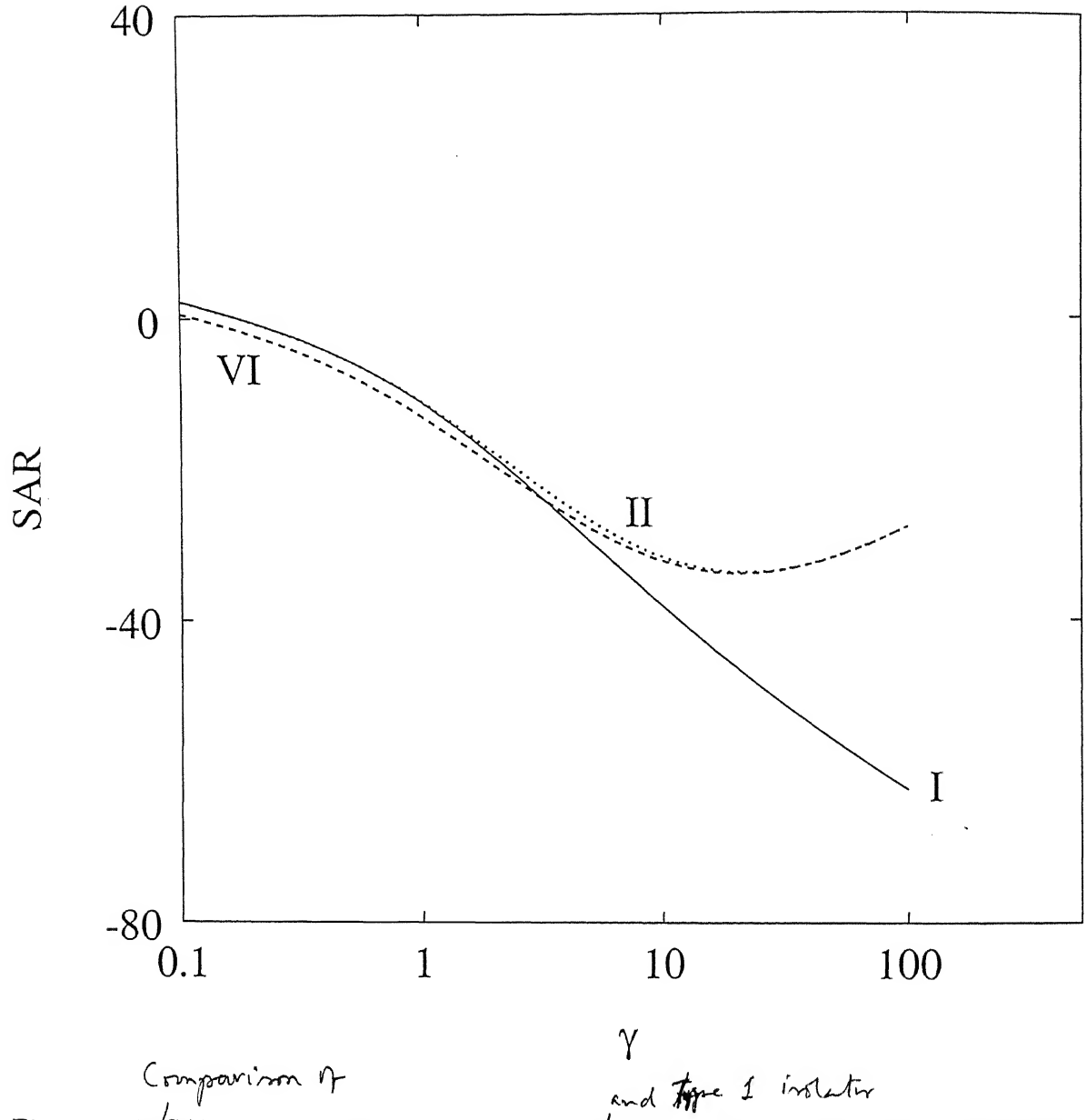

Figure 4.12: SAR curves in dB for type 3 isolator as a function of γ for the rounded step displacement. I. linear damping $\zeta = 0.1$, II. linear + cubic damping $\zeta = 0.1, \delta^* = 0.01$, VI. type 3 isolator $\zeta = 0.1, \delta^* = 0.01, n = 1, \delta_2 = 0.01, \mu = 0.5$

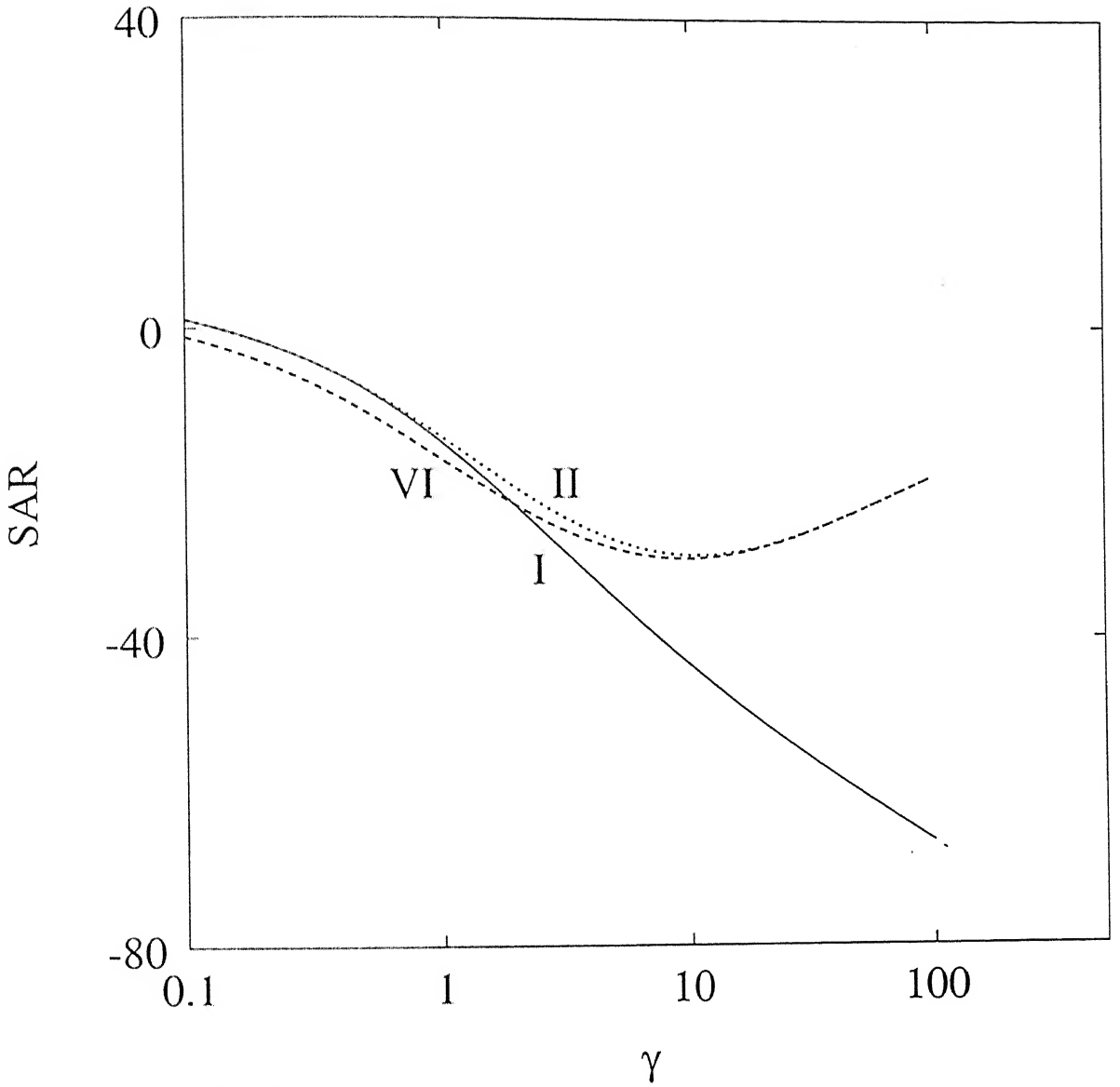

Comparison of and type 1 isolator

Figure 4.13: SAR curves in dB for type 3 isolator as a function of γ for the rounded pulse displacement. I. linear damping $\zeta = 0.1$ for type 1 isolator II. linear + cubic damping $\zeta = 0.1, \delta^* = 0.01$ for type 1 isolator VI. type 3 isolator $\zeta = 0.1, \delta^* = 0.01, n = 1, \delta_2 = 0.01, \mu = 0.5$

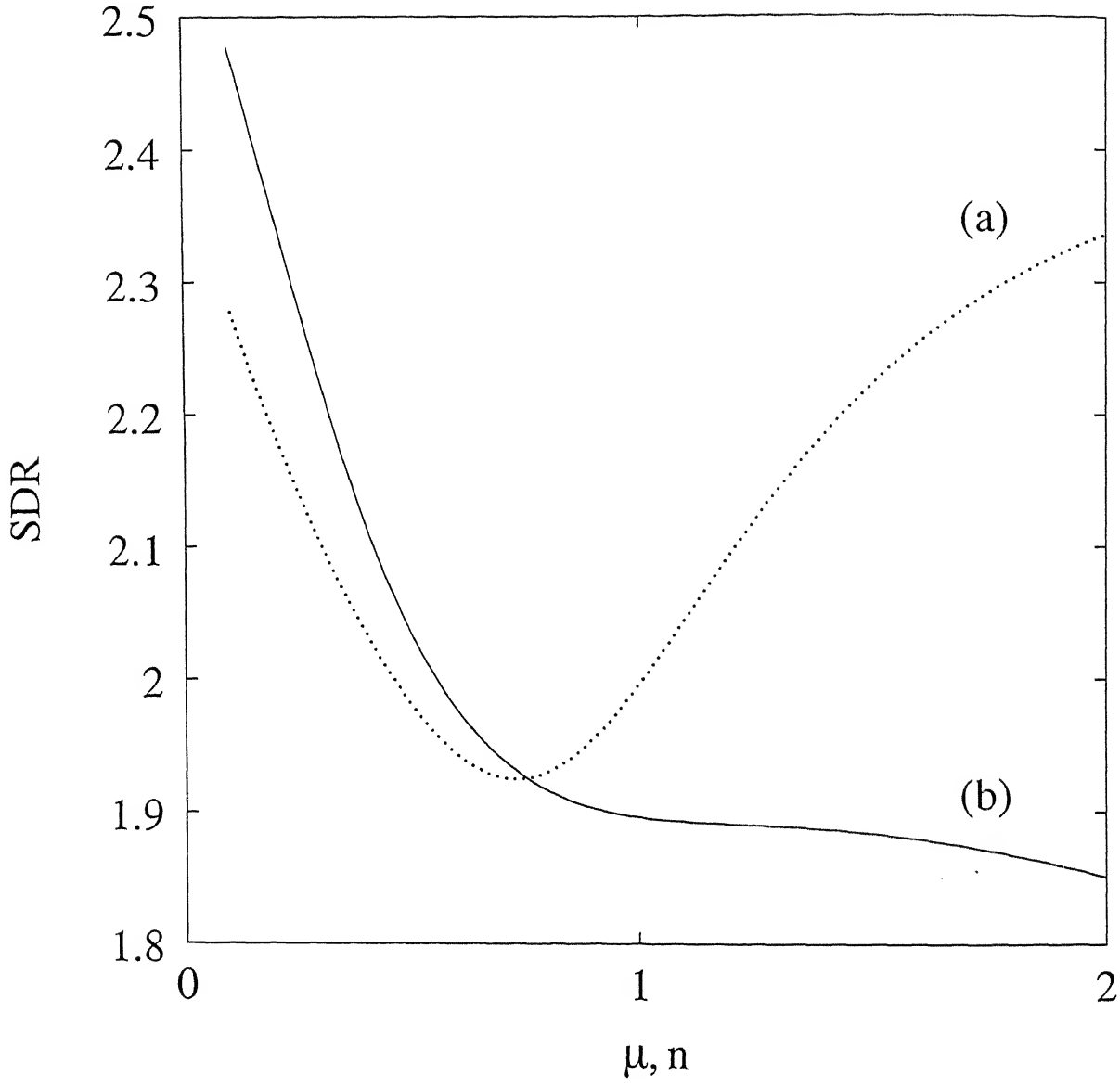

Figure 4.14: Curve (a): The effect of stiffness ratio (n) on the SDR in type 3 isolator, for the rounded step displacement at $\gamma = 50$ ($\zeta = 0.1, \delta^* = 0.01, \delta_2 = 0.01, \mu = 0.5$). Curve (b): The effect of mass ratio (μ) on the SDR in type 3 isolator, for the rounded step displacement at $\gamma = 50$ ($\zeta = 0.1, \delta^* = 0.01, \delta_2 = 0.01, n = 1.0$)

all severity parameters ($\gamma > 0.5$). From the results obtained (not presented here) the SDR curve for the rounded pulse is similar to that with the rounded step and the RDR curves for all the three types of excitations are qualitatively similar to the SDR curves. The SAR curves for the rounded step and the rounded pulse are shown in Figures 4.12 and 4.13, respectively. From these Figures we may conclude that the SAR values are not reduced by using a vibration absorber. Thus, inclusion of a vibration absorber may be useful only for the oscillatory step excitation, when the SDR and RDR values are reduced.

The effects of the mass ratio (μ) and the stiffness ratio (n) on the SDR are shown in Figure 4.14. It is readily seen that for $\mu > 0.7$, the SDR is almost independent of μ; whereas the SDR increases sharply with decreasing μ for $\mu < 0.7$. So far as the stiffness ratio is concerned, the SDR is minimum for $n = 0.8$. It was observed that this optimum value of n remains close to 0.8 for all values of μ. The RDR and the SAR values were found to be insensitive to the changes in the mass and stiffness ratios.

From a parametric investigation (not presented here), it has been found that the effects of the other secondary system parameters (ζ_2 and δ_2) on the SDR, RDR and SAR are not appreciable. The values of the SDR, RDR and SAR do not depend on whether the secondary system is linear or nonlinear. Thus, the absorber system may as well be linear.

4.3.4 Type 4 Isolator

In this section, the performance of a two stage isolator is compared with that of the (linear + cubic) damped isolator. Figures 4.15 and 4.16 show the SDR and SAR curves, respectively, as a function of the severity parameter γ. In these Figures, curve VII refers to a two stage isolator, for $\mu = 0.1$, with all other parameter values same as in the previous section.

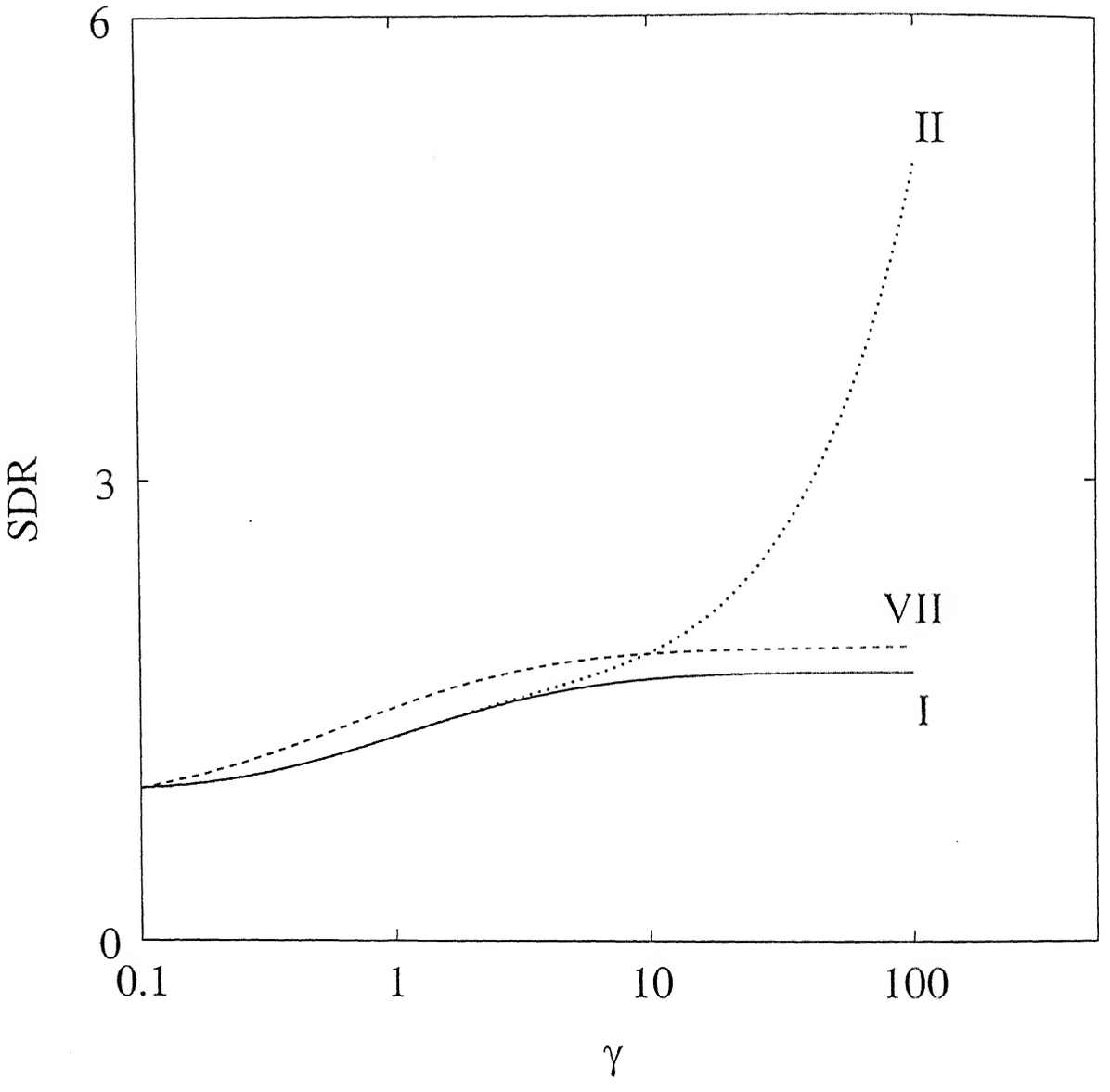

Figure 4.15: SDR curves for type 4 isolator as a function of γ for the rounded step displacement. I. linear damping $\zeta = 0.1$, II. linear + cubic damping $\zeta = 0.1, \delta^* = 0.01$, VII. type 4 isolator $\zeta = 0.1, \delta^* = 0.01, n = 1, \delta_2 = 0.01, \mu = 0.1$

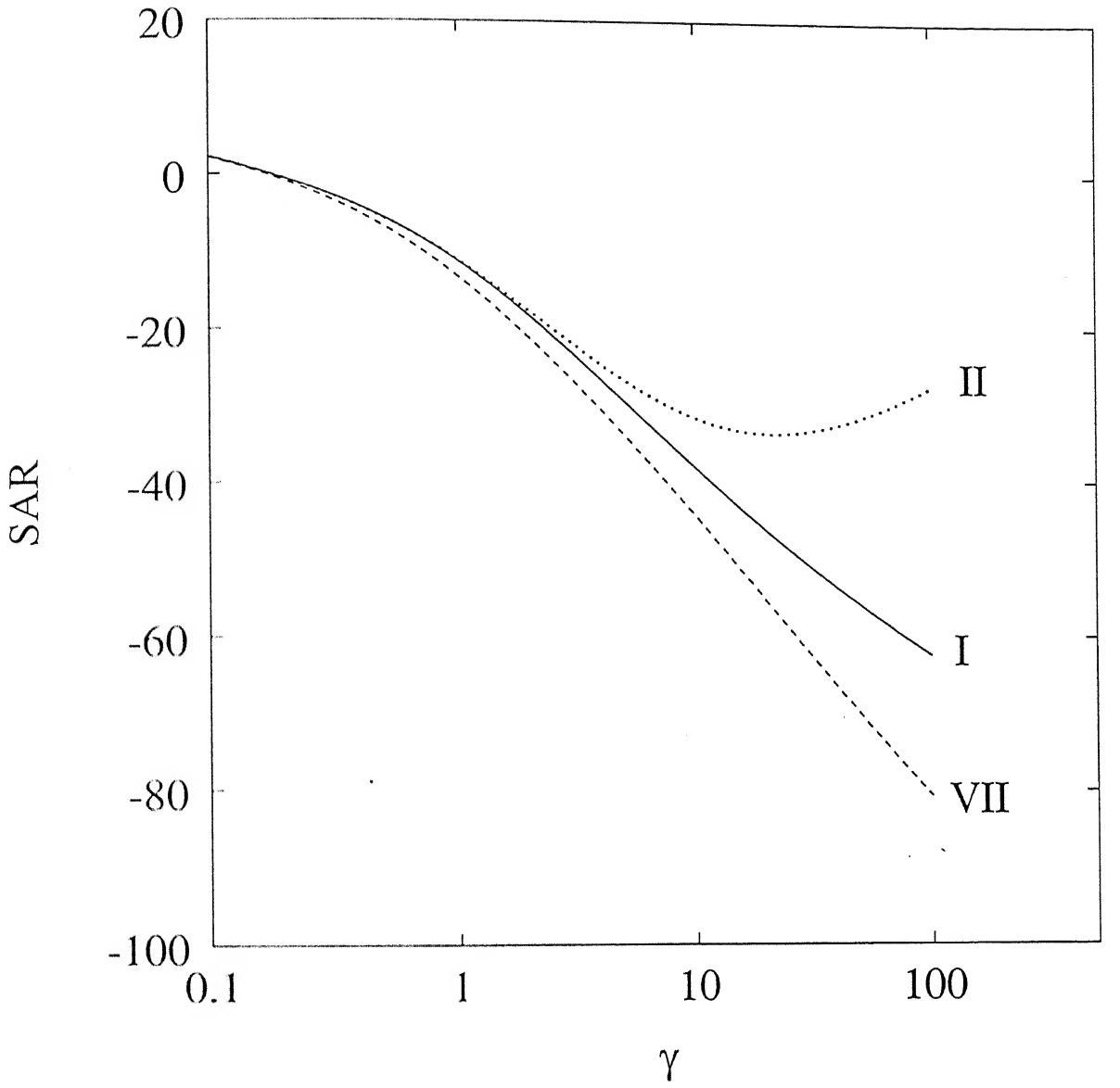

Figure 4.16: SAR curves in dB for type 4 isolator as a function of γ for the rounded step displacement. I. linear damping $\zeta = 0.1$, II. linear + cubic damping $\zeta = 0.1, \delta^* = 0.01$, VII. type 4 isolator $\zeta = 0.1, \delta^* = 0.01, n = 1, \delta_2 = 0.01, \mu = 0.1$

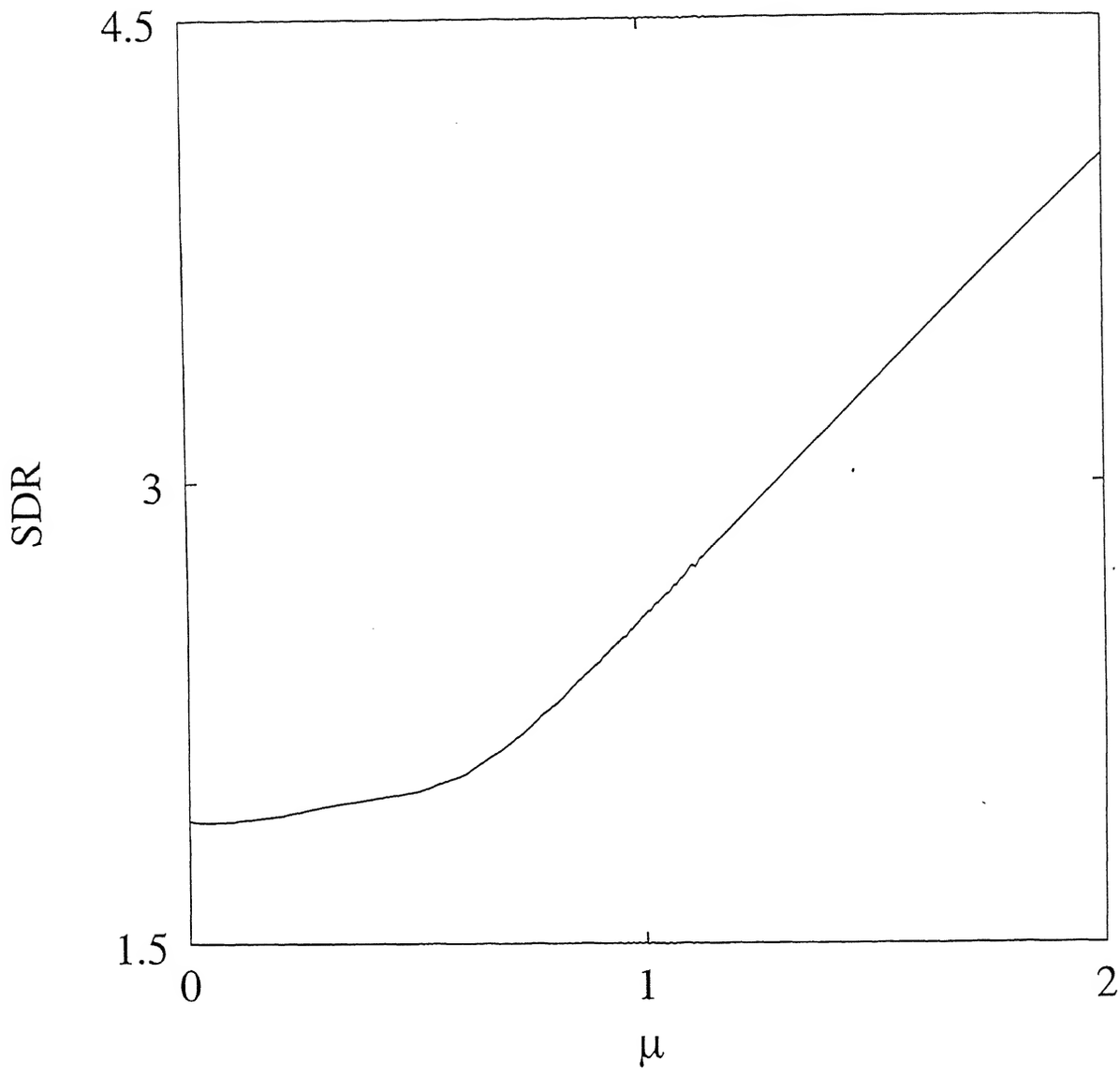

Figure 4.17: The effect of mass ratio (μ) on the SDR in type 4 isolator, for the rounded step displacement at $\gamma = 50$ ($\zeta = 0.1, \delta^* = 0.01, \delta_2 = 0.01, n = 1.0$)

As shown in Figure 4.15, the SDR curve for a two stage isolator is close to that of the linear isolator at all severity parameters for the rounded step excitation. The SAR curve for the two stage isolator is lower than that of the linear isolator at all severity parameters for the rounded step excitation as shown in Figure 4.16. The RDR curve (not shown here) is similar to the SDR curve for the rounded step excitation. For the rounded pulse and the oscillatory step excitations, the SDR, RDR and SAR curves (not shown here) were observed to be similar to those with the rounded step excitation. In the presence of cubic damping in the primary system, a two stage isolator is better than all other systems for reducing the SDR, RDR and SAR simultaneously at high severity parameters for all the three types of base excitations.

The effect of the mass ratio (μ) on the SDR is shown in Figure 4.17. For $\mu < 0.6$, the SDR is rather insensitive to the value of μ, but for $\mu > 0.6$, the SDR increases linearly with increasing mass ratio. This effect is opposite to what has been observed in the type 3 isolator.

It was further noted from the results not included here is that the SDR reduces with ζ_2 and n. The effect of the nonlinear damping of the secondary stage on SDR is negligible. Thus, like in the previous case, the secondary system may be taken as linear.

Chapter 5

2-DOF HEAVE-PITCH MODEL OF A VEHICLE FOR SHOCK EXCITATION

5.1 Introduction

In the previous chapters, we studied the effect of nonlinear damping on shock isolators in a single (heave) mode of vibration of a quarter-car vehicle model. In continuing with the investigation in a systematic manner, the next logical step would be to consider a two-dimensional (2-D) or half-car model, which includes vehicle pitch in addition to the sprung mass heave mode. The details of this 2-D model are given in the next section.

In this chapter, two of the four isolator (suspension) models discussed in chapter 4 are considered. The first one is a suspension system consisting of a two element isolator and the second one is elastically coupled three element isolator. With some special choice of parameters, equations are reduced to simpler forms amenable to analytical

solutions. For general nonlinear, coupled equations, numerical results are obtained with the rounded displacement step is considered as the input from the road bump. Like in a single (heave) mode SDOF model, it was observed that in this Heave-Pitch model also, nonlinear symmetric dissipative damping with positive coefficient is detrimental to shock isolation. The elastically coupled three element isolator nullifies the adverse effect of the nonlinear damping in this Heave-Pitch model as well.

5.2 System Models

5.2.1 Model I

The 2-DOF (Heave-Pitch) vehicle model with two element isolators is shown in Figure 5.1. The body structure of the vehicle is represented by a rigid body of mass m with moment of inertia I with respect to the centroidal axis perpendicular to the vehicle's plane of symmetry. The distances from the center of mass, to the front and rear axles, measured in the horizontal direction are a and b, respectively. The variables y_1 and y_2 denote base inputs due to road irregularities at the front and rear tyres, respectively. It is assumed that the rear tyres travel over the same path as the front tyres; hence y_2 is a delayed version of y_1, i.e., $y_2 = y_1(t - t_0)$, where $t_0 = \frac{a+b}{V}$, V is the forward speed, and $a + b = L$ is the vehicle wheel base. The body motion is described by the vertical displacement x of the center of mass and the angle of rotation θ about the centroidal axis, from the static equilibrium position shown in Figure 5.1.

From the previous chapters, we know that the effect of nonlinearity in stiffness on shock isolation performance is not predominant, so, here in model I shown in Figure 5.1, springs (k_1 and k_2) are considered linear. The dampers, however, are considered nonlinear with cubic nonlinearity superimposed on a linear term. Let x_1 and x_2 be

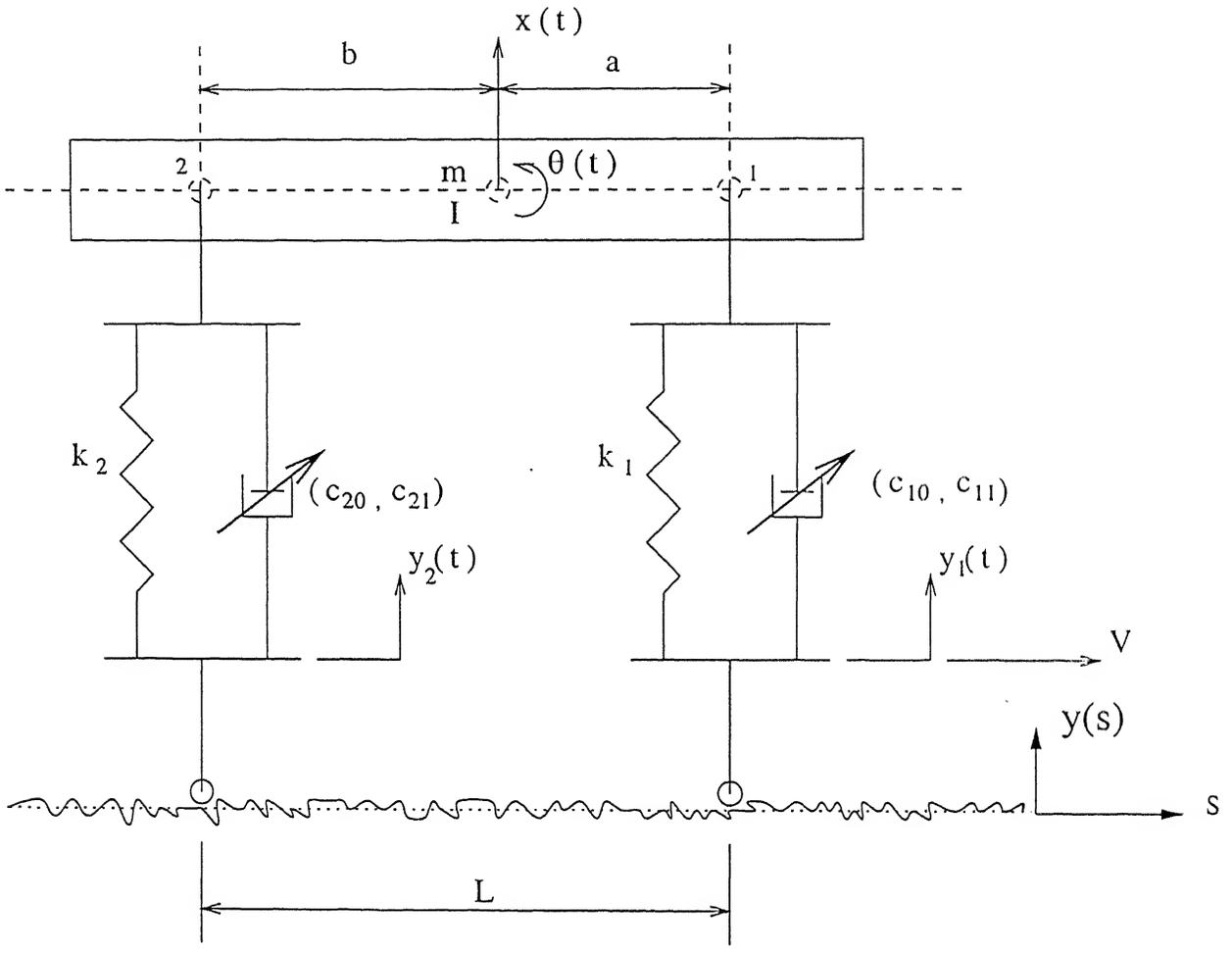

Figure 5.1: Heave-Pitch Model I

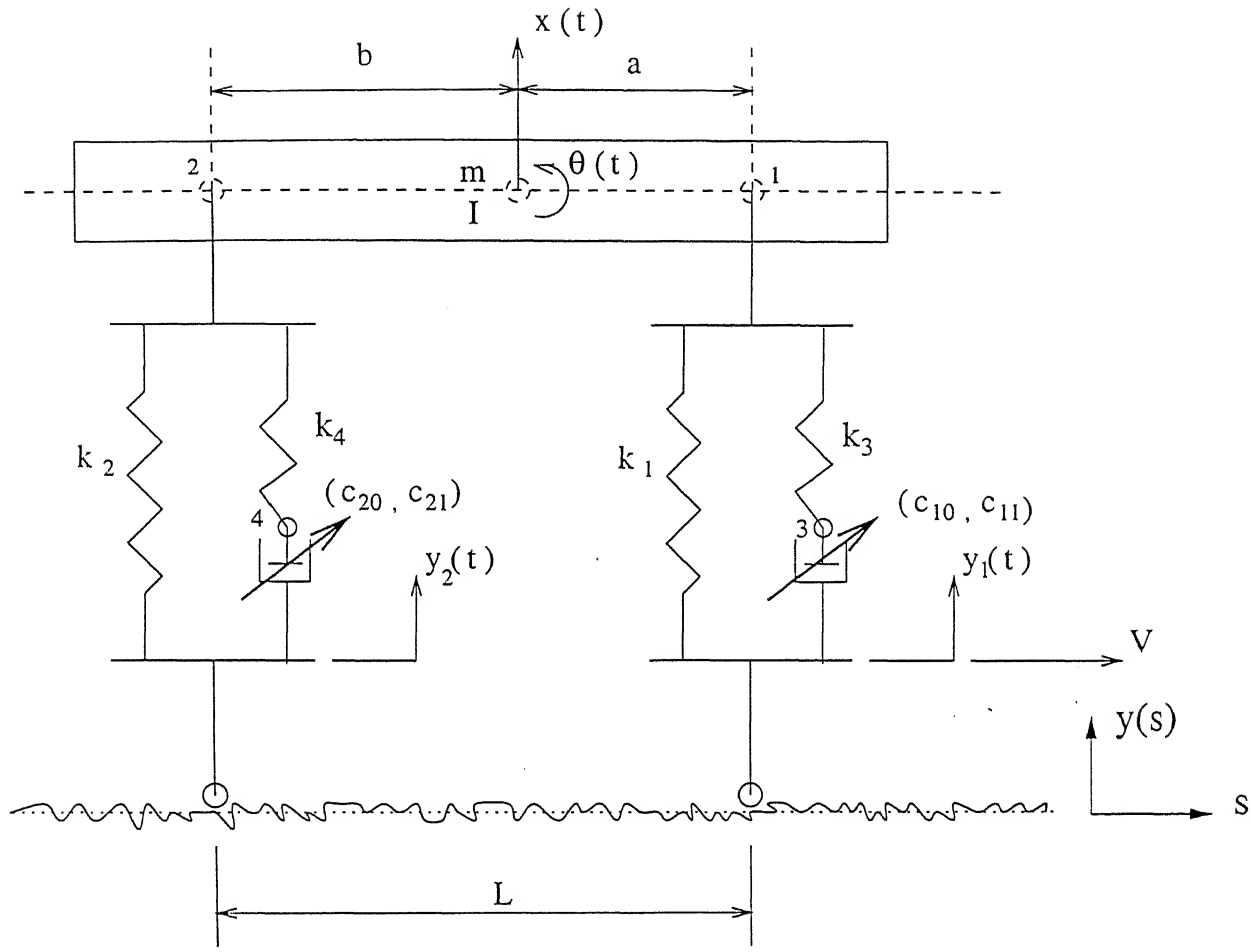

Figure 5.2: Heave-Pitch Model II

the vertical upward displacements, from the equilibrium position, at the points 1 and 2 respectively in Figure 5.1. The damping forces in the front and rear suspensions are $f_{d1} = c_{10}\dot{\Delta}_1 + c_{11}\dot{\Delta}_1^{\,3}$ and $f_{d2} = c_{20}\dot{\Delta}_2 + c_{21}\dot{\Delta}_2^{\,3}$ respectively; where, $\Delta_1 = x_1 - y_1$ and $\Delta_2 = x_2 - y_2$ are the relative displacements across the front and rear dampers in model I ; and dot denotes differentiation with respect to time t. It is assumed that the pitch motion, θ, is small.

Equations of motion for the model shown in Figure 5.1 are

$$m\ddot{x} + f_1 + f_2 = 0 \tag{5.1}$$

$$\text{and} \quad I\ddot{\theta} + f_1 a - f_2 b = 0 \tag{5.2}$$

where, f_1 and f_2 denote the downward front and rear suspension forces at points 1 and 2, and are given by

$$f_1 = k_1(x_1 - y_1) + c_{10}(\dot{x_1} - \dot{y_1}) + c_{11}(\dot{x_1} - \dot{y_1})^3 \tag{5.3}$$

$$\text{and} \quad f_2 = k_2(x_2 - y_2) + c_{20}(\dot{x_2} - \dot{y_2}) + c_{21}(\dot{x_2} - \dot{y_2})^3. \tag{5.4}$$

In addition, x_1 and x_2 are related to x and θ through

$$x_1 = x + a\theta \tag{5.5}$$

$$\text{and} \quad x_2 = x - b\theta. \tag{5.6}$$

In order to perform a parametric study, equations of motion (5.1) - (5.6) are written in non-dimensionalized form. The displacement variables are non-dimensionalized using y_{max}, which denotes the maximum value of the input displacement y_1 at the front wheel. The non-dimensionalized time is taken as $T = \omega_0 t$ where, $\omega_0 = \sqrt{(k_1 + k_2)/m}$. Thus the non-dimensional forms of equations (5.1) and (5.2) are

$$X'' + F_1 + F_2 = 0 \tag{5.7}$$

$$\text{and} \quad R^2 Z'' + F_1 - F_2 - \alpha(F_1 + F_2) = 0 \tag{5.8}$$

where, $X = \frac{x}{y_{max}}$; $Z = \frac{\theta L}{2y_{max}}$; $\alpha = \frac{b-a}{L}$; $R^2 = \frac{4I}{mL^2}$; $F_1 = \frac{f_1}{m\omega_0^2 y_{max}}$; $F_2 = \frac{f_2}{m\omega_0^2 y_{max}}$; prime denotes differentiation with respect to non-dimensionalized time T.

Equations (5.3) and (5.4) may be written in non-dimensionalized form as

$$F_1 = a_1(X_1 - Y_1) + 2\zeta_1(X_1' - Y_1') + \delta_1(X_1' - Y_1')^3 \tag{5.9}$$

$$\text{and} \quad F_2 = a_2(X_2 - Y_2) + 2\zeta_2(X_2' - Y_2') + \delta_2(X_2' - Y_2')^3. \tag{5.10}$$

where, $a_1 = \frac{k_1}{k_1+k_2}$; $a_2 = \frac{k_2}{k_1+k_2}$; $2\zeta_1 = \frac{c_{10}}{m\omega_0}$; $2\zeta_2 = \frac{c_{20}}{m\omega_0}$; $\delta_1 = \frac{c_{11}\omega_0 y_{max}^2}{m}$; $\delta_2 = \frac{c_{21}\omega_0 y_{max}^2}{m}$; $X_1 = \frac{x_1}{y_{max}}$; $X_2 = \frac{x_2}{y_{max}}$; $Y_1 = \frac{y_1}{y_{max}}$; and $Y_2 = \frac{y_2}{y_{max}}$.

From the geometry of the vehicle body, the relations between X_1, X_2, X, Z and α may be written as

$$X_1 = X + Z(1-\alpha) \tag{5.11}$$

$$X_2 = X - Z(1+\alpha) \tag{5.12}$$

$$X = [(1+\alpha)X_1 + (1-\alpha)X_2]/2 \tag{5.13}$$

$$\text{and} \quad Z = (X1 - X2)/2. \tag{5.14}$$

5.2.2 Model II

The 2-DOF (Heave-Pitch) vehicle model with three element isolators is shown in Figure 5.2. In this model II, both front and rear nonlinear dampers are elastically coupled. The front suspension nonlinear damper is coupled with a linear spring k_3 and the rear suspension nonlinear damper is coupled with a linear spring k_4. Like in model I, springs k_1 and k_2 are considered linear and all dampers $(C_{10}, C_{11}; C_{20}, C_{21})$ are considered nonlinear with cubic nonlinearity superimposed on a linear term. Let x_1, x_2, x_3 and x_4 be the vertical upward displacements, from equilibrium positions, at points 1,2,3 and 4 respectively, in Figure 5.2. The damping forces in the front and rear suspensions are

$f_{d1} = c_{10}\dot{\Delta}_1 + c_{11}\dot{\Delta}_1^{\,3}$ and $f_{d2} = c_{20}\dot{\Delta}_2 + c_{21}\dot{\Delta}_2^{\,3}$ respectively; where, $\Delta_1 = x_3 - y_1$ and $\Delta_2 = x_4 - y_2$ are the relative displacements across the front and rear dampers; and dot denotes differentiation with respect to time t. It is assumed that the pitch motion, θ, is small.

Equations of motion for the model shown in Figure 5.2 are

$$m\ddot{x} + f_1 + f_2 = 0 \tag{5.15}$$

$$\text{and} \quad I\ddot{\theta} + f_1 a - f_2 b = 0 \tag{5.16}$$

where, f_1 and f_2 denote the downward front and rear suspension forces at points 1 and 2 in Figure 5.2, and are given by

$$f_1 = k_1(x_1 - y_1) + k_3(x_1 - x_3) \tag{5.17}$$

$$\text{and} \quad f_2 = k_2(x_2 - y_2) + k_4(x_2 - x_4). \tag{5.18}$$

Equations of motion for the points 3 and 4 in Figure 5.2 may be written as

$$k_3(x_3 - x_1) + c_{10}(\dot{x}_3 - \dot{y}_1) + c_{11}(\dot{x}_3 - \dot{y}_1)^3 = 0 \tag{5.19}$$

$$\text{and} \quad k_4(x_4 - x_2) + c_{20}(\dot{x}_4 - \dot{y}_2) + c_{21}(\dot{x}_4 - \dot{y}_2)^3 = 0 \tag{5.20}$$

After non-dimensionalization, equations (5.15) - (5.20) may be written as

$$X'' + F_1 + F_2 = 0 \tag{5.21}$$

$$R^2 Z'' + F_1 - F_2 - \alpha(F_1 + F_2) = 0 \tag{5.22}$$

$$F_1 = a_1(X_1 - Y_1) + n_1(X_1 - X_3) \tag{5.23}$$

$$F_2 = a_2(X_2 - Y_2) + n_2(X_2 - X_4) \tag{5.24}$$

$$n_1(X_3 - X_1) + 2\zeta_1(X_3' - Y_1') + \delta_1(X_3' - Y_1')^3 = 0 \tag{5.25}$$

$$\text{and} \quad n_2(X_4 - X_2) + 2\zeta_2(X_4' - Y_2') + \delta_2(X_4' - Y_2')^3 = 0 \tag{5.26}$$

where $X_3 = \frac{x_3}{y_{max}}$; $X_4 = \frac{x_4}{y_{max}}$; $n_1 = \frac{k_3}{k_1+k_2}$; $n_2 = \frac{k_4}{k_1+k_2}$; and remaining other non-dimensionalized variables are same as those in model I.

5.3 Theoretical Analysis for Special Cases

In general, dynamic equations for both model I (equations (5.7) and (5.8)) and model II (equations (5.21) and (5.22)) are not amenable to theoretical analysis and also it is not possible to solve them analytically in closed form, because these equations are coupled and nonlinear. However, for some special choices of parameters, these equations are reduced to simpler forms. Under these conditions, some general isolation characteristics can be extracted without numerical integration of the equations of motion. In this section, we discuss these special cases. For all the dynamic equations of motion, initial conditions $X = X' = Z = Z' = 0$ at $T = 0$ are assumed.

5.3.1 Symmetric System

The simplest system is the symmetric system, in which the front and rear suspension characteristics are identical and the offset parameter α is zero. For $R = 1$ and $Y_2 = Y_1$, the symmetric system behaves like an SDOF system with $X = X_1 = X_2$ and $Z \equiv 0$. This SDOF system is similar to the two element isolator system without nonlinear stiffness in chapter 2 for model I and is similar to the three element isolator system in chapter 4 for model II.

From Chapter 2, we already know that the presence of nonlinear damping is detrimental to SDOF two element isolator. From Chapter 4, we know that the three element isolator nullifies the adverse effect of nonlinear damping.

5.3.2 Decoupled System

From equations (5.13), (5.14) and for

$$R^2 = 1 - \alpha^2, \tag{5.27}$$

equations (5.21) and (5.22) may be simplified as

$$(1+\alpha)X_1'' + 2F_1 = 0 \tag{5.28}$$

and

$$(1-\alpha)X_2'' + 2F_2 = 0. \tag{5.29}$$

Equation (5.27) implying $I = mab$ is called as the decoupling condition. If this condition is satisfied, then the 2-DOF system reduces to two SDOF systems (equations (5.28) and (5.29)) with mass $m_1 = mb/L$ at point 1 and mass $m_2 = ma/L$ at point 2, which are connected by a massless rod. The above nonlinear decoupled equations (5.28) and (5.29) for model I can be solved analytically by using the perturbation method, explained in the second chapter for shock excitations.

Without solving the decoupled equations (5.28) and (5.29); we can deduce the relation between X and Z for three special inputs of Y_1 and Y_2.

Case I: $Y_2 = 0$ **for** $T \geq 0$

This case occurs in practice, when the vehicle moves forward very slowly. Equation (5.29) gives $X_2 \equiv 0$ for $Y_2 = 0$ (see equation (5.9) for model I and equations (5.24) and (5.26) for model II). Equation (5.12) gives $X = Z(1+\alpha)$ and equation (5.14) gives $Z = X_1/2$ for $X_2 = 0$. In this case it is sufficient to solve only one equation viz., equation (5.28), to determine the responses X and Z. Heave and pitch modes are linearly dependent and their ratio $X/Z = 1+\alpha$ is a constant. For $\alpha = 0$, $X = Z$; this is an example of a repeated eigenvalue and eigenvectors problem in 2-DOF system and both natural frequencies and normal modes are identical.

Case II: $Y_2 = Y_1(T - T_0)$ **for** $T > 0$ **and** $T_0 = L\omega_0/V > 0$

In this case, the system behaviour is similar to the previous case, up to $T < T_0$; it means that the input at the rear wheel $Y_2(T) = 0$ for $T < T_0$; hence, $X_2(T) = 0; X(T) = (1+\alpha)Z(T)$ and $Z(T) = X_1(T)/2$ for $T < T_0$. At $T = T_0$, there will be a sudden change in the heave and pitch responses, due to input y_2 at the rear wheel. In shock excitations the maximum peak occurs during the first cycle. If T_0 is less than the time required to attain the maximum peak due to input y_1 at the front suspension, only then input y_2 can alter the maximum peak. So, it is important to study the response at low values of T_0, which correspond to high vehicle speeds.

Let us assume that

$$F_1 = (1+\alpha)\bar{F}(X_1, X_1', Y_1, Y_1') \tag{5.30}$$

and

$$F_2 = (1-\alpha)\bar{F}(X_2, X_2', Y_2, Y_2'), \tag{5.31}$$

then equations (5.28) and (5.29) may be rewritten as

$$X_1'' + 2\bar{F}(X_1, X_1', Y_1, Y_1') = 0 \tag{5.32}$$

and

$$X_2'' + 2\bar{F}(X_2, X_2', Y_2, Y_2') = 0. \tag{5.33}$$

Equations (5.32) and (5.33) are similar and independent of α. Since, Y_2 is a delayed version of Y_1; i.e., $Y_2(T) = Y_1(T - T_0)$; X_2 will also be a delayed version of X_1; i.e., $X_2(T) = X_1(T - T_0)$.

The assumption in equations (5.30) and (5.31) is indirectly putting a condition on the characteristics of the front and rear suspension springs and dampers. It implies that, the stiffness ratios $(a_1/a_2; n_1/n_2)$, the linear damping coefficients ratio (ζ_1/ζ_2) and the nonlinear damping coefficients ratio (δ_1/δ_2) of the front to the rear suspensions are simultaneously equal to $\frac{1+\alpha}{1-\alpha} = b/a$. In other words,

$$a_1/a_2 = \zeta_1/\zeta_2 = \delta_1/\delta_2 = n_1/n_2 = b/a. \tag{5.34}$$

This condition i.e., equation (5.34) may be called as the 'invariant ratio', which, when satisfied, renders X_1 and X_2 invariant to α. From equation (5.14) it can be deduced that, $Z(T)$ is also invariant to α.

Case III: $Y_2 = Y_1$

This case occurs in practice when the input excitation Y_1 is periodic with period $T_0 > 0$, that means both wheels are subjected to the same input simultaneously. For $Y_1 = Y_2$, equations (5.32) and (5.33) are identical to each other, which implies $X_1 = X_2$. From equations (5.13) and (5.14) it can be concluded that $X = X_1 = X_2$ and $Z \equiv 0$. Even though the system is asymmetric ($b > a$); in this special case $Y_2 = Y_1$ and under the assumption of invariant ratio given by equation (5.34), the decoupled system behaves as if it is symmetric (Section 5.3.1). We know from calculus of variations that a symmetric system always gives optimum response. In our vehicle model, to satisfy the assumption of invariant ratio, front to rear stiffness and damping ratios should be b/a, which is always greater than unity, for forward center of mass ($b > a$).

The discussions presented above for the three special cases are true for any type of excitation (i.e., harmonic, random and transient).

5.3.3 Linear System

In this section, the solution of a linear system for model I is obtained by using Laplace transform. This solution has been used for studying the effect of linear damping on vehicle suspension performance for model I. For the linear system ($\delta_1 = \delta_2 = 0$), equations of motion (5.7) - (5.10) reduce to

$$X'' + F_1 + F_2 = 0, \tag{5.35}$$

$$R^2 Z'' + F_1 - F_2 - \alpha(F_1 + F_2) = 0, \tag{5.36}$$

$$F_1 = a_1(X_1 - Y_1) + 2\zeta_1(X_1' - Y_1') \tag{5.37}$$

$$\text{and} \quad F_2 = a_2(X_2 - Y_2) + 2\zeta_2(X_2' - Y_2'). \tag{5.38}$$

The solution of linear equations (5.35) and (5.36) for initial conditions $X = X' = Z = Z' = 0$ at $T = 0$ is expressed as the algebraic sum of two responses one due to only input Y_1 and the other due to only input $Y_2 = Y_1(T - T_0)$.

Let X_f and X_b be the heave mode responses due to inputs Y_1 and Y_2, respectively, and Z_f and Z_b be the pitch mode responses due to inputs Y_1 and Y_2, respectively. Now, the heave (X) and pitch (Z) mode responses may be expressed as

$$X(T) = X_f(T) + X_b(T - T_0)u(T - T_0) \tag{5.39}$$

$$\text{and} \quad Z(T) = Z_f(T) - Z_b(T - T_0)u(T - T_0), \tag{5.40}$$

$$\text{where} \quad X_f(T) = X_0(a_1, \zeta_1, h_{11}, h_{12}, h_{13}, T); \tag{5.41}$$

$$X_b(T) = X_0(a_2, \zeta_2, h_{14}, h_{15}, h_{16}, T); \tag{5.42}$$

$$Z_f(T) = X_0(a_1, \zeta_1, h_{21}, h_{22}, h_{23}, T); \tag{5.43}$$

$$Z_b(T) = X_0(a_2, \zeta_2, h_{24}, h_{25}, h_{26}, T) \tag{5.44}$$

and u is a unit step function, and the functional form of X_0 and expressions for other variables are given in Appendix B for input Y_1 given in the next section.

5.4 Input from The Road Irregularities

In this chapter, a rounded displacement step has been assumed as input to the vehicle front and rear suspensions from the road irregularities. This rounded displacement step represents a sudden bump on the road. The expressions for the rounded displacement step in spatial co-ordinate s are given below:

$$y_1(s) = y_{1max}\left[1 - (1 + \gamma_s s/L)\, e^{(-\gamma_s s/L)}\right] \quad \text{for } s \geq 0 \tag{5.45}$$

$$\text{and} \quad y_2(s) = y_1(s - L)u(s - L) \tag{5.46}$$

where, γ_s is the spatial severity parameter and L is the wheel base of the vehicle.

Equations (5.45) and (5.46) may be written in temporal co-ordinate t as,

$$y_1(t) = y_{1max}\left[1-(1+\gamma_s Vt/L)\,e^{(-\gamma_s Vt/L)}\right] \quad \text{for} \quad t \geq 0 \tag{5.47}$$

$$\text{and} \quad y_2(t) = y_1(t-t_0)u(t-t_0) \tag{5.48}$$

where, $t = s/V$ and $t_0 = L/V$ is the time delay.

In non-dimensionalized form

$$Y_1(T) = \left[1-(1+\gamma_s T/T_0)\,e^{(-\gamma_s T/T_0)}\right] \quad \text{for} \quad T \geq 0 \tag{5.49}$$

$$\text{and} \quad Y_2(T) = Y_1(T-T_0)u(T-T_0) \tag{5.50}$$

where $T_0 = L\omega_0/V$ is the non-dimensionalized time delay.

5.5 Results and Discussions

The coupled nonlinear equations (5.7) and (5.8) are numerically integrated by using Runge-Kutta Method. The performance of the vehicle suspension is evaluated by using the following four indices:

Heave Displacement Ratio (HDR) $= \frac{|X|_{max}}{y_{1max}}$;

Pitch Displacement Ratio (PDR) $= \frac{|Z|_{max}}{y_{1max}}$;

Heave Acceleration Ratio (HAR) $= 20\log_{10}\frac{|X''|_{max}}{y''_{1max}}$;

Pitch Acceleration Ratio (PAR) $= 20\log_{10}\frac{|Z''|_{max}}{y''_{1max}}$.

In general, four wheeled vehicles have forward center of mass ($\alpha > 0$) and $R > 1$. Here, we have considered $\alpha = 0.2$ and $R = 1.5$ for the purpose of numerical integration. Spatial severity parameter, $\gamma_s = 10$ has been considered. The effects of linear and nonlinear damping on HDR, PDR, HAR and PAR are discussed.

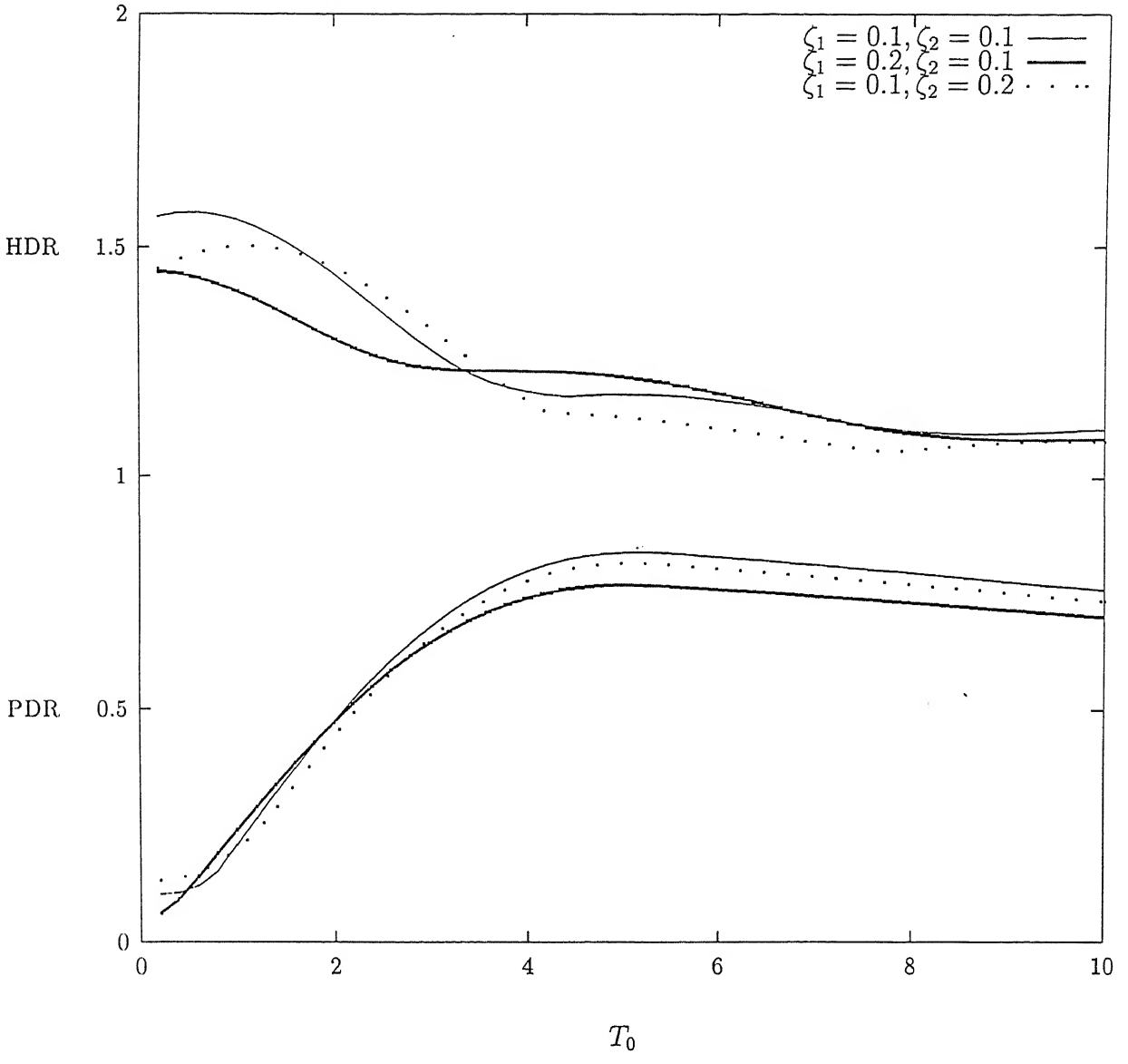

Figure 5.3: Effect of Linear Damping on HDR and PDR for Model I

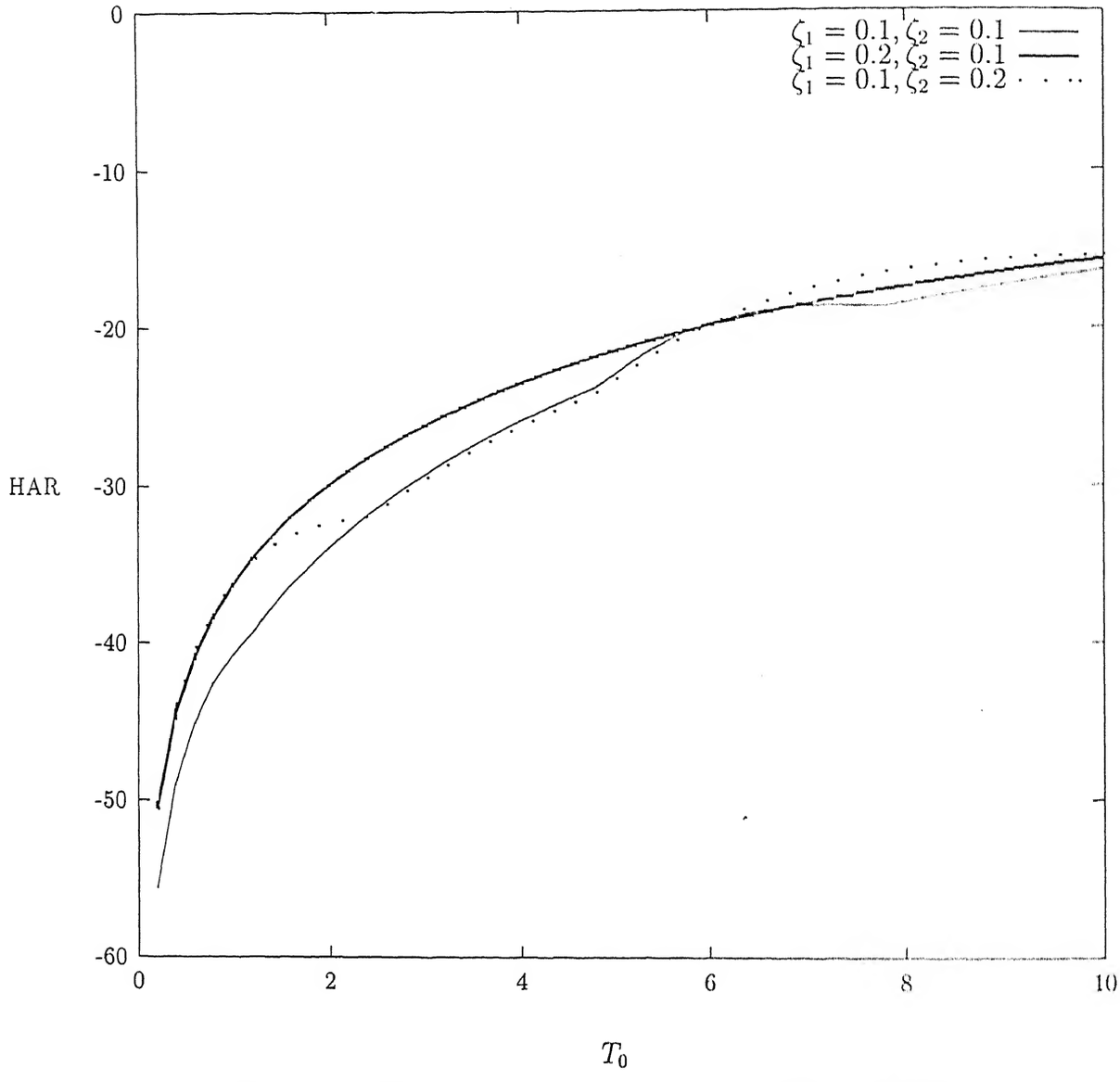

Figure 5.4: Effect of Linear Damping on HAR for Model I

5.5.1 Effect of Linear Damping

Model I

Numerical results are obtained for various values of damping by using the closed form solution given by equations (5.39) and (5.40). From the decoupled system (see section 5.3.2), i.e., with $R^2 = 1 - \alpha^2$, if the stiffness ratio and damping ratio of front to rear suspensions are simultaneously equal to the invariant ratio (see equation (5.34)), then we get optimum X and Z. For forward center of mass ($\alpha = 0.2$), the invariant ratio ($b/a = \frac{1+\alpha}{1-\alpha}$) is greater than unity; it means that high damping and high stiffness at the front suspension rather than at the rear suspension give the optimum response for the decoupled case. This is especially so at very high vehicle speed (i.e. T_0 is close to zero). Figure 5.3 shows the effect of linear damping on HDR and PDR for the coupled system (model I). By increasing the total damping ($\zeta_1 + \zeta_2$) in the system, HDR decreases at high speeds ($T_0 < 2$). For a given total damping ($\zeta_1 + \zeta_2$), at high speeds ($T_0 < 3$), ($\zeta_1 > \zeta_2$) as compared to ($\zeta_1 < \zeta_2$) gives low HDR. At low speeds ($T_0 > 3.5$), ($\zeta_1 = 0.1, \zeta_2 = 0.2$) gives lower HDR than for other damping coefficients ($\zeta_1 = 0.1, \zeta_2 = 0.1$) and ($\zeta_1 = 0.2, \zeta_2 = 0.1$). Similar observations were found for various values of damping coefficients.

At high speeds (see Figure 5.3), PDR does not change much by varying damping either in the front or in the rear suspension. For all damping values, PDR initially increases with T_0 up to ($T_0 \approx 4$), after that it is almost constant. At low speeds ($T_0 > 4.5$), if the total damping ($\zeta_1 + \zeta_2$) in the system increases, then PDR decreases marginally. For a given total damping ($\zeta_1 + \zeta_2$), reduction in PDR is more for ($\zeta_1 > \zeta_2$) than with ($\zeta_1 < \zeta_2$).

Figure 5.4 shows the effect of linear damping on HAR for model I. At high speeds, HAR increases with increasing total damping ($\zeta_1 + \zeta_2$) in the system. This observation

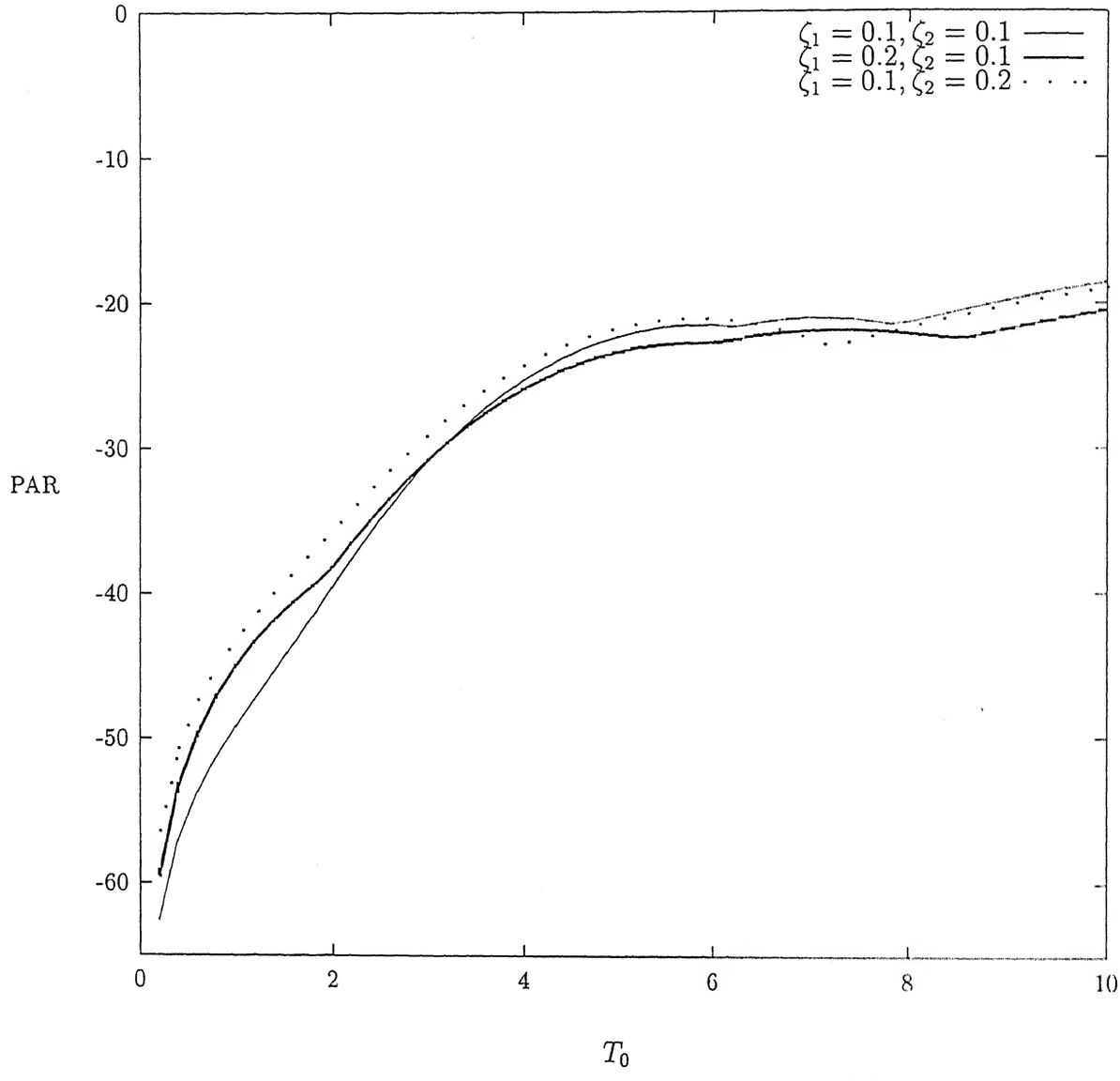

Figure 5.5: Effect of Linear Damping on PAR for Model I

is similar to that for the SDOF system [4], in which SAR increases at high severity parameters with increasing damping value. For a given total damping $(\zeta_1+\zeta_2)$, at very high speeds $(T_0 < 1)$, HAR is insensitive to whether $(\zeta_1 < \zeta_2)$ or $(\zeta_1 > \zeta_2)$.

Figure 5.5 shows the effect of linear damping on PAR for model I. For a given total damping $(\zeta_1 + \zeta_2)$, $(\zeta_1 > \zeta_2)$ gives lower PAR than that with $(\zeta_1 < \zeta_2)$ almost at all speeds. By increasing the total damping $(\zeta_1 + \zeta_2)$ in the system, PAR increases with increasing vehicle speeds up to $T_0 < 3$.

In conclusion, for a given total damping $(\zeta_1 + \zeta_2)$, at high speeds $(\zeta_1 > \zeta_2)$ gives lower HDR and PAR as compared to those with $(\zeta_1 < \zeta_2)$. At high speeds, increasing the total damping in the system reduces HDR, but increases HAR and PAR. For better isolation, all four indices, viz., HDR, HAR, PDR and PAR should be simultaneously as low as possible. These are conflicting requirements which can be fulfilled only partially by a two-element isolator (model I). The three-element isolator model with linear damping is discussed next to see if both HDR and HAR can be simultaneously brought down.

Model II

In the fourth chapter (see Figure 4.7), it has been observed that the optimum SDR occurs at a spring ratio parameter, $n = 1.0$. So, here we have considered $n_1 = n_2 = 1.0$ in model II. $\zeta_1 = \zeta_2 = 0.1$ has been taken in both model I and model II. Figure 5.6 shows comparison of models I and II for HDR and PDR. At all speeds, there is hardly any difference in the performance of these two models so far as HDR and PDR values are concerned.

Figure 5.7 shows comparison of models I and II for HAR and PAR. At high speeds $(T_0 < 0.2)$, there is considerable reduction in both HAR (about 6 dB) and PAR (about 10 dB) values for model II as compared those of model I. However, at lower speed regimes, both models yield similar values for HAR and PAR.

In conclusion, at high vehicle speeds model II performs better than model I by reducing HAR and PAR, while maintaining similar values of HDR and PDR.

5.5.2 Effect of Nonlinear Damping

Model I

From chapter two, we know that nonlinear damping is detrimental for shock isolation in SDOF system especially at high severity parameters (see section 2.4.2). Figure 5.8 shows the effect of nonlinear damping on HDR and PDR for model I, with linear damping coefficients $\zeta_1 = \zeta_2 = 0.1$ and nonlinear damping coefficients $\delta_1 = \delta_2 = 0.01$. As in the SDOF system (see Figure 2.10), here also the nonlinear damping is detrimental to the shock isolation for model I at high speeds. It is evident from Figure 5.8 that both HDR and PDR are increased due to nonlinear damping. At low velocities ($T_0 > 1$), however, the effect of nonlinear damping is negligible. Figure 5.9 shows the effect of nonlinear damping on HAR and PAR. Both HAR and PAR increase due to nonlinear damping up to $T_0 \approx 2$. After $T_0 > 2$, again the effect of nonlinear damping is negligible.

Therefore, due to nonlinear damping, all the four performance indices, HDR, PDR, HAR and PAR are larger at high speeds. It was observed that the distribution of damping between the front and rear suspension does not improved the vehicle suspension performance unlike in linear damping case, since the presence of nonlinear damping itself is deteriorated the vehicle suspension performance.

In the next section, performance of models I and II are compared in the presence of nonlinear damping.

Model II

Figure 5.10 shows the comparison of models I and II with reference to HDR and PDR values. For model I, $\zeta_1 = \zeta_2 = 0.1$ and $\delta_1 = \delta_2 = 0.01$ and for model II,

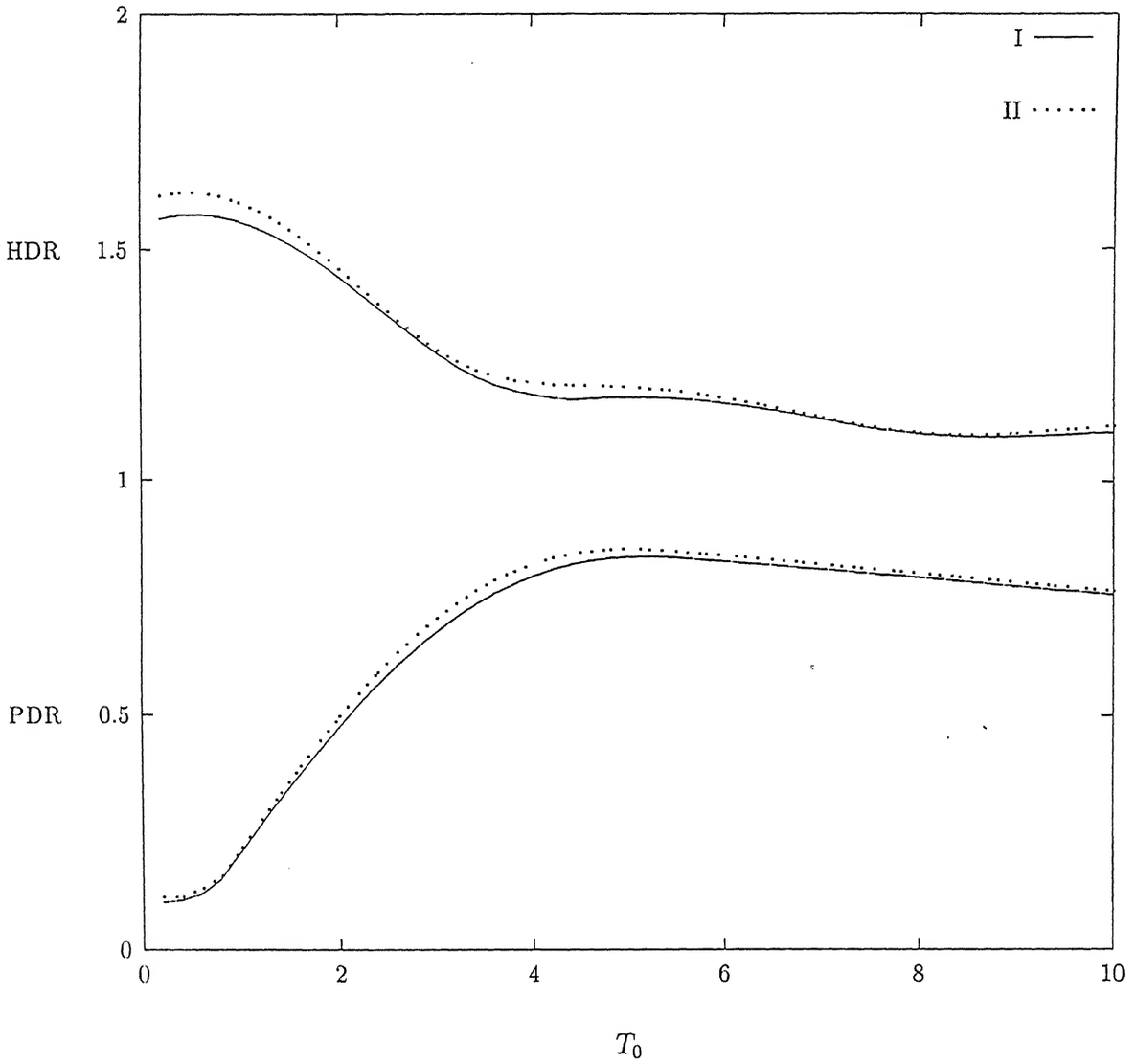

Figure 5.6: Comparison of Model I and II for HDR and PDR, linear damping case

$\zeta_1 = \zeta_2 = 0.1$; $\delta_1 = \delta_2 = 0.01$ and $n_1 = n_2 = 1$ have been used. At high speeds ($T_0 < 1$), both HDR and PDR values are effectively reduced in model II when compared to those in model I. However, at lower speed regimes, both models I and II yield almost similar values for HDR and PDR.

HAR and PAR values are presented in Figure 5.11 for both models I and II. At high vehicle speeds ($T_0 < 1.5$), reduction in both HAR and PAR values is very high for model II when compared to those of model I. For example, this reduction is 25 dB and 35 dB in HAR and PAR, respectively, at ($T_0 = 0.2$). At lower speed regimes ($T_0 > 1.5$), the difference between models I and II for both HAR and PAR values are negligible. The adverse effect of nonlinear damping is completely nullified in model II. Like in SDOF system, it is better to mount the nonlinear damper elastically, in this 2-DOF model also, to get better isolation performance.

It is evident, by comparing Figure 5.6 with Figure 5.10 and Figure 5.7 with Figure 5.11 respectively, that the performance of model II is similar for both linear and nonlinear damping cases. In conclusion, model II reduces all four performance indices HDR, PDR, HAR and PAR in the presence of both linear and nonlinear damping.

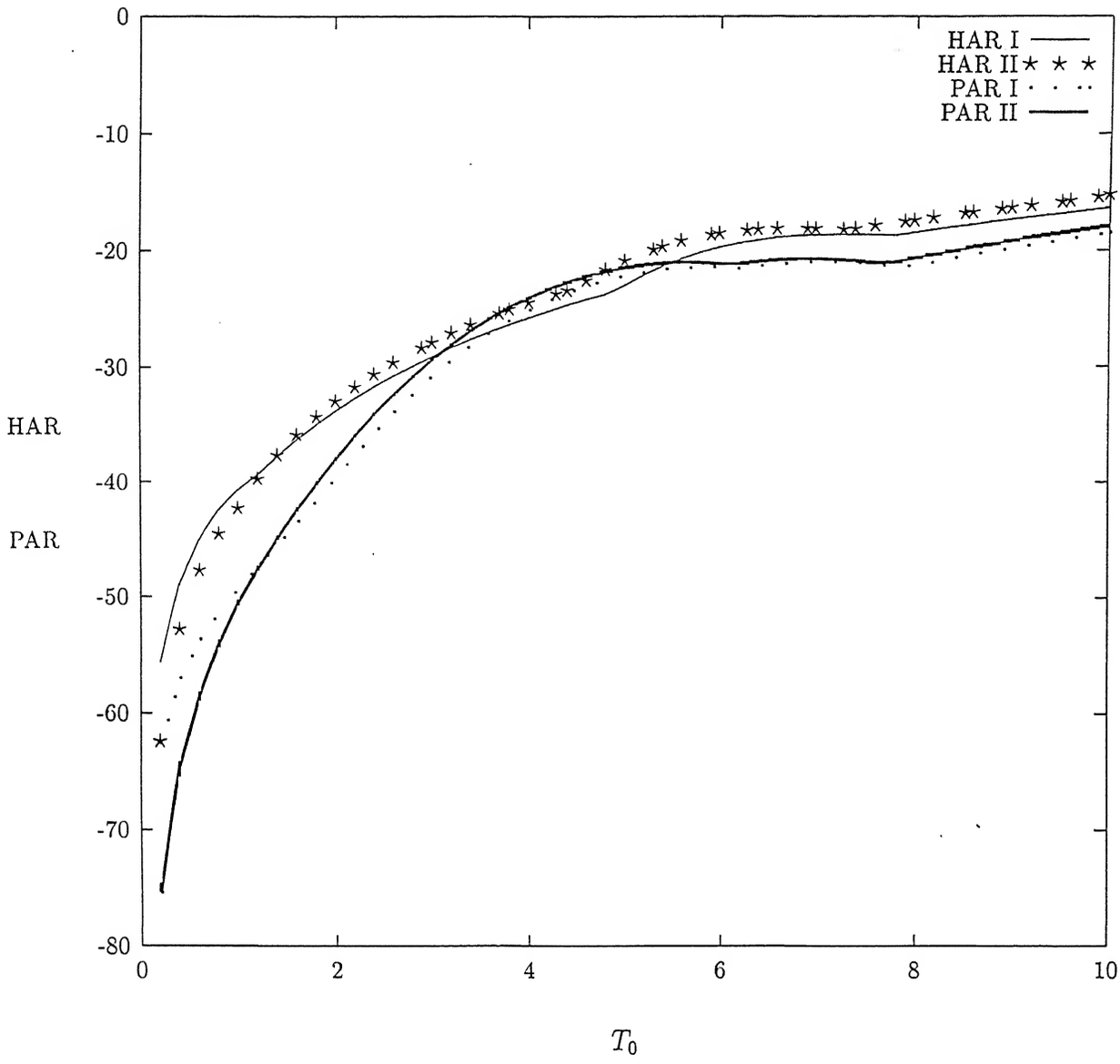

Figure 5.7: Comparison of Model I and II on HAR and PAR, linear damping case

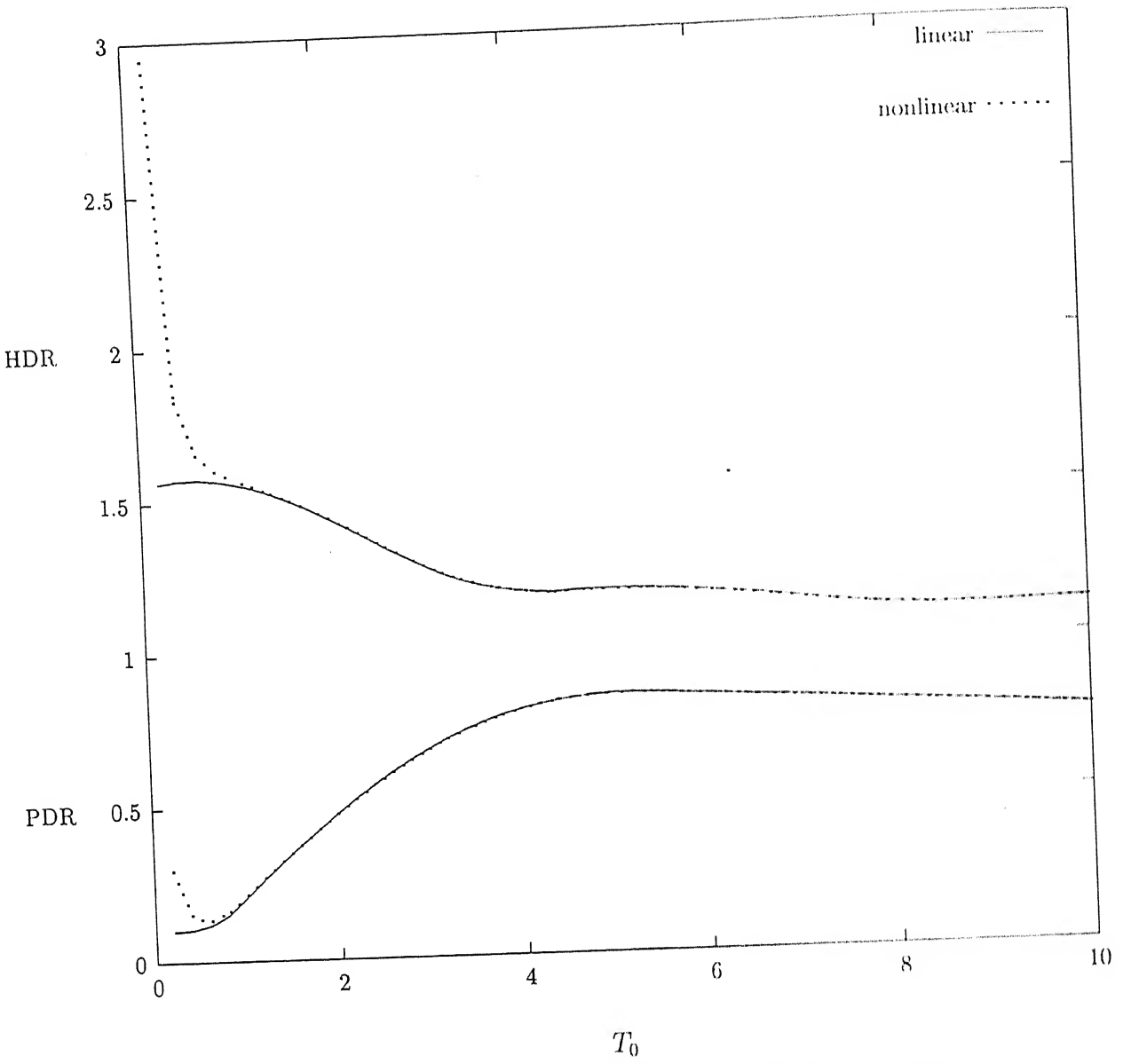

Figure 5.8: Effect of Nonlinear Damping on HDR and PDR

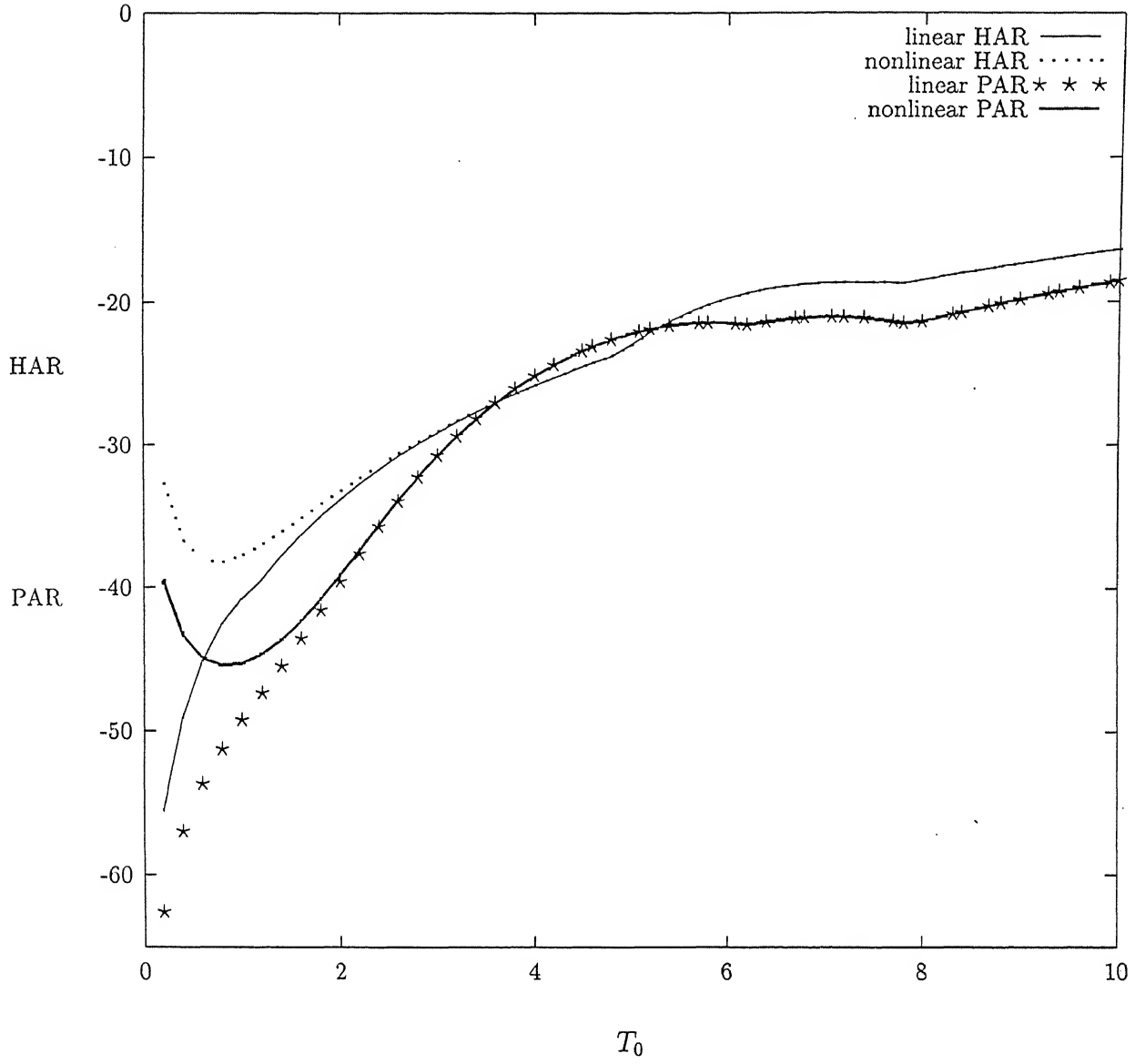

Figure 5.9: Effect of Nonlinear Damping on HAR and PAR

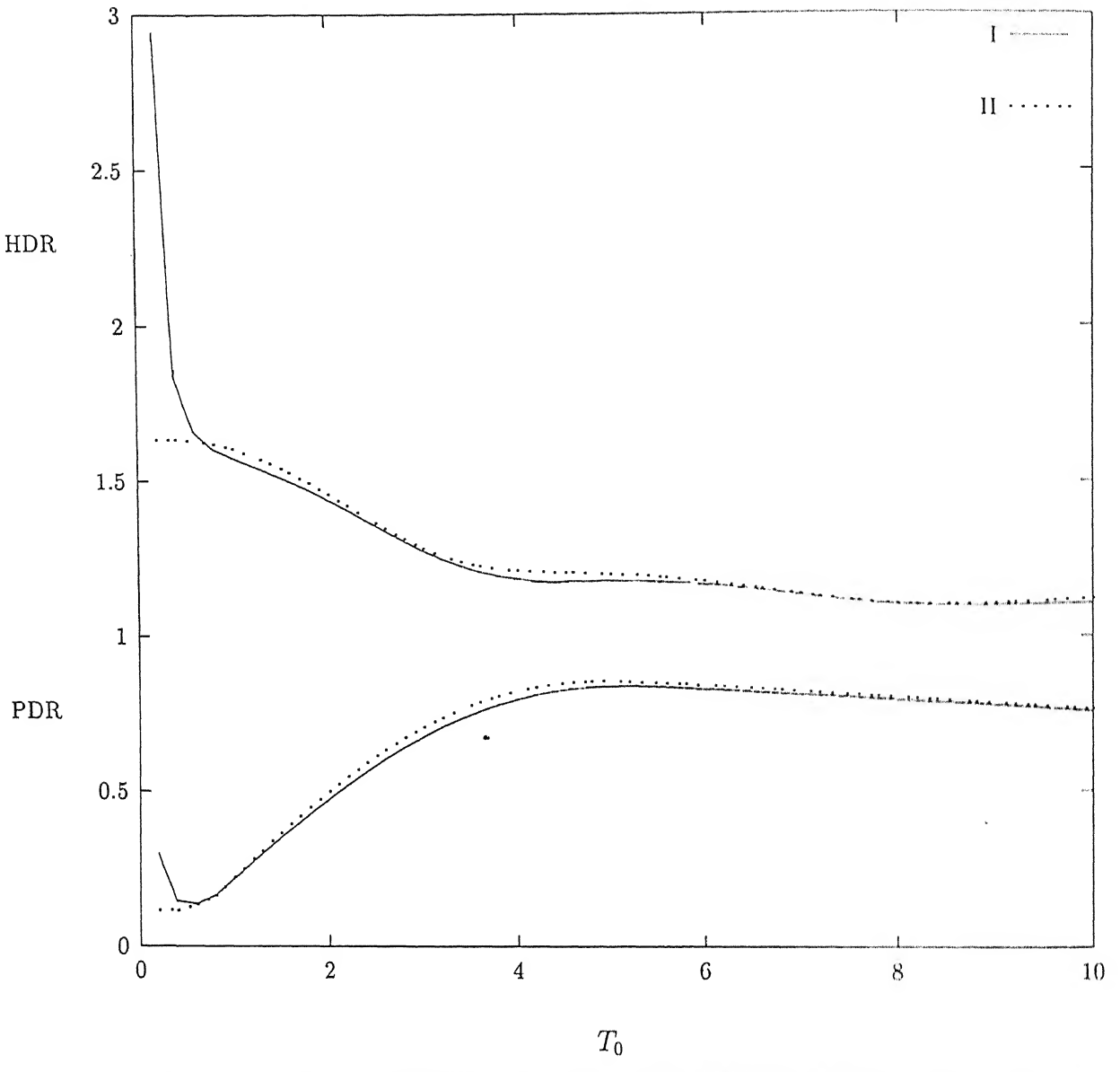

Figure 5.10: Comparison of Model I and II for HDR and PDR, nonlinear damping case

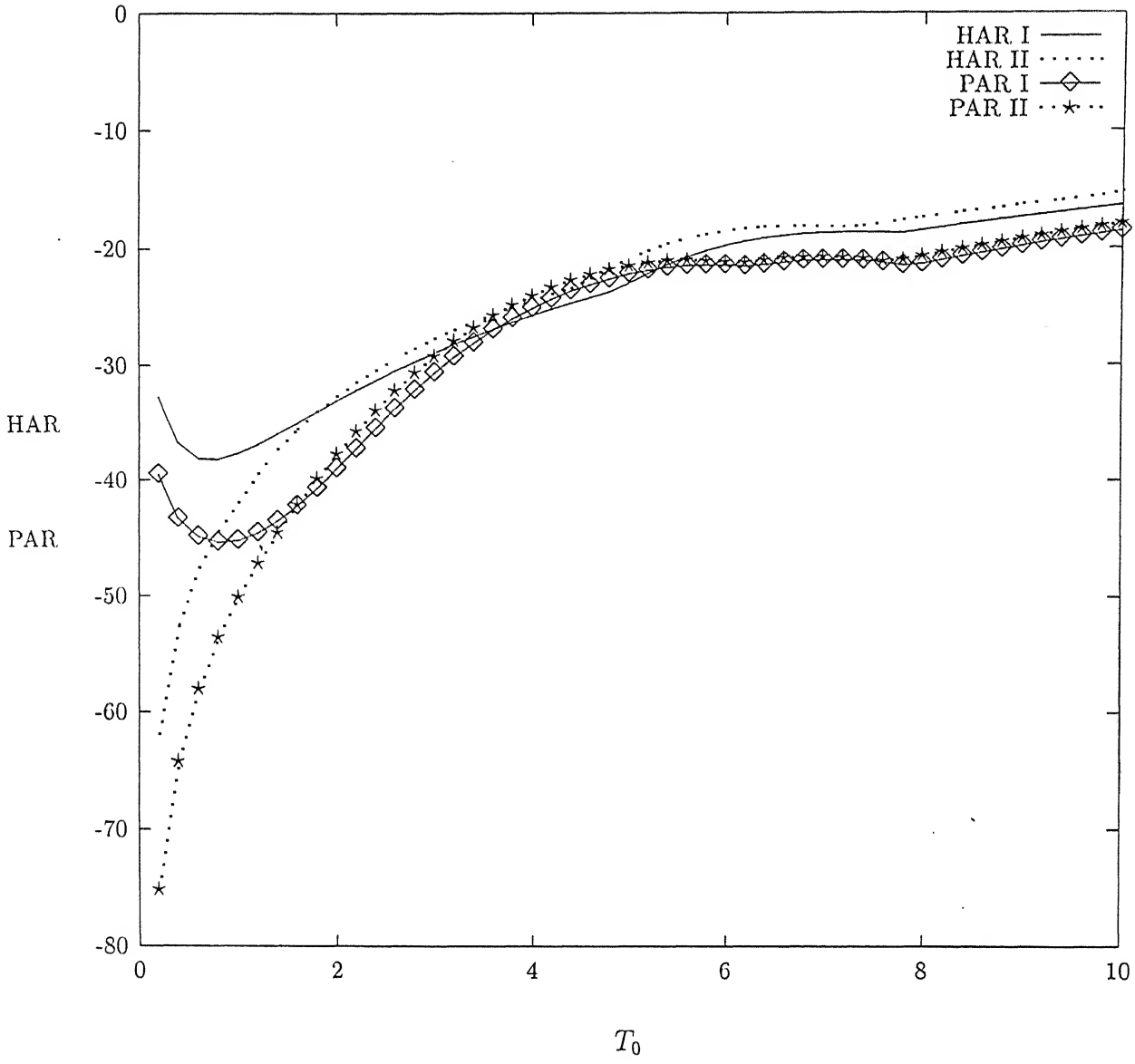

Figure 5.11: Comparison of Model I and II for HDR and PDR, nonlinear damping case

Chapter 6

2-DOF HEAVE-PITCH MODEL OF A VEHICLE FOR RANDOM EXCITATION

6.1 Introduction

In the previous chapter, the performance of nonlinear suspension system has been studied in the context of a 2-DOF heave-pitch model of a vehicle subjected to shock excitation has been studied. In this chapter, the same model of a vehicle subjected to random excitation is investigated. The road surface profile on which the vehicle is traversing is modelled as the output of a first order shaping filter to white noise excitation. To determine the response of the vehicle, Monte Carlo simulation has been employed. The road surface excitation has been simulated as a series of cosine functions with weighted amplitudes at evenly spaced frequencies and random phase angles. Only a two element isolator model is considered. Root Mean Square (RMS) values of response variables are treated as performance indices. It is observed that the

nonlinear cubic damping reduces the RMS heave and pitch displacements but increases both the RMS heave and pitch accelerations.

6.2 Equations of Motion

The 2-DOF (Heave-Pitch) vehicle model with two element isolators, shown in Figure 5.1, is considered again. The description of the vehicle model remains same as given in the previous chapter, but the input excitations y_1 and y_2 are now considered as of stochastic nature. Equations of motion are also identical to the equations of motion given by equations (5.1) - (5.2). The non-dimensional forms of equations of motion given by equations (5.7) - (5.12) are repeated below for the sake of completeness:

$$X'' + F_1 + F_2 = 0 \tag{6.1}$$

$$R^2 Z'' + F_1 - F_2 - \alpha(F_1 + F_2) = 0 \tag{6.2}$$

$$F_1 = a_1(X_1 - Y_1) + 2\zeta_1(X_1' - Y_1') + \delta_1(X_1' - Y_1')^3 \tag{6.3}$$

$$F_2 = a_2(X_2 - Y_2) + 2\zeta_2(X_2' - Y_2') + \delta_2(X_2' - Y_2')^3 \tag{6.4}$$

$$X_1 = X + Z(1 - \alpha) \tag{6.5}$$

$$X_2 = X - Z(1 + \alpha). \tag{6.6}$$

As in the previous chapter, $Y_2(T)(= y_2/y_{max})$ is considered as the delayed version of $Y_1(T)(= y_1/y_{max})$ with $Y_2(T) = Y_1(T - T_0)$, but y_{max} here denotes the RMS value of the input displacement y_1 at the front wheel. All the non-dimensional variables are identical to those given in the previous chapter. In the next section, the statistical properties of y_1 are described.

6.3 Road Profile Model

The classification of rough surfaces has received much attention over the years. Different models of the road surface roughness are described in the literature [79-84]. Among various methods of analysis, the most common one is via wave number spectra or covariance properties. The techniques rely on one crucial assumption that a rough ground profile may be regarded as the output of a white-noise excited, spatial shaping filter.

Consider a road surface which is homogeneous and isotropic, with a displacement profile $y(s)$, where s is the horizontal distance, assumed to be a member function of an ergodic random process $\{y(s)\}$[80]. The profile autocorrelation function may be defined in terms of the horizontal lag, h, by

$$R_y(h) = E[y(s)y(s+h)] \tag{6.7}$$

where E indicates the expectation operator taken over all members of the process. When a vehicle travels across a road surface, the displacement experienced at its front wheel must be expressed as a function of time, $y_1(t)$, with magnitude equivalent to the profile displacement at the point of contact at that instant: thus if at time t_1 the point of contact is at s_1 we may write

$$y_1(t_1) = y(s_1). \tag{6.8}$$

The distance s will be a known function of t and $s = Vt$ for a constant vehicle speed V. The autocorrelation function may be expressed as a function of expectations at the two instants of time concerned. Thus

$$R_{y_1}(t_1, t_2) = E[y_1(t_1)y_2(t_2)] \doteq E[y(s_1)y(s_2)] = R_y(s_1, s_2). \tag{6.9}$$

For the constant speed V, the input random process y is stationary. For a stationary

random process, $y(s)$, equation (6.9) may be written as

$$R_{y_1}(\tau) = R_y(h) \tag{6.10}$$

where $\tau = t_2 - t_1$; $\quad h = s_2 - s_1 \quad$ and $\quad \tau = h/V$.

The temporal power spectral density $S_{y_1}(\omega)$ is given by[85],

$$S_{y_1}(\omega) = \frac{1}{2\pi}\int_{-\infty}^{\infty} R_{y_1}(\tau)e^{-i\omega\tau}d\tau \tag{6.11}$$

and the corresponding spatial spectral density is

$$S_y(\nu) = \frac{1}{2\pi}\int_{-\infty}^{\infty} R_y(h)e^{-i\nu h}dh \tag{6.12}$$

where $\omega = 2\pi/T_p$ is the circular frequency; $\nu = 2\pi/\lambda$ is the wave number; T_p is the time period and λ is the wavelength.

From equations (6.9)-(6.12), the relation between $S_{y_1}(\omega)$ and $S_y(\gamma)$ may be written as

$$S_{y_1}(\omega) = \frac{1}{V}S_y(\nu = \omega/V) \tag{6.13}$$

The power spectral density (psd) function of road irregularity is assumed to be of the form [60]

$$S_{y_1}(\omega) = \frac{\sigma^2 qV}{\pi[\omega^2 + (qV)^2]} \tag{6.14}$$

where V is the vehicle forward speed, ω is circular frequency, σ^2 denotes the variance of the road irregularity and q is a coefficient depending on the type of road surface. The process $y_1(t)$ described by equation (6.14) is the output of a linear first order filter with white noise input given by

$$\dot{y}_1(t) + qVy_1(t) = W(t). \tag{6.15}$$

$W(t)$ is a white noise process with covariance function

$$E[W(t)W^T(t)] = 2\sigma^2 qV\delta(t_2 - t_1) \tag{6.16}$$

$E[\cdot]$ denotes the expectation operator and δ represents the Dirac-delta function.

The psd function of road irregularity given by equation (6.14) may be expressed in terms of non-dimensional parameters as

$$S_{Y_1}(\Omega) = \frac{(\sigma^2/\pi)\beta T_0}{(\Omega T_0)^2 + (\beta)^2} \tag{6.17}$$

where, $\Omega = \omega/\omega_0, \quad \omega_0 = \sqrt{(k_1 + k_2)/m} \quad$ and $\quad \beta = qL.$

Similarly, the autocorrelation function for the psd given by equation (6.17) may be written as

$$R_{Y_1}(\tau) = \sigma^2 \exp(|\ -\beta\tau/T_0\ |). \tag{6.18}$$

6.4 Monte Carlo Simulation

The Monte Carlo simulation is a statistical sampling experiment[86,87]. It involves a repeated generation of random variates and a subsequent determination of the system response for each realization of the random variates by using deterministic methods. Proper statistical processing provides estimates of useful response statistics.

The random input process $Y_1(T)$ from the road surface is simulated by using the Shinozuka's spectral representation method[65]. In this method, sample functions of the stochastic process are generated using a cosine series formula. These sample functions accurately reflect the prescribed probabilistic characteristics of the stochastic process when the number N of the terms in the cosine series is large. The ensemble-averaged power spectral density or autocorrelation function approaches the corresponding target (actual) function as the sample size increases. In addition, the generated sample functions possess ergodic characteristic in the sense that the temporally-averaged mean value and the autocorrelation function are identical with the corresponding targets, when the averaging takes place over the fundamental period of the cosine series. The

autocorrelation function and consequently the power spectral density respectively converge at the rate $1/N^2$ to the target autocorrelation and target power spectral density of the random process when $N \rightarrow \infty$. The most important property of the simulated stochastic process is that it is asymptotically Gaussian as $N \rightarrow \infty$ by virtue of the central limit theorem.

Simulation Formula

The random input process $Y_1(T)$ with mean value equal to zero and autocorrelation function $R_{Y_1}(\tau)$ given by equation (6.18) can be simulated by the following series with $N \rightarrow \infty$[65];

$$Y_1(T) = (\sqrt{2}/y_{max}) \sum_{n=0}^{N-1} [A_n \cos(\Omega_n' T + \phi_n)] \tag{6.19}$$

where, $A_n = \sqrt{2 S_{Y_1}(\Omega_n) \Delta\Omega}$.

$S_{Y_1}(\Omega_n)$ is the psd of road surface given by equation (6.17), which is of insignificant magnitude (or may be assumed to be zero) below a lower limit Ω_l and beyond an upper limit Ω_u. Thus, Ω_n is considered in the range

$$\Omega_l \leq \Omega_n < \Omega_u;$$

ϕ_n is the random phase angle uniformly distributed between 0 and 2π;

$$\begin{aligned} \Omega_n &= \Omega_l + (n - 1/2)\Delta\Omega, \\ \Omega_n' &= \Omega_n + \delta\Omega_n, \quad n = 1, 2, ..., N; \\ \Delta\Omega &= (\Omega_u - \Omega_l)/N, \end{aligned}$$

with N being the number of intervals. A small random frequency $\delta\Omega_n$ is introduced to avoid the periodicity of the simulated process and is uniformly distributed between $-\Delta\Omega'/2$ and $\Delta\Omega'/2$ with $\Delta\Omega' \ll \Delta\Omega$. The input random process $Y_1(T)$ is simulated with $N = 1000, \Omega_l = 0, \Omega_u = 50$ Hz and $\Delta\Omega' = \Delta\Omega/20$.

The autocorrelation function of the simulated (generated) random process $Y_1(T)$ is compared in the next section with the actual (target) autocorrelation function given by equation (6.18).

6.5 Results and Discussions

Road roughness parameter $q = 0.15$ and $\sigma^2 = 9.0 \times 10^{-6} m^2$ for asphalt road have been reported in several references [79-84]. For a wheel base $L = 2.5$ m, $\beta = qL$ value comes out to be 0.375. For $\omega_0 = 10$ rad/sec, $T_0 = 1$ represents vehicle speed $V = 25$ m/sec (i.e., 90 Km/h). In Figure 6.1, the generated autocorrelation function is compared with the target autocorrelation function given by equation (6.18) with $\beta = 0.375$ and $T_0 = 1$. It is seen that the generated autocorrelation function is matching very well with the target autocorrelation function for all τ. Similar matching was observed for other values of T_0 also. Both autocorrelation functions are asymptotically approaching the mean value which is zero according to our assumption.

In all the results, like in the previous chapter, $R = 1.5$, $\alpha = 0.2$, $\zeta_1 = \zeta_2 = 0.1$ and $\delta_1 = \delta_2 = 0.01$ have been considered. Equations (6.1) and (6.2) are integrated numerically by using Runge-Kutta method for the input sample functions generated by equation (6.19). Figure 6.2 shows the effect of nonlinear cubic damping on RMS heave displacement. It may be observed that nonlinear cubic damping reduces the RMS heave displacement at all speeds $T_0 > 0.2$. Here, high T_0 corresponds to low speeds and low T_0 corresponds to high speeds. $T_0 = 0.2$ represents a speed of 125 m/sec (450 Km/h) and $T_0 = 10$ represents a speed of 2.5 m/sec (9 Km/h) for $\omega_0 = 10$ rad/sec. At low speed regimes ($T_0 > 3$), there is not much difference between linear and nonlinear responses, although the nonlinear response is somewhat lower than the linear response. Both, linear and nonlinear responses are increased with an increase in speed up to $T_0 = 1.0$.

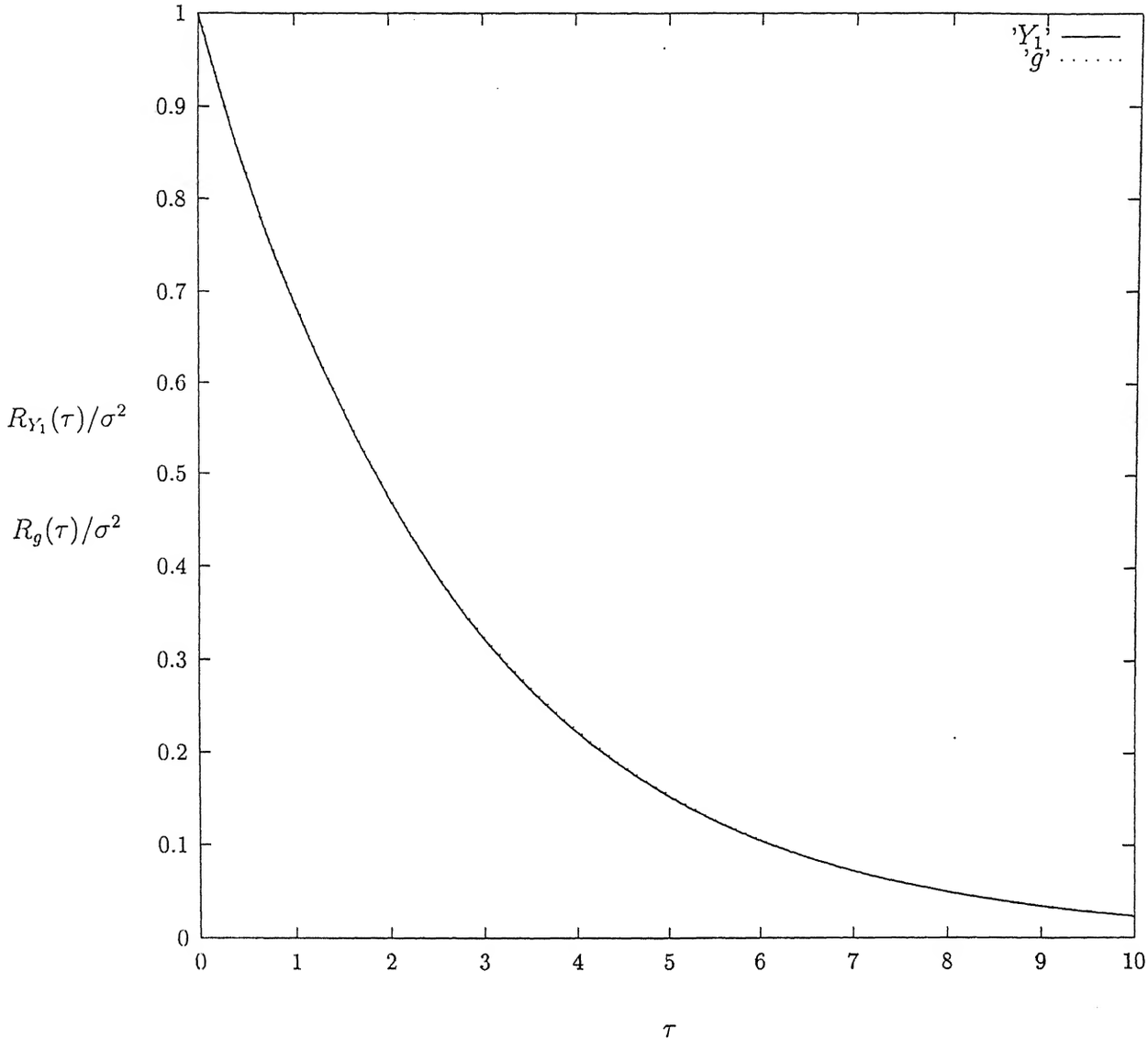

Figure 6.1: Comparison of generated autocorrelation function with target autocorrelation function. Y_1: target; g: generated.

While the nonlinear response increases monotonically with increasing speed, the linear response exhibits a resonance type phenomenon at $T_0 = 1.0$. For $T_0 < 1$, linear response decreases with increasing speed. This result seems to be paradoxical, since it is expected that the response increases with increasing vehicle speed. However, it is observed that beyond a critical speed, the performance of vehicle suspension improves rapidly with speed increment. Similar behaviour has been reported in physics literature [88-91] for linear and nonlinear stochastic systems, with nonlinear models consisting of only nonlinearity in stiffness and not in damping. This phenomenon termed 'stochastic resonance' was explained analytically only for soft Duffing oscillators having double-well potentials. Hitherto, there is no explanation available for this phenomenon for hard Duffing oscillators with a single well potential. The system under consideration here also has a single well potential (due to the linear springs). However, it may be pointed out that the critical speed for the present system, beyond which the linear response decreases with increasing speed, is found to be very high (beyond the range of practical interest).

Figure 6.3 shows the effect of nonlinear damping on RMS heave acceleration. Here, the nonlinear response is higher than the linear response at all speed regimes. At high speed regimes, the difference is very high. At $T_0 = 1$, the difference is 8 dB, but at $T_0 = 10$ the difference is only 1 dB.

Figure 6.4 and 6.5 show the effect of nonlinear damping on RMS pitch displacement and acceleration respectively. In Figure 6.4, both linear and nonlinear responses show a critical speed around $T_0 = 4$, which gives a peak RMS pitch displacement. The nonlinear RMS pitch displacement is always lower than the linear RMS pitch displacement. The difference between the linear and nonlinear responses is maximum at the critical speed.

The RMS pitch acceleration (see Figure 6.5) is always more in the presence of

nonlinear damping. The difference between the linear and nonlinear responses is very high at high speed regimes. The linear response shows a critical speed at which the RMS acceleration reaches a maximum value, whereas the nonlinear response shows a monotonic increase with increasing speed.

In summary, stochastic resonance was observed for both heave and pitch displacements when the damping is linear. Unlike for shock excitations, in this case the nonlinear cubic damping reduces both heave and pitch displacements. However, the presence of nonlinearity in the damping force increases both heave and pitch accelerations at high speed regimes.

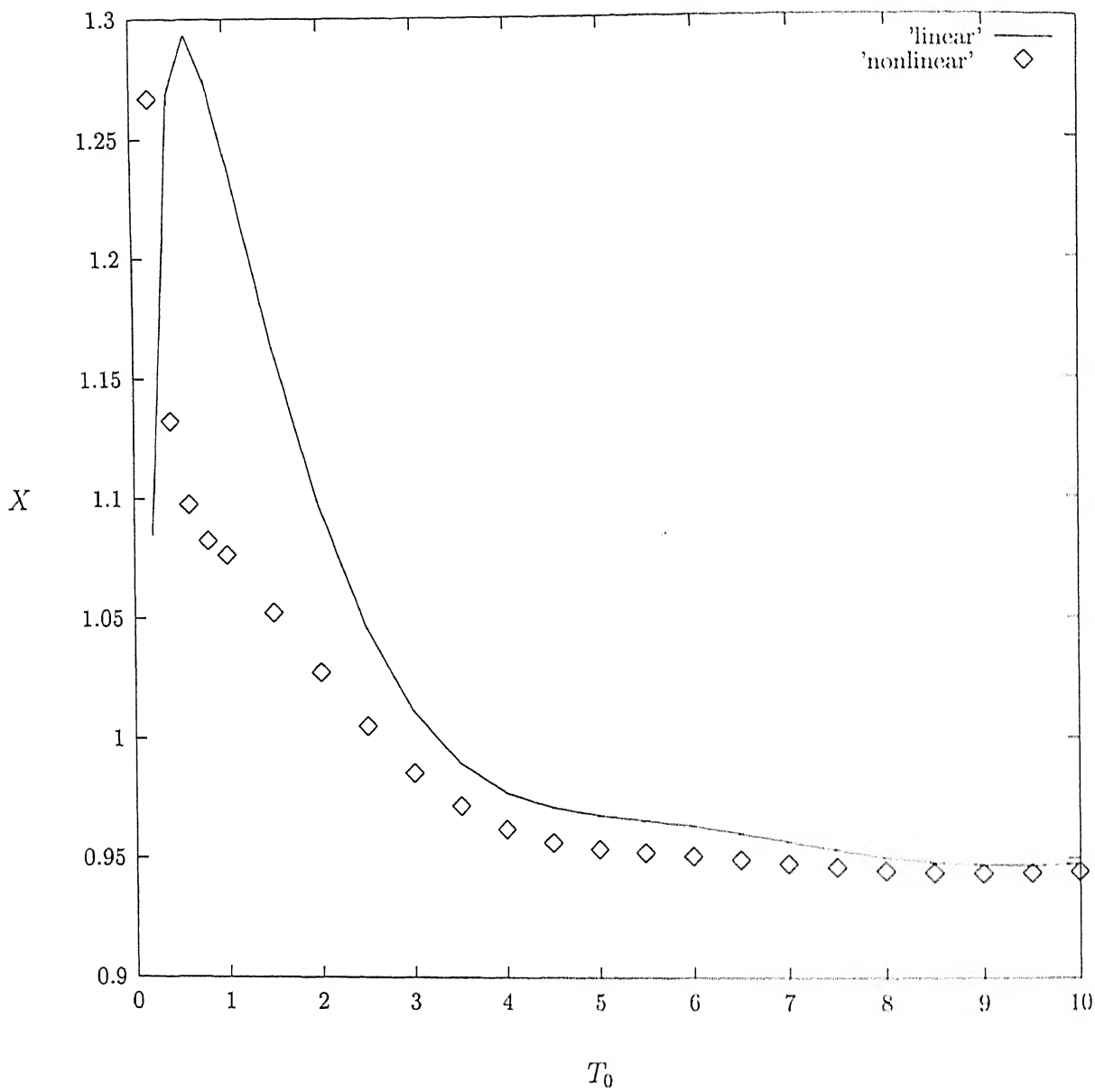

Figure 6.2: Effect of nonlinear damping on RMS Heave displacement.

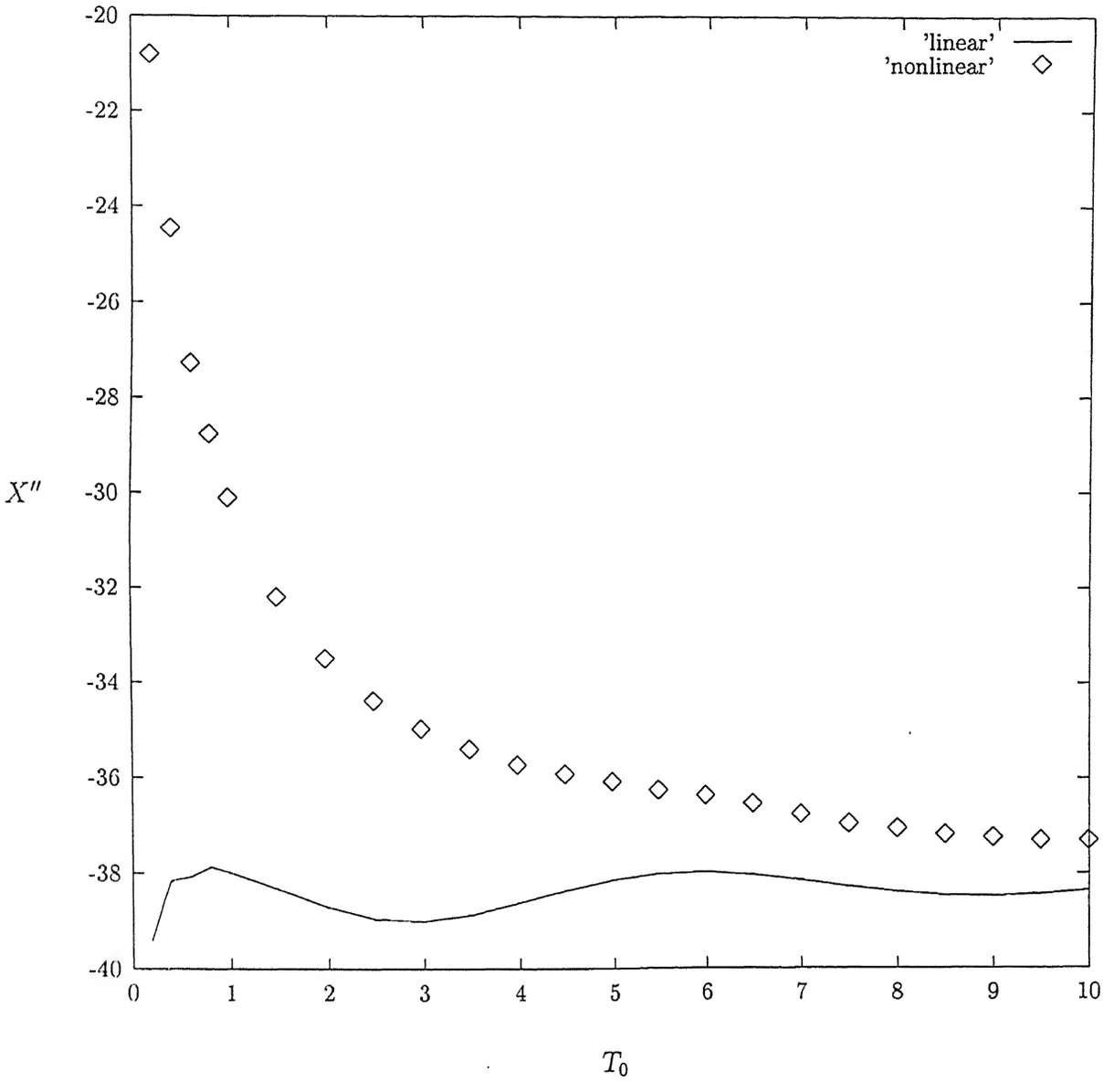

Figure 6.3: Effect of nonlinear damping on RMS Heave acceleration in dB.

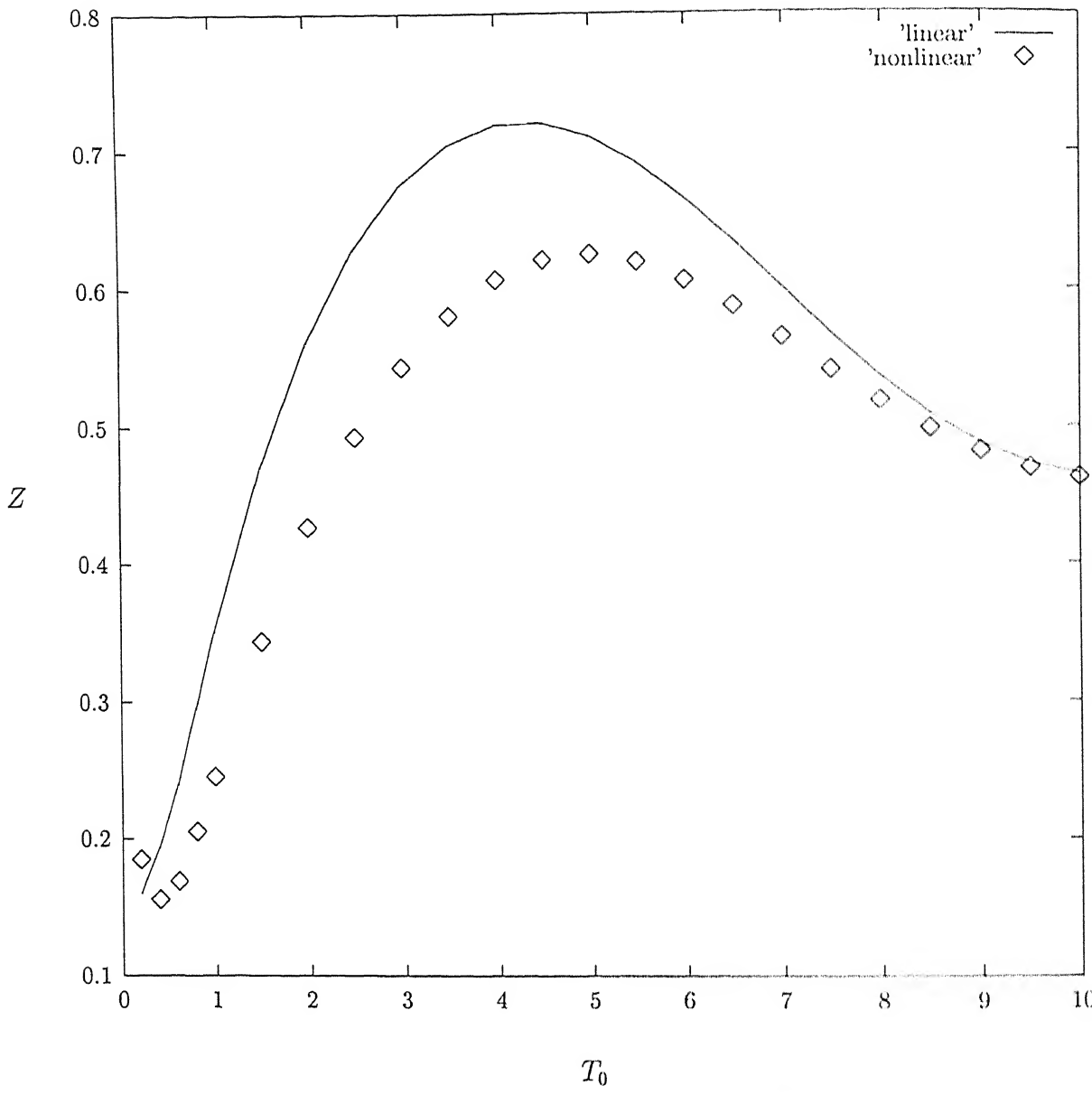

Figure 6.4: Effect of nonlinear damping on RMS Pitch displacement.

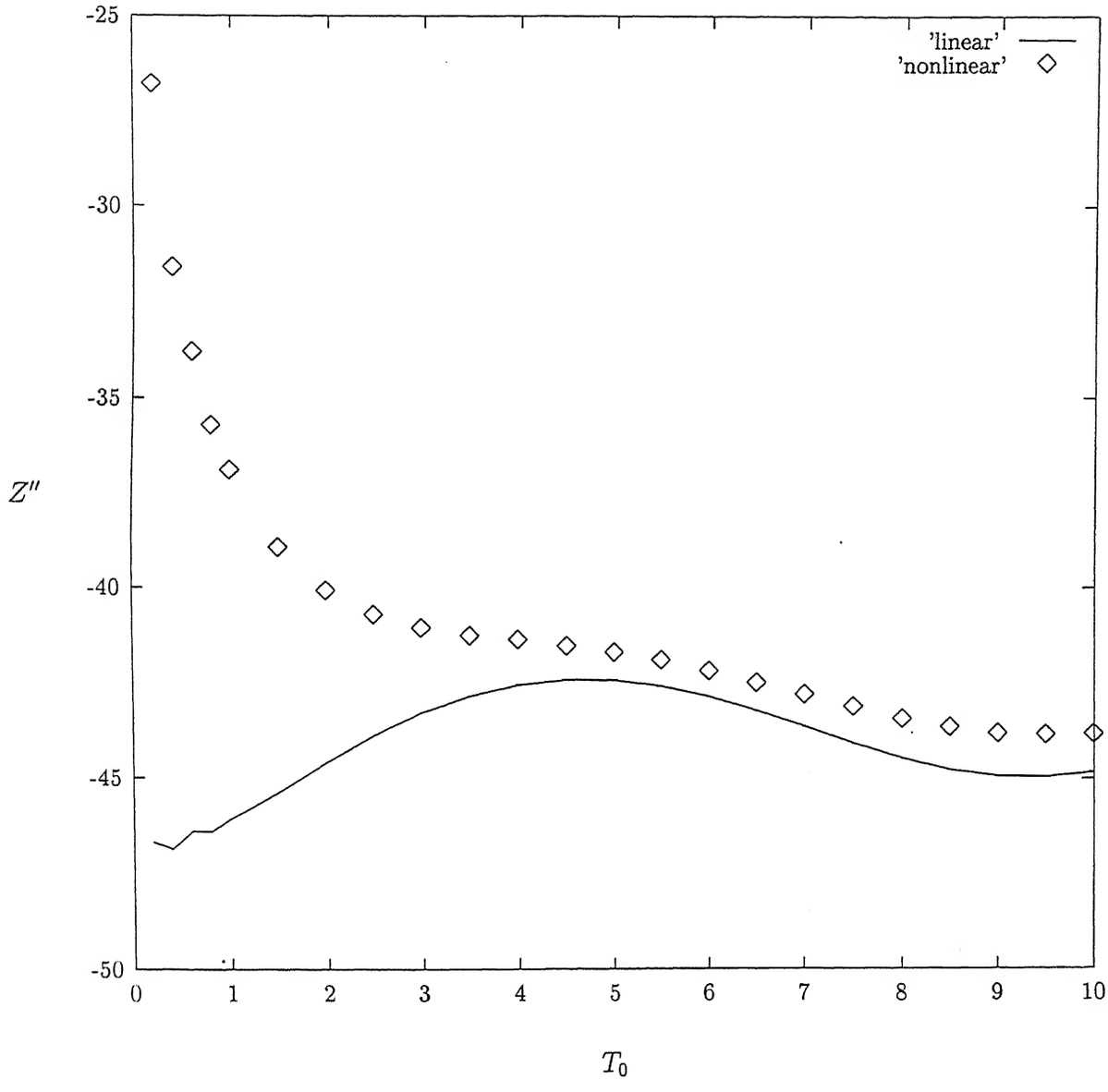

Figure 6.5: Effect of nonlinear damping on RMS Pitch acceleration in dB.

Chapter 7

CONCLUSIONS

7.1 Conclusions

In this thesis, the effect of nonlinearity in the isolator elements has been investigated for shock and random excitations. Both base and force excitations have been studied. A simple analytical method has been developed using perturbation method with Laplace transform to determine the transient response of a single degree-of-freedom (SDOF) system in the presence of nonlinear, dissipative shock isolators. This method is applicable for any order of nonlinearity, both in the restoring and damping forces, expressed in the form of polynomials. However, the closed form results are obtained with only cubic nonlinearity both in the restoring and damping forces. Three types of base excitations, namely, the rounded step, the rounded pulse and the oscillatory step are considered. Analytical results obtained by the present method are compared with those obtained by direct numerical integration. Numerical results are included for a typical elastomeric damper which can be modelled by a combination of linear viscous damping and a dissipative quadratic damping with a negative coefficient. In the presence of inherent cubic damping in a nonlinear shock isolator with base excitation, four

different modifications of the isolator are considered to improve its performance. A two degree-of-freedom (2-DOF) model for a vehicle undergoing heave and pitch motions is investigated for both shock and random excitations. It is assumed that the vehicle is moving with a constant speed so that the rear wheels are subjected to the same input as the front wheels but with a time delay. Shinozuka's spectral method is used for generation of the random input process. Monte-Carlo simulation has been employed to find the response of the vehicle.

The major conclusions of the present thesis are listed below:

(i) A simple analytical method has been developed using perturbation technique in conjunction with Laplace transform to determine the transient response of an SDOF system in the presence of nonlinear, dissipative shock isolators. It is observed that in most cases, the closed form perturbed solution match well with the numerically integrated results.

(ii) It has been established that the effect of nonlinear damping is more predominant than the effect of nonlinear stiffness so far as the performance of shock isolators for base excitation is concerned. The presence of nonlinear n^{th} power-law damping, with a positive coefficient and the index n greater than unity, is harmful for base excited shock isolators. However, quadratic damping with a negative coefficient improves the performance of a shock isolator.

(iii) With force excitation, the presence of nonlinearity in damping does not deteriorate the performance of a shock isolator, rather it marginally improves the performance of a linear shock isolator.

(iv) To improve the performance of a shock isolator with base excitation, in the presence of nonlinear cubic damping, four methods, namely, Coulomb damped isolator, three element isolator, vibration absorber and two stage isolator have been considered. Overall, a three element isolator and a two stage isolator are shown to nullify the

adverse effect of cubic damping nonlinearity.

(v) 2-DOF coupled nonlinear asymmetric systems behave like a symmetric system for a particular choice of parameter values. At very high speeds and for forward center of mass, high damping and high stiffness at the front suspension rather than at the rear suspension give the optimum response for the decoupled system.

(vi) The detrimental effect of nonlinear cubic damping in a two element isolator and its mitigation by using a three element isolator are exhibited by both SDOF and 2-DOF models.

(vii) With a random base excitation, 'Stochastic Resonance' type phenomenon is observed for both heave and pitch displacements when the damping is linear. Unlike for shock excitations, in this case the nonlinear cubic damping reduces heave and pitch displacements. However, the presence of nonlinearity in the damping force increases both heave and pitch accelerations.

7.2 Scope of Future Work

The following are the directions along which future research can be carried out:

(i) In 2-DOF vehicle model, speed of the vehicle is assumed constant. The effects of variable speed with acceleration/deceleration can be looked into.

(ii) 2-DOF heave-pitch vehicle model can be extended to heave-pitch-roll vehicle model with four inputs at the four wheels. Extra degrees-of- freedom can be introduced to treat the sprung and unsprung masses.

(iii) It was observed that the nonlinear asymmetric system behaves like a symmetric nonlinear system for a particular choice of parameter values in 2-DOF vehicle model. One can extend this work to investigate whether the behaviour of nonlinear asymmetric system (discrete or continuous) in general can be studied as a perturbation on nonlinear

symmetric systems.

(iv) The phenomenon of stochastic resonance can be investigated in nonlinear continuous systems also.

REFERENCES

1. C.E. Crede 1951 *Vibration and Shock Isolation.* New York: Wiley.

2. C.M. Harris 1988 *Shock and Vibration Handbook.* New York: McGraw-Hill; Third edition.

3. A.K. Mallik 1990 *Principles of Vibration Control.* New Delhi: Affiliated East-West Press.

4. J.C. Snowdon 1968 *Vibration and Shock in Damped Mechanical Systems.* New York: John Wiley and sons, Inc.

5. J.C. Snowdon 1970 *41st Shock and Vibration Bulletin* 2, 21-45. Isolation from mechanical shock with a mounting system having nonlinear dual-phase damping.

6. R.R. Guntur and S. Sankar 1982 *Journal of Sound and Vibration* 84, 253-267. Performance of Different kinds of dual-phase damping shock mounts.

7. M.S. Hundal 1980 *12th Shock and Vibration Digest* 9, 17-21. Literature review - Pneumatic shock absorbers and isolators.

8. M.S. Hundal 1981 *Journal of Sound and Vibration* 76, 273-281. Response of shock isolators with linear and quadratic damping.

9. C.A. Mercer and P.L. Rees 1971 *Journal of Sound and Vibration* 18, 511-520. An optimum shock Isolator.

10. R.L. Eshleman and P.N. Rao 1969 *Shock and Vibration Bulletin* 40 (5), 217-234. The response of mechanical shock isolation elements to high rate input loading.

11. M.S. Hundal 1982 *Journal of Sound and Vibration* 84, 1-9. Passive pneumatic shock isolator: Analysis and Design.

12. M.S. Hundal and D.J. Fitzmorris 1985 *Shock and Vibration Bulletin* 55 (1), 139-154. Response of a symmetric self damped pneumatic shock isolator to an acceleration pulse.

13. M.S. Hundal 1985 *Journal of Sound and Vibration* 101, 33-40. Shock response of a symmetric pneumatic spring to a velocity pulse.

14. M.S. Hundal 1983 *Shock and Vibration Bulletin* 53(4), 73-83. Damped pneumatic spring as shock isolator: generalized analysis and design procedure.

15. M.S. Hundal 1983 *Journal of Sound and Vibration* 86, 293-296. Linear shock isolator: response to velocity pulse.

16. S. Rakheja and S. Sankar 1985 *Transactions of the ASME, Journal of Vibration, Acoustics, Stress and Reliability in Design* 107, 398-403. Vibration and shock isolation performance of a semi-active 'on-off' damper.

17. J. Alanoy and S. Sankar 1988 *Journal of Sound and Vibration* 126, 145-156. Semi-active force generators for shock isolation.

18. B. El-Asir et. al. 1994 *Journal of Sound and Vibration* 174, 115-121. A new approximate analytical analysis of the response of nonlinear damped systems subjected to step function excitation.

19. V.A. Bapat and R. Srinivasan 1970 *Journal of Sound and Vibration* 13, 51-65. Step function response of nonlinear spring mass systems in the presence of Coulomb damping.

20. G.L. Anderson 1974 *Journal of Sound and Vibration* 32, 101-108. Application of ultra-spherical polynomials to nonlinear, non-conservative systems subjected to step function excitation.

21. S.C. Sinha and P. Srinivasan 1972 *Journal of Sound and Vibration* 22, 211-219. An approximate analysis of nonlinear, non-conservative systems subjected to step function excitation.

22. H.R. Srirangarajan and P. Srinivasan 1976 *Journal of Sound and Vibration* 44, 369-377. The pulse response of nonlinear systems.

23. H.F. Bauer 1971 *International Journal of Nonlinear Mechanics* 6, 529-543. Vibrational behaviour of nonlinear systems to pulse excitations of finite duration.

24. H.R. Srirangarajan and P. Srinivasan 1973 *Journal of Sound and Vibration* 29, 215-226. The transient response to certain third-order nonlinear systems.

25. R. G. White 1973 *Journal of Sound and Vibration* 29, 295-307. Effects of nonlinearity due to large deflections in the derivation of frequency response data from the impulse response of structures.

26. A.H. Nayfeh and D.T. Mook 1979 *Nonlinear Oscillations.* New York: John Wiley.

27. D.W. Jordan and P. Smith 1987 *Nonlinear Ordinary Differential Equations.* Oxford: Clarendon Press; second edition.

28. C.M. Bender and S.A. Orszag 1978 *Advanced Mathematical Methods for Scientists and Engineers.* New York: McGraw-Hill.

29. J.A. Murdock 1991 *Perturbation Theory and Methods.* New York: John Wiley and Sons, Inc.

30. A.H. Nayfeh 1981 *Introduction to perturbation Techniques.* New York: Wiley.

31. A.H. Nayfeh 1973 *Perturbation Methods.* New York: Wiley.

32. N. Chandra Shekhar, H. Hatwal and A.K. Mallik 1998 *Journal of Sound and Vibration* 214, 589-603. Response of nonlinear dissipative shock isolators.

33. N. C. Nigam and S. Narayanan 1994 *Applications of Random Vibrations* Narosa Publishing House, New Delhi.

34. D. Hrovat 1991 *Journal of Sound and Vibration* 146, 93-110. Optimal suspension performance for 2-D vehicle models.

35. F. Oueslati and S. Sankar 1994 *Journal of Sound and Vibration* 172, 391-411. A class of semi-active suspension schemes for vehicle vibration control.

36. D. Yadav and H.C. Upadhyay 1992 *Journal of Sound and Vibration* 156, 247-268. Dynamics of vehicle in variable velocity runs over non-homogeneous flexible track and foundation with two point input models.

37. T.J. Gordon and R.S. Sharp 1998 *Journal of Sound and Vibration* 217, 163-182. On improving the performance of automotive semi-active suspension systems through road preview.

38. R.F. Harrison and J.K. Hammond 1986 *Journal of Sound and Vibration* 105, 361-371. Approximate, time-domain, non-stationary analysis of stochastically excited, non-linear systems with particular reference to the motion of vehicles on rough ground.

39. R.C. Redfield and D.C. Karnopp 1989 *Transactions of ASME, Journal of Dynamic Systems, Measurement and Control* 111, 51-59. Performance sensitivity of an actively damped vehicle suspension to feedback variation.

40. C. Yue, T. Butsuen and J.K. Hedrick 1989 *Transactions of ASME, Journal of Dynamic Systems, Measurement and Control* 111, 286-291. Alternative control laws for automotive active suspensions.

41. A. Hac 1995 *Transactions of ASME, Journal of Dynamic Systems, Measurement and Control* 117, 478-483. Decentralized control of active vehicle suspensions with preview.

42. A. Hac 1985 *Journal of Sound and Vibration* 100, 343-357. Suspension optimization of a 2-DOF vehicle model using a stochastic optimal control technique.

43. C.L. Kirk 1988 *Journal of Sound and Vibration* 124, 157-182. Non-linear random vibration isolators.

44. Y.A. Khulief and S.P. Sun 1989 *Transactions of ASME, Journal of Dynamic Systems, Measurement and Control* 111, 521-527. Finite element modeling and semi-active control of vibrations in road vehicles.

45. A. Hac and I. Youn 1992 *Transactions of ASME, Journal of Vibration and Acoustics* 114, 84-92. Optimal semi-active suspension with preview based on a quarter car model.

46. A. Hac and I. Youn 1993 *Transactions of ASME, Journal of Vibration and Acoustics* 115, 498-508. Optimal design of active and semi-active suspensions including time delays and preview.

47. D.A. Crolla and M.B.A. Abdel-Hady 1991 *Vehicle System Dynamics* 20, 107-120. Active suspension control: Performance comparisons using control laws applied to a full vehicle model.

48. D. Karnopp and G. Heess 1991 *Vehicle System Dynamics* 20, 207-217. Electronically controllable vehicle suspensions.

49. YE. Lin and H.P. Willumeit 1991 *Vehicle System Dynamics* 20, 353-369. The dynamics of the vibrator controlled adaptive damper and its potentials in vibration isolation.

50. N. Lovam, D.A. Wilson and R.S. Sharp 1992 *Vehicle System Dynamics* 21, 39-63. Optimization and performance enhancement of active suspensions for automobiles under preview of the road.

51. S.Y. Bhave 1992 *Vehicle System Dynamics* 21, 225-245. Effect of connecting the front and rear air suspension of a vehicle on the transmissibility of road undulation inputs.

52. M.G. Fodor and R. Redfield 1993 *Vehicle System Dynamics* 22, 1-20. The variable linear transmission for regenerative damping in vehicle suspension control.

53. R.G.M. Huismann, F.E. Veldpauss, H.J.M. Voets and J.J. Kok 1993 *Vehicle System Dynamics* 22, 43-55. An optimal continuous time control strategy for active suspensions with preview.

54. D. Ryba 1993 *Vehicle System Dynamics* 22, 79-95. Semi-active damping with an electromagnetic force generator.

55. A. Moran and M. Nagai 1993 *Vehicle System Dynamics* 22, 321-334. Optimal preview control of rear suspension using nonlinear neural networks.

56. S. Narayanan and G.V. Raju 1990 *Journal of Sound and Vibration* 141, 449-463. Stochastic optimal control of non-stationary response of a single-degree-of-freedom vehicle model.

57. G.V. Raju and S. Narayanan 1990 *International congress on recent developments in air and structure-born sound and vibration.* 687-694, Auburn University, USA. Active control of non-stationary response of a 2-DOF vehicle model.

58. G.V. Raju and S. Narayanan 1991 *Journal of Sound and Vibration.* 149, 413-428. Optimal estimation and control of non-stationary response of a two-degree-of-freedom vehicle model.

59. G.V. Raju and S. Narayanan 1995 *Sadhana.* 20, 489-499. Active control of non-stationary response of a two-degree-of-freedom vehicle model with nonlinear suspensions.

60. S. Narayanan and S. Senthil 1998 *Journal of Sound and Vibration.* 211, 495-506. Stochastic optimal active control of a 2-DOF quarter car model with non-linear passive suspension elements.

61. J.A. Tamboli and S.G. Joshi 1999 *Journal of Sound and Vibration* 219, 193-205. Optimum design of a passive suspension system of a vehicle subjected to actual random road excitations.

62. S.T. Ariaratnam and Wei-Chau Xie 1994 *International Journal of Nonlinear Mechanics* 29, 197-204. Almost-sure stochastic stability of coupled non-linear oscillators.

63. M. M. Doyle, N. Sri Namachchivaya and H. J. Van Roessel 1997 *International Journal of Nonlinear Mechanics* 32, 681-692. Asymptotic stability of structural

system based on Lyapunov exponents and moment Lyapunov exponents.

64. R.D. Blevins 1997 *Journal of Sound and Vibration* 208, 617-652. Probability density of finite Fourier series with random phases.

65. M. Shinozuka 1972 *Journal of Sound and Vibration* 25, 111-128. Digital simulation of random processes and its applications.

66. M. Shinozuka and G. Deodatis 1991 *Transactions of ASME, Applied Mechanics Reviews* 44, 191-203. Simulation of stochastic processes by spectral representation.

67. Y.S. Zhou, Z.K. Hou, M.F. Dimentberg and M.N. Noori 1997 *Journal of Sound and Vibration* 203, 607-620. A model for general periodic excitation with random disturbance and its application.

68. E.A. Johnson, S.F. Wojtkiewicz, L.A. Bergman and B.F. Spencer Jr 1997 *International Journal of Nonlinear Mechanics* 32, 721-734. Observations with regard to massively parallel computation for Monte Carlo simulation of stochastic dynamical systems.

69. B.A. Zeldin and P.D. Spanos 1996 *Transactions of the ASME, Journal of Applied Mechanics* 63, 946-952. Random field representation and synthesis using wavelet bases.

70. O.P. Agrawal 1998 *Transactions of ASME, Journal of Vibration and Acoustics* 120, 763-769. Application of wavelets in modeling stochastic dynamic systems.

71. F.W. Elliot Jr., D.J. Horntrop and A.J. Majda *Journal of Computational Physics* 132, 384-408. A Fourier-wavelet Monte Carlo method for fractal random fields.

72. B. Ravindra and A.K. Mallik 1993 *International Journal of Nonlinear Mechanics* 28, 427-440. Hard Duffing-type vibration isolator with combined Coulomb and viscous damping.

73. B. Ravindra and A.K. Mallik 1994 *Journal of Sound and Vibration* 170, 325-337. Performance of nonlinear vibration isolators under harmonic excitation.

74. B. Ravindra and A.K. Mallik 1995 *Journal of Sound and Vibration* 182, 345-353. Chaotic response of a harmonically excited mass on an isolator with nonlinear stiffness and damping characteristics.

75. A.K. Mallik, V. Kher, M. Puri and H. Hatwal 1999 *Journal of Sound and Vibration* 219, 239-253. On the modelling of non-linear elastomeric vibration isolators.

76. W. Rudin 1990 *Principles of Mathematical Analysis.* New York: McGraw-Hill; third edition.

77. N. Chandra Shekhar, H. Hatwal and A.K. Mallik 1999 *Journal of Sound and Vibration* Performance of nonlinear isolators and absorbers to shock excitations. (in press)

78. William H. Press, Saul A. Teukolsky, William T. Vetterling and Brian P. Flannery, 1993 *Numerical Recipes in Fortran*, second edition, Cambridge University Press.

79. V.J. Virchis and J.D. Robson 1971 *Journal of Sound and Vibration* 18, 423-427. Response of an acceleration vehicle to random road undulation.

80. C.J. Dodds and J.D. Robson 1973 *Journal of Sound and Vibration* 31, 175-183. The description of road surface roughness.

81. K. Sobczyk, D. B. Macvean and J.D. Robson 1977 *Journal of Sound and Vibration* 52, 37-49. Response to profile imposed excitation with randomly varying traversal velocity.

82. K.M.A. Kamash and J.B. Robson 1978 *Journal of Sound and Vibration* 57, 89-100. The description of road surface roughness.

83. R.F. Harrison and J.K. Hammond 1985 *Journal of Sound and Vibration* 99, 437-447. A systems approach to the characterization of rough ground.

84. A.N. Heath 1987 *Journal of Sound and Vibration* 115, 131-144. Application of the isotropic road roughness assumption.

85. D.E. Newland 1993 *An Introduction to Random Vibrations, Spectral and Wavelet analysis* Longman House, Harlow, England.

86. M. Shinozuka and G. Deodatis 1996 *Applied Mechanics Reviews* 49, 29-53. Simulation of multidimensional Gaussian fields by spectral representation.

87. P.D. Spanos and B.A. Zeldin 1998 *Applied Mechanics Reviews* 51, 219-237. Monte Carlo treatment of random fields: A broad perspective.

88. K. Wiesenfeld 1993 *Annals New York Academy of Sciences* 706, 13-25. An introduction to stochastic resonance.

89. L. Gammaitoni, P. Hanggi, P. Jung and F. Marchesoni 1998 *Reviews of Modern Physics* 70, 223-287. Stochastic resonance.

90. S. Mitaim and B. Kosko 1998 *Proceedings of the IEEE* 86, 2152-2183. Adaptive stochastic resonance.

91. K. Wiesenfeld and F. Jaramillo 1998 *Chaos* 8, 539-548. Minireveiw of stochastic resonance.

Appendix A

Solution of Ordinary Second Order Differential Equations for Three Special Non-homogeneous Functions

In this appendix the solution of linear second order differential equations with time-invariant coefficients for three types of generalized non-homogeneous functions, with initial conditions $x = \dot{x} = 0$ at $t = 0$, are presented.

Consider the equation

$$\ddot{x} + 2\zeta\dot{x} + x = f(t) \tag{A.1}$$

with initial conditions $x(0) = \dot{x}(0) = 0$.

Solution of equation (A.1) is obtained by using Laplace transformations for three types of non-homogeneous functions $f(t)$.

Case (i) $\quad f(t) = e^{at}\left[\sum_{m=0}^{N} A_m t^m\right]$

This is the generalized form of both rounded step and rounded pulse inputs. Solution of equation (A.1) may be written as

$$
\begin{aligned}
x(t) &= x_1(t) + x_2(t) \\
\text{where,} \quad x_1(t) &= e^{-\zeta t}\left[P_1\cos(\beta t) + Q_1\sin(\beta t)\right]/\beta \\
\text{and} \quad x_2(t) &= e^{at}\left[\sum_{m=0}^{N} B_{m+1}t^m/m!\right] \\
\beta &= \sqrt{(1-\zeta^2)}; \\
\alpha &= -\zeta + i\beta; \\
i &= \sqrt{(-1)}; \\
Q_1 + iP_1 &= \left[\sum_{m=0}^{N}(N-m)!A_{N-m}(\alpha-a)^m\right]/(\alpha-a)^{N+1}; \\
B_{N+1} &= N!A_N/\Gamma; \\
B_N &= \left[(N-1)!A_{N-1} - 2(a+\zeta)B_{N+1}\right]/\Gamma, \\
B_{N+1-m} &= \left[(N-m)!A_{N-m} - 2(a+\zeta)B_{N+2-m} - B_{N+3-m}\right]/\Gamma;\ \Gamma = a^2 + 2a\zeta + 1
\end{aligned}
$$

for $2 \le m \le N$.

Case (ii) $f(t) = e^{at}\left[\sum_{m=0}^{N}\{C_m\cos(\omega_m t) + D_m\sin(\omega_m t)\}\right]$

This function is a generalization of the oscillatory step input. Solution of equation (A.1) then may be written as

$$
\begin{aligned}
x(t) &= x_1(t) + x_2(t) \\
\text{where,} \quad x_1(t) &= e^{-\zeta t}\left[P_2\cos(\beta t) + Q_2\sin(\beta t)\right]/\beta \\
\text{and} \quad x_2(t) &= e^{at}\left[\sum_{m=0}^{N}\{R_m\cos(\omega_m t) + S_m\sin(\omega_m t)\}\right] \\
\text{where,} \quad \beta &= \sqrt{(1-\zeta^2)}; \\
\alpha &= -\zeta + i\beta; \\
i &= \sqrt{(-1)};
\end{aligned}
$$

$$
\begin{aligned}
Q_2 + iP_2 &= \sum_{m=0}^{N} \frac{C_m(\alpha - a) + D_m\omega_m}{(\alpha - a)^2 + \omega_m^2} \\
\text{and} \quad \alpha_m &= a + i\omega_m; \\
S_m + iR_m &= \frac{D_m + iC_m}{\alpha_m^2 + 2\zeta\alpha_m + 1}.
\end{aligned}
$$

Case (iii) $f(t) = e^{at}\left[E\cos(\Omega t) + F\sin(\Omega t)\right]\left(\sum_{m=0}^{N} A_m t^m\right)$

This type of non-homogeneous terms occur in equations (17) and (18) and it is similar to equation (19). Solution of equation (A.1) may be written as

$$
\begin{aligned}
x(t) &= x_1(t) + x_2(t) \\
\text{where,} \quad x_1(t) &= e^{-\zeta t}\left[P_3\cos(\beta t) + Q_3\sin(\beta t)\right]/\beta \\
\text{and} \quad x_2(t) &= e^{at}\left[\sum_{m=0}^{N}\left\{R_m\cos(\Omega t) + S_m\sin(\Omega t)\right\}t^m/m!\right] \\
\text{where,} \quad \beta &= \sqrt{(1-\zeta^2)}; \\
\alpha &= -\zeta + i\beta; \\
\text{and} \quad i &= \sqrt{(-1)}; \\
U_m &= \left[\sum_{k=0}^{\lceil m/2\rceil}(-1)^k \begin{pmatrix} m+1 \\ 2k \end{pmatrix}(\alpha - a)^{m+1-2k}\Omega^{2k}\right] \\
V_m &= \left[\sum_{k=0}^{\lfloor m/2\rfloor}(-1)^k \begin{pmatrix} m+1 \\ 2k+1 \end{pmatrix}(\alpha - a)^{m-2k}\Omega^{2k+1}\right] \\
G &= (\alpha - a)^2 + \Omega^2; \\
Q_3 + iP_3 &= \left[\sum_{m=0}^{N} m!A_m\left(EU_m + V_mF\right)G^{N-m}\right]/G^{N+1}; \\
\alpha_2 &= a + i\Omega; \\
\Gamma_2 &= \alpha_2^2 + 2\zeta\alpha_2 + 1; \\
B_{N+1} &= N!A_N/\Gamma_2; \\
B_N &= B_{N+1}\left[(N-1)!A_{N-1} - 2(\alpha_2 + \zeta)B_{N+1}\right]/(N!A_N);
\end{aligned}
$$

$$B_{N+1-m} = B_{N+1}\left[(N-m)!A_{N-m} - 2(\alpha_2+\zeta)B_{N+2-m} - B_{N+3-m}\right]/(N!A_N);$$
$$\text{for} \quad 2 \le m \le N.$$

$$S_m + iR_m = (F+iE)B_{N+1-m} \qquad \text{for} \quad 0 \le m \le N.$$

Appendix B

Laplace Transform of Equation (5.41) and Its Inverse

The Laplace transform of X_0 given in equation (5.41) may be written as

$$\bar{X}_0(s) = \frac{N(s)}{D(s)}; \tag{B.1}$$

where, $N(s) = N_{01}(s)\bar{Y}_1(s)$; $N_{01}(s) = (a_1 + 2\zeta_1 s)(h_{11}s^2 + h_{12}s + h_{13})$;

$h_{11} = 1$; $h_{12} = 4\zeta_2(1+\alpha)/R^2$; $h_{13} = 2a_2(1+\alpha)/R^2$;

$\bar{Y}_1(s) = \gamma^2/(s(s+\gamma)^2)$ for the rounded step; $\gamma = \gamma_s/T_0$;

$D(s) = s^4 + q_3 s^3 + q_2 s^2 + q_1 s + q_0$;

$q_3 = 2[(1+\alpha^2+R^2)(\zeta_1+\zeta_2) - 2\alpha(\zeta_1-\zeta_2)]/R^2$;

$q_2 = [1 - 2\alpha(a_1 - a_2) + \alpha^2 + R^2 + 16\zeta_1\zeta_2)]/R^2$;

$q_1 = 8[\zeta_1 a_2 + \zeta_2 a_1]/R^2$; $\quad q_0 = 4a_1a_2/R^2$.

The factorization of denominator $D(s)$ in equation (B.1) may be expressed as

$D(s) = \psi_1(s)\psi_2(s)$;

where, $\psi_1(s) = [(s+\alpha_1)^2 + \beta_1^2]$; $\quad \psi_2(s) = [(s+\alpha_2)^2 + \beta_2^2]$.

Let us assume that $\lambda_1 = -\alpha_1 + i\beta_1$; $\quad \lambda_2 = -\alpha_2 + i\beta_2$; are the complex roots of

the polynomial $D(s)$ and $\lambda_1 \neq \lambda_2$ then the inverse Laplace transform of $\bar{X}_0(s)$ may be written as

$X_0(T) = X_{00} + X_{01}(T) + X_{02}(T) + X_{03}(T)$

where, $X_{00} = h_{13}a_1/q_0$;

$X_{01}(T) = \exp(-\gamma T)(A_{01} + B_{01}T)$;

$B_{01} = Q_{010}(-\gamma)$; $\quad Q_{010}(s) = \frac{\gamma^2 N_{01}(s)}{sD(s)}$;

$A_{01} = Q_{011}(-\gamma)$; $\quad Q_{011}(s) = Q'_{010}(s)$

here, $(')$ denotes differentiation with respect to s,

$X_{02}(T) = \exp(-\alpha_1 T)(A_{02}\cos(\beta_1 T) + B_{02}\sin(\beta_1 T))/\beta_1$;

$B_{02} + iA_{02} = Q_{02}(\lambda_1)$;

$Q_{02}(s) = \frac{N_{01}(s)\bar{Y}_1(s)}{\psi_1(s)}$;

let $X_{020}(\lambda_1, \lambda_2, T) = X_{02}(T)$ then

$X_{03}(T) = X_{020}(\lambda_2, \lambda_1, T)$.

The other parameters used in equations (5.39)-(5.41) are

$h_{14} = 1$; $\quad h_{15} = 4\zeta_1(1-\alpha)/R^2$; $\quad h_{16} = 2a_1(1-\alpha)/R^2$;

$h_{21} = (1-\alpha)/R^2$; $\quad h_{22} = 4\zeta_2/R^2$; $\quad h_{23} = 2a_2/R^2$;

$h_{24} = (1+\alpha)/R^2$; $\quad h_{25} = 4\zeta_1/R^2$; $\quad h_{26} = 2a_1/R^2$.